Relaxation analysis of $LiNiO_2$-based cathode materials in the deeply lithium extracted region

Jian Kang

Department of Fundamental Energy Science

Graduate School of Energy Science

Kyoto University

2022

Table of contents

Chapter 1 Introduction

1.1 Lithium ion batteries

A chemical battery that converts the energy of chemical reactions into electrical energy is called a primary battery if its mission ends when the stored chemical energy is released, and a secondary battery if the released energy can be recovered and reused by recharging. Lithium ion battery (LIB) is a type of secondary battery. Since its commercialization in 1991, LIBs have been widely used in portable electronic devices, such as laptop computers and mobile phones, due to their excellent energy and power densities. Since their commercialization in 1991, they have been widely used in portable electronic devices such as laptop computers and mobile phones, due to their superior energy density and power density. Currently, secondary batteries are largely used for resource and energy conservation.[1-3]

A lithium ion battery consists of a positive electrode (active material, binder, conductive aid, current collecting foil), an anode (active material, binder, current collecting foil), electrolyte (solvent, supporting salt, additives), separator, and cell case. The typical lithium ion battery uses $LiCoO_2$ as the positive electrode, graphite as the negative electrode, $LiPF_6$ as the electrolyte, and a polyolefin separator.[2]

Lithium ion secondary batteries have the following characteristics:

(1) High energy density (compared to nickel / cadmium and nickel / hydrogen), small size, and light weight.

(2) High electromotive force of 4 V or more.

(3) High current discharge is possible.

(4) Low self-discharge.

(5) No harmful substances such as lead and cadmium.

(6) No memory effect (a decrease in discharge capacity when the battery is recharged without being used up).

These features are the reasons why rechargeable batteries have been used more commonly than conventional batteries.[3]

Figure 1.1 schematically shows the reaction during charging and discharging of a lithium secondary battery.[4] During charging, lithium ions are produced in the positive electrode, which move through the electrolyte and are inserted into the carbon interlayer of the negative electrode.

During charging, the reaction at each electrode is represented as

$$\text{(Anode)} \quad C_6 + xLi^+ + xe^- \rightarrow Li_xC_6$$

$$\text{(Cathode)} \quad LiCoO_2 \rightarrow Li_{1-x}CoO_2 + xLi^+ + xe^-.$$

Here, graphite is denoted by C_6 while the composition of the filled graphite interlayer is LiC_6. Therefore, the total charging reaction is described as

$$C_6 + LiCoO_2 \rightarrow Li_xC_6 + Li_{1-x}CoO_2.$$

During discharge, lithium ion is released from the carbon interlayers of the anode and return to the lithium portion of the $LiCoO_2$ cathode. In this process, the decrease in Gibbs free energy due to the redox reaction is taken out as electrical work. The properties and combinations of the cathode, anode, separator, and electrolyte are important to achieve high-performance in lithium ion batteries. The following sections 1.2 and 1.3 describe the details of the cathode and anode, which are particularly important in battery development.

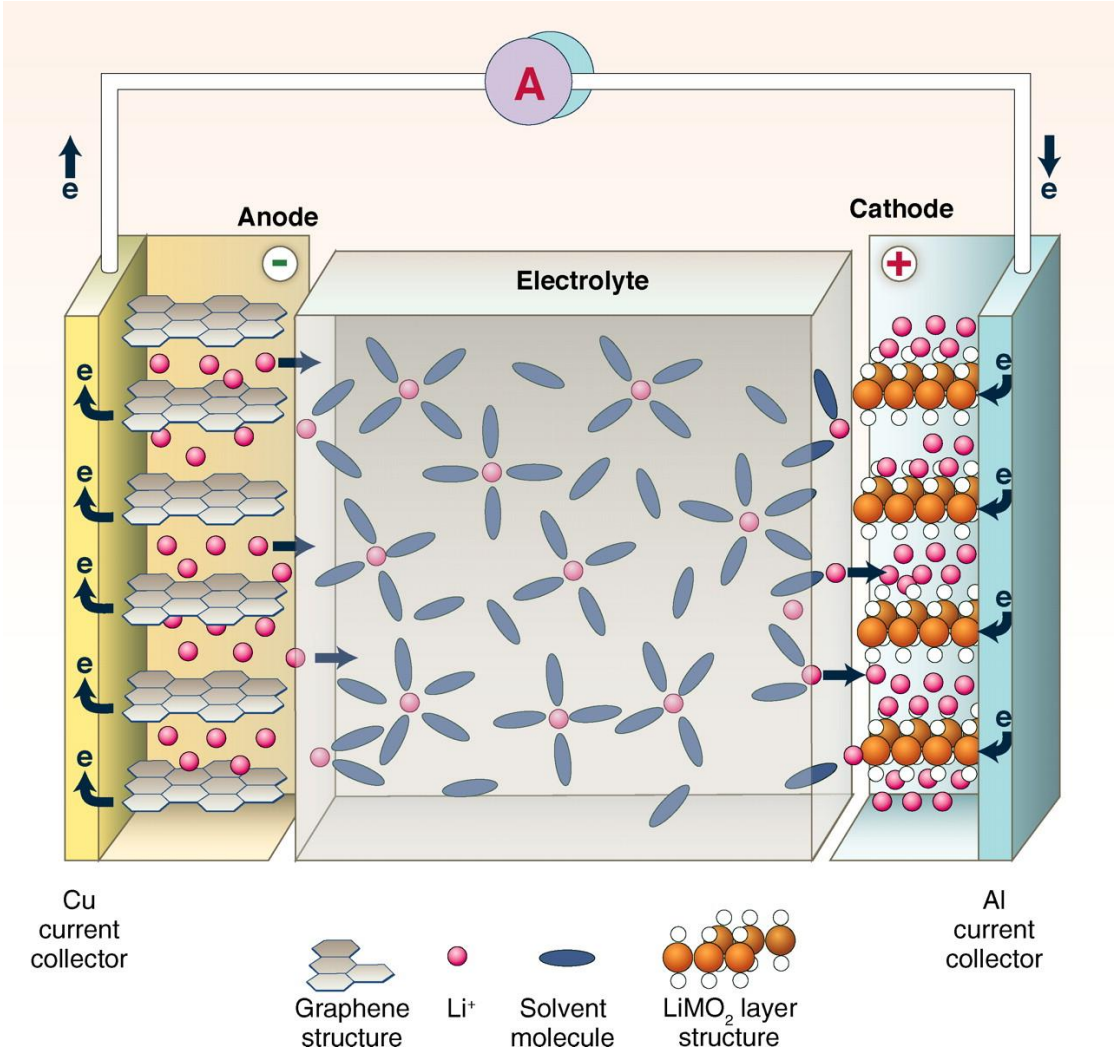

Figure 1.1 Schematic diagram of lithium ion secondary battery.

1.2 Cathode

High voltage and high capacity lithium ion secondary batteries are expected to be used not only as small scale power sources for electronic devices but also at larger scale such as automobiles. To realize this, it is important to develop cathode materials with higher output, more lithium ions storage, faster lithium insertion and extraction and have less capacity degradation over cycles. In other words, in addition to high electromotive force, high charge / discharge capacity, high rate characteristics, and good cycle retention, safety and economic efficiency are also required of electrode materials.[5-7]

The cathode materials for lithium ion batteries currently available for practical use are layered $LiCoO_2$ or compounds modified by doping with small amounts of foreign elements. However, the biggest problem with the commercialized LIBs so far is the use of cobalt, a scarce and expensive metal element, which accounts for about 30% of the total production cost. Small LIBs, such as those for cell phone, use only a small amount of cobalt per battery, so the cost effectiveness (cost / performance) difference between LIBs and other batteries can be negligible. The cost of Co becomes a more serious issue for larger and higher capacity LIBs such as those for HEVs (Hybrid Electric Vehicles). For PHEVs (Plug-in Hybrid Electric Vehicles) and electric vehicles, which require even larger capacities, the cost of may even lead to the depletion of resources as the use of Co increases. In order to cope with this problem, various non-cobalt cathode materials have been investigated as alternatives to $LiCoO_2$. For example, $LiNiO_2$, which has the same layered rock salt structure and contains less expensive and less toxic Ni, $LiMn_2O_4$, which has a spinel structure, and $LiFePO_4$, which has an olivine structure. The comparison of these materials is summarized in Table 1.1.[8,9]

Table 1.1 Comparison of typical cathode materials.

Electrode material	Average voltage (V)	Specific capacity ($mAh \cdot g^{-1}$)	Advantages	Disadvantages
$LiCoO_2$	3.8	274	performance	expensive and toxic Co
$LiNiO_2$	3.8	275	low cost and high capacity	limited cycle life and poor safety
$LiMn_2O_4$	4.1	148	low cost	limited cycle life, low capacity
$LiFePO_4$	3.4	170	low cost, good cycle life	low voltage and capacity

1.2.1 $LiCoO_2$ (LCO)

The $LiCoO_2$ was discovered by Goodenough *et at*., and has been mainly applied as a cathode material for lithium ion batteries, which are widely used in current mobile devices due to its easy synthesis and stable performance. The fractional coordinates of Li, Co, and O are shown in Table 1.2. The theoretical capacity of $LiCoO_2$ is 273.8 $mAh \cdot g^{-1}$. But in practice, the extraction of more than 0.5 of lithium for the formula from the crystal structure causes a large structural change and therefore reduces the reversibility as well as degrades the battery performance. Then, only half of the theoretical capacity of 140 $mAh \cdot g^{-1}$ is practical used for charge-discharge process in battery. In addition, it is difficult to use $LiCoO_2$ as a power source for medium to large size devices, although it is useful in the field of small devices, due to the problem of Co reserves and uneven distribution as the main raw material, as well as its large environmental impact. Therefore, in recent years, research on $LiNiO_2$-based materials using Ni has been actively conducted to avoid such problem.[2]

Table 1.2 The fractional coordinates of $LiCoO_2$.

atom	Wyckoff symbol	x	y	z	Site occupancy (*g*)
Li	3*a*	0	0	1/2	1
Co	3*b*	0	0	0	1
O	6*c*	0	0	0.258	1

1.2.2 $LiNiO_2$ (LNO)

$LiNiO_2$ is a cathode material that has been studied for a long time as an alternative to $LiCoO_2$. $LiNiO_2$ was first synthesized by Dyer *et al*. in 1954, and was later widely studied by Dahn *et al*. and Ohzuku *et al*. in the 1990s. $LiNiO_2$ has the same layered rock salt type structure as $LiCoO_2$, so it is expected to have the similar characteristics as $LiCoO_2$. When nickel is used, although the potential is slightly lower than that of cobalt, the theoretical capacity is almost the same as that of $LiCoO_2$. However, the available charge / discharge capacity is about 1.2 times larger (lithium ion desorption up to about 0.7 is possible). In addition, nickel is more abundant than cobalt and would make for a cheaper alternative, and it is also superior in terms of low toxicity.[3]

From this point of view, $LiNiO_2$ is considered to be the best alternative material, but there is a problem in terms of synthesis. Since nickel is more easily reduced to divalent in comparison with cobalt, lithium deficiency due to volatilization of the raw lithium salt tends to occur during high temperature sintering, resulting in the formation of $Li_{1-x}Ni_{1+x}O_2$ with a non-stoichiometric composition. Almost identical ionic radius of Li^+ (0.76 Å) and Ni^{2+} (0.69 Å) allows the mixing of nickel ions into the vacant site. When Ni^{2+} occupies the lithium 3*a* site, the region can be regarded as a local NiO irregularly arranged rock salt layer ($Fm\bar{3}m$), which is called a rock salt domain. The rock salt domain is not only electrochemically inert, but also prevents the battery reaction in the rock salt layer which is inherently active, because the Ni^{2+} in the lithium sites inhibits the two-dimensional solid phase diffusion of the single lithium layer.[2]

This non-stoichiometric composition causes problems such as a decrease in the diffusion rate of lithium ions and degradation of the cycle performance. In addition, when Li is desorbed from $LiNiO_2$, Ni moves to the Li position, and when there is a large amount

of Li, the Ni position is occupied, which adversely affects the charge / discharge performance. A further major problem is thermal stability, where the decomposition reaction associated with oxygen occurs at temperatures about 50 ℃ lower than the $LiCoO_2$ case. This is a major issue in view of the recent strong demand for safety.[10-13]

Figure 1.2 shows the structural change of $Li_{1-x}NiO_2$ during charge / discharge, where H is hexagonal (space group: $R\bar{3}m$) and M is monoclinic (space group: $C2/m$).[14-17] Figure 1.3 shows the hexagonal and monoclinic crystal structures. The crystal structure change of $Li_{1-x}NiO_2$ proceeds in the following manner: hexagonal (H1) → monoclinic (M) → hexagonal (H2) → hexagonal (H3), and such crystal structure change is a major cause of degradation of electrode materials. It has been reported that a phase transformation of H2-H3 occurs when it is charged up to 4.15V. In the H2-H3 phase transformation, the *a*-axis shows a slight contraction, but *c*-axis decreases sharply. The large change in the *c*-axis between the H2-H3 phases indicates that there will be a significant strain at the interface between the two phases, which affects mainly in the primary particle level, but also on the secondary particles. This strain is released by the formation of cracks during cycling. The cracks provide a pathway for the liquid electrolyte to infiltrate the particles inside. This can exacerbate side reactions such as electrolyte decomposition and dissolution of metal ions in the material. In addition, the rigidity of solid electrolyte interphase (SEI) formed by the side reaction can increase the charge transfer impedance, and phase transformation can occur on the exposed surface of the material. Such processes would result in reduced cycling and thermal stability.

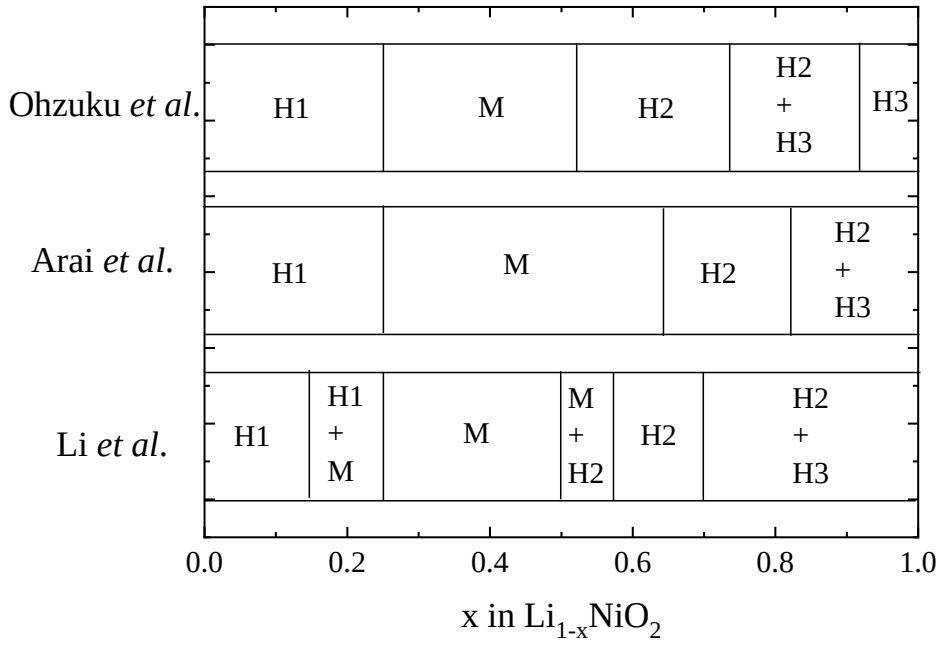

Figure 1.2 Structural changes in $Li_{1-x}NiO_2$.

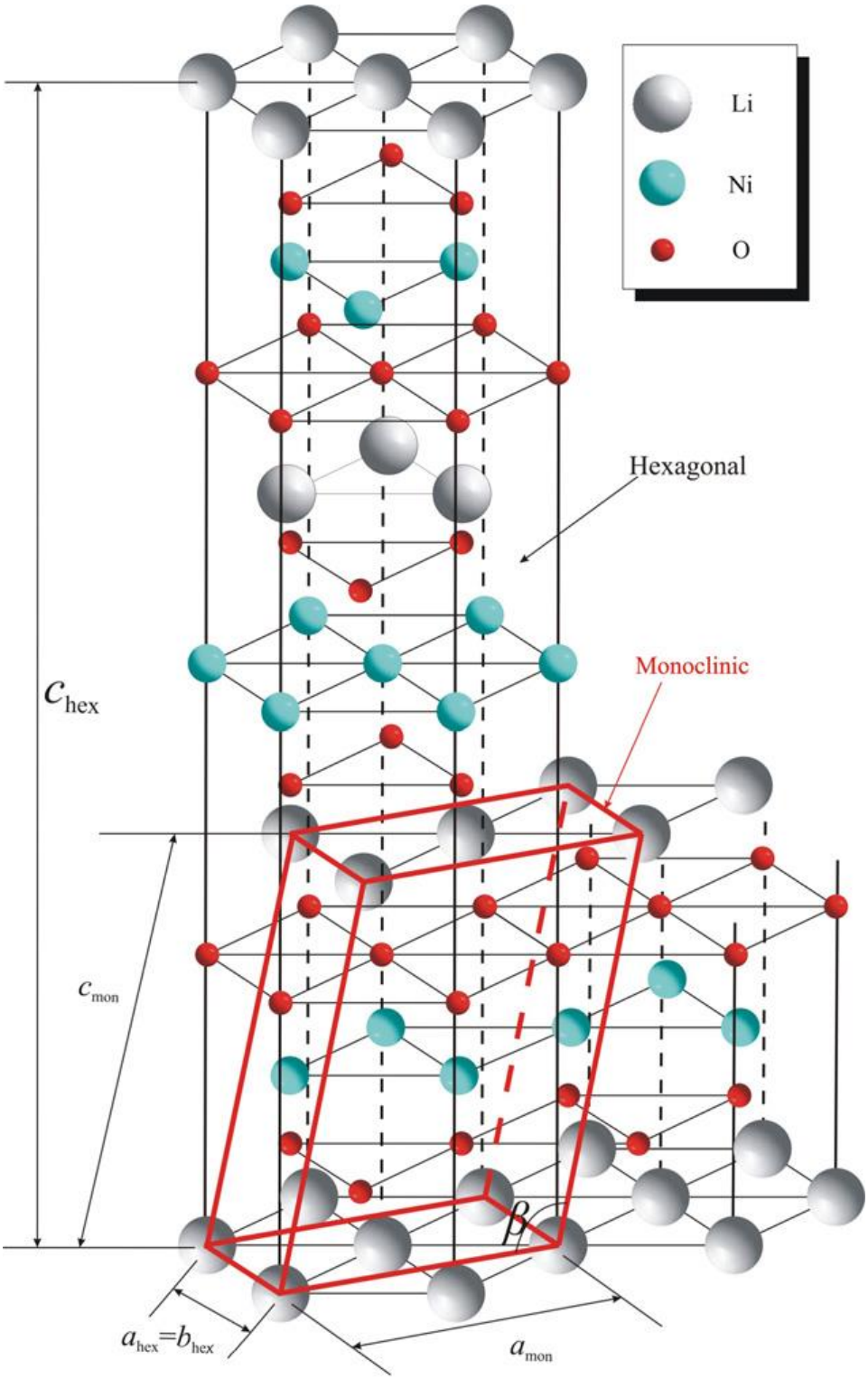

Figure 1.3 Crystal structure of space group $R\bar{3}m$ and space group $C2/m$.

1.2.3 $LiNi_aCo_bAl_{1-a-b}O_2$ (NCA) and $LiNi_aCo_bMn_{1-a-b}O_2$ (NCM)

Although $LiNiO_2$ has been studied for a long time as an alternative material to $LiCoO_2$, it has not been put to practical use due to the above problems, and the use of $LiNiO_2$ alone seems to be difficult. In this study, a variety of solid solution compounds based on $LiNiO_2$ have been investigated. In particular, $LiNi_{1-a-b}Co_aAl_bO_2$ (NCA) in which the Ni in $LiNiO_2$ is partially replaced by Co and Al, has attracted considerable attention. NCA has the same crystal structure as $LiNiO_2$, but has a higher specific capacity and improved structural, chemical, and thermal stability compared to $LiNiO_2$. It is also advantageous in terms of cost because it reduces the amount of Co used.[18-22] However, it is known that NCA exhibits hexagonal two-phase ($R\bar{3}m$) coexistence reaction as well as $LiNiO_2$ in the high potential region.[20,23,24]

Among the NCAs, $LiNi_{0.8}Co_{0.15}Al_{0.05}O_2$ has excellent performance and has been widely studied.[18-20] However, this composition of NCA also shows hexagonal two-phase ($R\bar{3}m$) coexistence reaction in the high potential region.[18,25] On the other hand, due to the high cost and toxicity of Co, NCAs with less Co substitution are currently being investigated.[21]

In recent years, it has been also reported that partial substitution of Ni by Co and Mn ($LiNi_{1-a-b}Co_aMn_bO_2$) would improve the electrochemical performance in $LiNiO_2$-based electrode materials.[26-30] $LiNi_{1-a-b}Co_aMn_bO_2$ (NCM) are regarded as a promising cathode material due to their relatively low cost, high capacity and excellent cycle performance.[31-33] In the NCM-based cathode material, the $LiNi_{1/3}Co_{1/3}Al_{1/3}O_2$ (NCM-333),[34] $LiNi_{0.5}Co_{0.2}Al_{0.3}O_2$ (NCM-523),[35] $LiNi_{0.6}Co_{0.2}Al_{0.2}O_2$ (NCM-622)[36] and $LiNi_{0.8}Co_{0.1}Al_{0.1}O_2$ (NCM-811)[37] were widely investigated. Even though Ni-lean NCM (Ni < 60%) provides the excellent cycle performance and thermal properties, it gave a

relatively low practical specific capacity (< 200 $mAh \cdot g^{-1}$) and thus could not meet the industrial demand for large scale energy storage devices. Therefore, Ni-rich cathode materials (Ni > 60%) are attractive alternative candidates that can provide a specific capacity of more than 200 $mAh \cdot g^{-1}$. In the Ni-rich NCM system, Co and Mn contribute to improvement of electric conductivity and structural stability, respectively. $LiNi_{0.8}Co_{0.1}Al_{0.1}O_2$ (NCM-811), for its larger capacity, has been also investigated mainly focused on the application of EVs or power storage systems. However, it is difficult to commercialize due to several instability issues during the charge and discharge. For example, the possible reaction between highly oxidizing Ni^{4+} and electrolyte to form NiO-like rock salt type layer in the high potential region. The NiO-like rock salt layer is thought to increase the charge transfer resistance leading capacity fade.[38,39] In addition, increasing the Ni content in Ni-rich systems has a negative impact on capacity degradation, which prevents large scale commercialization[40,41]. To solve these problems, many experimental methods have been explored, such as surface coating,[42] making single crystal particles,[43,44] and core shell / concentration gradient structures.[45,46]

1.3 Anode

The anode of battery must have a low discharge potential and high energy extraction per unit weight and volume. From these perspectives, metallic lithium has the most favorable characteristics due to its low redox potential (-3.040 V compared to standard hydrogen electrode) and large specific capacities per weight and volume (3860 $mAh \cdot g^{-1}$ and 2047 $mAh \cdot cm^{-3}$, respectively).[47-49] It has already been used as an anode material for primary batteries, but there have been practical problems with its use in secondary batteries. The lithium metal elutes as Li cation in the electrolyte during discharge, and precipitates as Li metal in the liquid during charging, forming dendrites or fine particles. In addition, isolated lithium is also formed by dropping out of the dendrite and losing conductivity at its interface through reaction with the solvent, resulting in poor current efficiency. For this reason, carbon materials are widely used as the anode in lithium ion batteries currently on the market.[3]

Although the specific capacity of carbon materials is inferior to that of lithium metals, they exhibit excellent cycle performance because charging and discharging proceed at a low potential comparable to that of lithium metals.

Carbon materials are mainly graphite, easily graphitizable carbon (soft carbon), and difficult to graphitize carbon (hard carbon). Of these, graphite is currently the most widely used LIB anode material. The theoretical capacity of graphite is 372 $mAh \cdot g^{-1}$.[49,50] When Li is inserted, at 0.6 V - 1.3 V vs. Li^+ / Li, the graphite and electrolyte form a compound and a thin film called solid electrolyte interphase (SEI) is formed between the graphite and electrolyte. This SEI is ion conductive but non electronically conductive and, once formed, effectively prevents the irreversible reduction of the electrolyte.

In general, graphite has the following characteristics.[2]

(1) High discharge capacity per volume

(2) High initial charge / discharge efficiency (low irreversible component)

(3) Flat discharge curve

(4) High average discharge voltage

In addition, propylene carbonate (PC) can be used as the electrolyte solvent for soft carbon and hard carbon in the case of the anode, but not for graphite because the decomposition reaction of PC precedes the doping of Li^+. In general, ethylene carbonate (EC) is used instead of PC.

In addition to carbon materials, there are other tin-based materials such as carbon silicon (Si) and tin (Sn). These materials have a capacity per volume comparable to that of lithium metal.[49,50] However, because tin-based materials can absorb a large amount of lithium, they undergo a fourfold change in volume upon lithium absorption, and collapses upon repeated lithium absorption and release. In order to solve this problem, tin-based oxide anode materials or tin-based amorphous anode materials are used. Among them, anode materials using multiple elements such as tin, cobalt, and carbon can achieve both high dose and improved cycle life characteristics.[2]

1.4 Relaxation analysis

In general, it is known that the crystal structure of the electrode material of lithium ion batteries changes with the change in electrode potential during charge / discharge. Although there have been many reported on the crystal structure change during charging and discharging, there are very few reports on the crystal structure change during the pause time after charging and discharging. T. Yao *et al*. clarified that the change in state of materials from kinetic to thermodynamic processes by analyzing the materials over time in the open-circuit state after charge / discharge is stopped.[51]

Relaxation analysis stands on that the kinetics dominates during charging and discharging, while the equilibrium dominates during quiescence. Our group have previously reported the results of relaxation analysis for γ-Fe_2O_3,[51,52] $LiFePO_4$,[53] $LiMn_2O_4$,[54,55] $LiMn_{0.75}Fe_{0.25}PO_4$,[56-58] $LiCoO_2$,[59] graphite,[60,61] $LiNiO_2$ and $LiNi_{0.933}Co_{0.031}Al_{0.036}O_2$.[62]

In the case of γ-Fe_2O_3 and $LiFePO_4$, the iron site shift was observed after the cessation of charging and discharging, indicating that the kinetic stability of Li is at 8*a* site, while the equilibrium stability is at 16*c* site.[52,53] It was also found that Li-rich and Li-lean phases coexist in $LiFePO_4$, with the Li-lean phase favoring Li diffusion during charging and discharging, and the Li-rich phase favoring Li diffusion at the relaxation.[54]

There is a great possibility that a similar relaxation decrease can be observed for other electrode materials, and our group are currently conducting relaxation analyses for various electrode materials.

1.5 Motivation and objective of thesis

Lithium ion secondary batteries are currently used in many electronic devices due to their excellent performance. In the future, it would be necessary to develop even higher performance electrode materials for large scale applications such as PHEVs and electric vehicles that require high capacity. In lithium secondary batteries, upon charging, lithium ions break the chemical bonds at the cathode and leave the cathode, forming new chemical bonds at the anode, and *vice versa*. As described above, very intense chemical reactions are constantly occurring in electrode materials, and electrode materials must be able to withstand these harsh conditions. In order to develop superior electrode materials, it is important to analyze structural changes and ion diffusion behavior from the atomic level.

Among the cathode materials NCAs, $LiNi_{0.8}Co_{0.15}Al_{0.05}O_2$ has excellent performance and has been widely studied. However, it shows two-phase coexistence reaction of hexagonal crystal in high potential region, which causes degradation. On the other hand, due to the expensive and toxic nature of Co, NCA with less Co substitution is also important and is currently being studied. In the previous study, relaxation analyses were performed for $LiNiO_2$ and $LiNi_{0.933}Co_{0.031}Al_{0.036}O_2$ (Co-3.1 NCA) with a small amount of Co substitution in the high potential region. Figure 1.4 shows the relaxation behavior of the mole fraction of H3 phase in Li_xNiO_2 and $Li_xNi_{0.933}Co_{0.031}Al_{0.036}O_2$ measured after lithium extraction up to x = 0.12, 0.09 and 0.06 at 0.01 C. The results shows that the mole fraction of H3 phase in all the samples decrease with a small amount of Co substitution.[63]

In this thesis, in order to discuss the contribution of Co substitution in the high potential region, relaxation analyses were performed on $Li_xNi_{0.874}Co_{0.090}Al_{0.036}O_2$ (Co-9.0 NCA) and $Li_xNi_{0.815}Co_{0.149}Al_{0.036}O_2$ (Co-14.9 NCA) after the lithium extraction up to high voltage region ($0.06 \leq x \leq 0.12$). Furthermore, in order to clarify the contribution of Co

to NCM-based cathode materials, I also investigated the structural changes in the relaxation process after the $Li_xNi_{0.8}Co_{0.1}Mn_{0.1}O_2$ (NCM-811) and $Li_xNi_{0.35}Co_{0.35}Mn_{0.30}O_2$ (NCM-353530) was charged to the high voltage region ($0.06 \leq x \leq 0.12$).

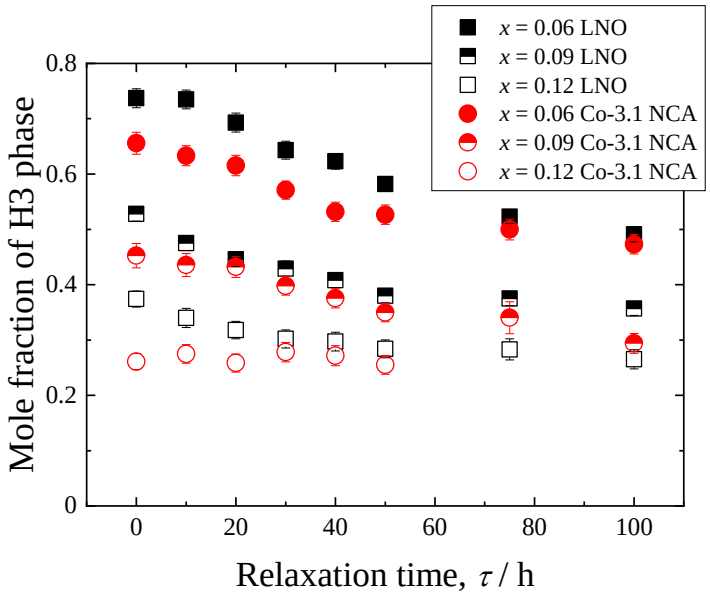

Figure 1.4 Calculated mole fraction change of H3 phase for Li_xNiO_2 and $Li_xNi_{0.933}Co_{0.031}Al_{0.036}O_2$ (x = 0.12, 0.09 and 0.06).

Reference

[1] 工藤徹一, 日比野光宏, 本間格, リチウムイオン電池の科学, ホスト･ゲスト系電極の物理化学からナノテク材料まで, 内田老鶴圃 (2010).

[2] 堀江英明, リチウムイオン電池, 基礎と応用, 培風館 (2010).

[3] 小久見善八, 安部武志, 稲葉稔, 内本善晴, リチウム二次電池, オーム社 (2008).

[4] M. M. Thackeray, C. Wolverton, and E. D. Isaacs, *Energy Environ. Sci*., **5**, 7854 (2012).

[5] K. Kang, Y. S. Meng, J. Breger, C. P. Grey, and G. Ceder, *Science*, **311**, 977 (2006).

[6] P. Simon, and Y. Gogotsi, *Nat. Mater*., **7**, 845 (2008).

[7] J. B. Goodenough, and K. S. Park, J. Am. *Chem. Soc*., **135**, 1167 (2013).

[8] N. Nitta, F. X. Wu, J. T. Lee, and G. Yushin, *Mater. Today*, **18**, 252 (2015).

[9] A. Manthiram, *J. Phys.Chem. Lett*., **2,** 176 (2011).

[10] C. S. Yoon, M. J. Choi, D. W. Jun, Q. Zhang, P. Kaghazchi, K. H. Kim, and Y. K. Sun,*Chem. Mater*., **30**, 1808 (2018).

[11] K. M. Shaju, G. V. Subba, and B. V. R. Chowdari, *Electrochimica Acta*, **48**, 145 (2002).

[12] C. Li, H. P. Zhang, L. J. Fu, H. Liu, Y. P. Wu, E. Rahm, R. Holze, and H. Q. Wu, *Electrochimica Acta*, **51**, 3872 (2006).

[13] A. Kraytsberg, and Y. Ein-Eli, *Adv. Energy Mater*., **2**, 922 (2012).

[14] T. Ohzuku, A. Ueda, and M. Nagayama, *J. Electrochem. Soc*., **140**, 7, 1862 (1993).

[15] H. Arai, S. Okada, H. Ohtsuka, M. Ichimura, J. Yamaki, *Solid State Ionics* **80**, 261 (1995).

[16] W. Li, J. N. Reimers and J. R. DahnSolid, *State Ionics* **67**, 123 (1993).

[17] H. Y. Li, N. Zhang, J. Li, and J. R. Dahn, *J. Electrochem. Soc*., **165**, A2985 (2018).

[18] R. Amin, D. B. Ravansbæk, and Y. Chiang, *J. Electrochem. Soc*., **162**, A1163 (2015).

[19] H. B. Xie, K. Du, G. R. Hu, J. G. Duan, Z. D. Peng, Z. J. Zhang, and Y. B. Cao, *J. Mater. Chem. A*, **3**, 20236 (2015).

[20] R. Robert, C. Bunzli, E. J. Berg, and P. Novak, *Chem. Mater*., **27**, 526 (2015).

[21] M. Jo, M. Noh, P. Oh, Y. Kim, and J. Cho, *Adv. Energy Mater*., **4**, 1301583 (2014)

[22] Y. Makimura, T. Sasaki, T. Nonaka, Y. F. Nishimura, T. Uyama, C. Okuda, Y. Itou, and Y. Takeuchi, *J. Mater. Chem. A*, **4**, 8350 (2016).

[23] W. S. Yoon, K. Y. Chung, J. McBreen, and X. Q. Yang, *Electrochem. Commun*., **8**, 1257 (2006).

[24] Y. L. Lin, M. Q. Xu, Y. Y. Tian, W. Z. Fan, L. Y, and W. S. Li, *Mater. Chem. Phys*., **211**, 200 (2018).

[25] R. Robert and P. Novak, *J. Electrochem. Soc*., **162**, A1823 (2015).

[26] A. Rougier, I, Saadoune, P. Gravereau, P. Willmann, and C. Delams, *Solid State Ionics*, **90**, 83 (1996).

[27] J. M. Tarascon, G. Vaughan, Y. Chabre, L. Seguin, M. Anne, P. Strobel, and G. Amatucci, *J. Solie State Chem*., **147**, 410 (1999).

[28] E. Mccalla, and J. R. Dahn, *Solid State Ionics*, **242**, 1 (2013).

[29] T. Ohzuku, A. Ueda, and M. Kouguchi, *J. Electrochem. Soc*., **142**, 4033 (1995).

[30] L. Croguennec, Y. Shao-Horn, A. Gloter, C. Colliex, M. Guilmard, F. Fauth, and C. Delmas, *Chem. Mater*., **21**, 1051 (2009).

[31] T. Ohzuku, and Y. Makimura, *Chem. Lett*., **30**, 642 (2001).

[32] S. Gao, Y. Cheng, and M. Shirpour, *ACS. Appl. Mater. Interfaces*, **11**, 982 (2019).

[33] N. Voronina, Y. K. Sun, and S. T. Myung, *ACS. Energy Lett*., **5**, 1814 (2020).

[34] J. Xu, F. Lin, M. Doeff, and W. Tong, *J. Mater. Chem. A*, **5**, 874 (2017).

[35] S. Myung, A. Ogata, K. Lee, S. Komaba, Y. Sun, and H. Yashiro, *J. Electrochem. Soc*., **155**, A374 (2008).

[36] Y. Zhu, X. Tian, X. Zhou, P. Zhang, N. Angulakshmi, and Y. Zhou, *Electrochimica Acta*, **328**, 135116 (2019).

[37] S. Gao, Y. Cheng, and M. Shirpour, ACS. Appl. *Mater. Interfaces*, **11**, 982 (2019).

[38] C. Yoon, K. Park, U. Kim, K. Kang, H. Ryu, and Y. Sun, *Chem. Mater*., **29**, 10436 (2017).

[39] J. Pender, G. Jha, D. H. Youn, J. M. Ziegler, I. Andoni, E. J. Choi, A. Heller, B. S. Dunn, P. S. Weiss, R. M. Penner, and C. B. Mullins, *ACS Nana*., **14**, 1243 (2020).

[40] F. Wu, N. Liu, L. Chen, N. Li, J. Dong, Y. Lu, G. Tan, M. Xu, D. Cao, Y. Liu, Y. Chen, and Y. Su, *J. Energy Chem*., **62**, 351 (2021).

[41] Y. You, H. Celio, J. Li, A. Dolocan, and A. Manthiram, *Angew. Chem. Int. Ed*., **57**, 6480 (2018).

[42] F. Schipper, H. Bouzaglo, M. Dixit, E. M. Erickson, T. Weigel, M. Talianker, J. Grinblat, L. Burstein, M. Schmidt, J. Lampert, C. Erk, B. Markovsky, D. T. Major, and D. Aurbach, Angew. *Adv. Energy Mater*., **8**, 1701682 (2018).

[43] G. Qian, Y. Zhang, L. Li, R. Zhang, J. Xu, Z. Cheng, S. Xie, H. Wang, Q. Rao, Y. He, Y. Shen, L. Chen, M. Tang, and Z. Ma, *Energy Storage Mater*., **27**, 140 (2020).

[44] H. Li, J. Li, X. Ma, and J. R. Dahn, *J. Electrochem. Soc*., **165**, A1038 (2018).

[45] Y. Sun, S. Myung, M. Kim, J. Prakash, and K. Amine, *J. Am. Chem. Soc*., **127**, 13411 (2005).

[46] Y. Sun, D. Kim, H. Jung, S. Myung, and K. Amine, *Electrochimica Acta*, **55**, 8621 (2010).

[47] W. Xu, J. Wang, F. Ding, X. Chen, E. Nasybulin, Y. Zhang, and J. Zhang, *Energy Environ. Sci*., **7**, 513 (2014).

[48] X. Cheng, R. Zhang, C. Zhao, and Q. Zhang, *Chem. Rev*., **117**, 10403 (2017).

[49] W. Zhang, *J. Power Sources*, **196**, 13 (2011).

[50] Q. Wang, B. Mao, S. I. Stoliarov, and J. Sun, *Progress in Energy and Combustion Science,* **73**, 95 (2019).

[51] S. Park, M. Oda, and T. Yao, *Solid State Ionics*, **203**, 29 (2011).

[52] S. Park, S. Ito, K. Takasu and T. Yao, *Electrochemistry*, **80**, 804 (2012).

[53] S. Park, K. Kameyama, and T. Yao, *Electrochemical and Solid-State Letters*, **15,** A49 (2012).

[54] I. S. Seo, S. Park, and T. Yao, *ECS Electrochem. Lett.*, **2**, A6 (2013).

[55] S. Takai, T. Tawa, M. Takemoto, J. Kang, T. Yabutsuka, and T. Yao, *J. Ceramic Soc. Japan*. **129**, 744 (2021)

[56] Y. Satou, S. Komine, S. Park, and T. Yao, *Solid State Ionics*, **262**, 35 (2014).

[57] Y. Satou, S. Komine, S. Takai, and T. Yao, J. Electrochem. Soc., **161**, A1759 (2014).

[58] Y. Satou, S. Komine, S. Takai, and T. Yao, *ECS Electrochem. Lett*., **4**, A37 (2015).

[59] I. Seo, S. Nagashima, S. Takai, and T. Yao, *ECS Electrochem. Lett.*, **2**, A72 (2013).

[60] T. Kitamura, S. Takai, T. Yabutsuka, and T.Yao, *J. Physice and Chemistry of Solids.,* **142**, 109440 (2020).

[61] S. Takai, T. Kitamura, T. Yabutsuka, and T. Yao, *Electrochem.,* **88**, 434 (2020).

[62] T. Tamura, S. Takai, T. Yabutsuka, and T. Yao, *J. Electrochem. Soc*., **164**, A1514 (2017).

Chapter 2 Structural Relaxation of $Li_xNi_{0.874}Co_{0.090}Al_{0.036}O_2$ after lithium extraction up to high voltage region ($0.06 \leq x \leq 0.12$) at 0.01 C

2.1 Introduction

$LiNiO_2$ is one of the promising cathode materials for batteries used in electric vehicles due to its high capacity and low cost.[1,2] It has been known that $LiNiO_2$ undergo phase changes in the following order when lithium is extracted: hexagonal (H1), monoclinic (M), hexagonal (H2), hexagonal (H3).[3] Such a change in crystal structure can cause degradation of the electrode material. In particular, a two-phase coexistence (H2 + H3 phases) region exists when charged to a high potential region, and the large difference in *c*-axis between the H2 and H3 phases restrict the reversible electrode reaction resulting in the degradation of cycle performance.[4] $LiNi_{1-a-b}Co_aAl_bO_2$ (NCA) (Co and Al co-doped) are currently being used in electric vehicles due to the good cycle performance and high temperature stability, but it is also known that a two-phase coexistence region still occurs when lithium extracted from NCA up to a high potential region.[5,6] To use the batteries with the capacity beyond 200 $mAh \cdot g^{-1}$, it is necessary to investigate the charge-discharge process and structural stability in this higher voltage region. In addition, difference in structure between charging / discharging and equilibrium states would be of importance for the battery performance to follow the phase transition. Our group have investigated the transient from kinetically favorable toward equilibrium structure by relaxation time dependent XRD analysis.

In recent years, our group have investigated the structural change in electrode materials after the termination of lithium insertion or extraction by using X-ray diffraction accompanied by the Rietveld analysis. During the lithium insertion or extraction, electrode materials possess the kinetically preferred structure, which is sometimes

different from the thermodynamically stable structure. Yao *et al*. named this technique as "Relaxation analysis" and applied to various cathode or anode materials.

In the previous study, Tamura *et al*. investigated the relaxation analyses on Li_xNiO_2 and $Li_xNi_{0.933}Co_{0.031}Al_{0.036}O_2$ (Co-3.1 NCA) after lithium extraction up to high potential region (x = 0.12, 0.09 and 0.06). It was found that the appearance of the H3 phase could be suppressed by substitution a small amount of Co.[7] In order to further investigate the effect of increasing Co substitution, in the chapter 2, I have carried out the relaxation analysis on $LiNi_{0.874}Co_{0.090}Al_{0.036}O_2$ (Co-9.0 NCA) with increased Co substitution to compare with the previous study on $LiNiO_2$ and Co-3.1 NCA.

2.2 Experiment

2.2.1 Electrochemical lithium extraction

I used the $LiNi_{0.874}Co_{0.090}Al_{0.036}O_2$ (Co-9.0 NCA) with the typical particle size of 5.7 μm (Sumitomo Metal Mining Co., Ltd.) as a cathode material. Mixing the active materials (Co-9.0 NCA) with Acetylene Black (AB) and PVdF power with the ratio of 80:10:10 in weight and spreading on Al foil with a small amount of NMP, the test electrode was prepared. Lithium metal was used for counter electrode and the electrolyte employed was 1 $mol \cdot dm^{-3}$ $LiPF_6$ in a mixture of ethylene carbonate (EC) and dimethyl carbonate (DMC) solution (2:1 v / v, Kishida chemical Co., Ltd). A two-electrode type metal cell (Figure 2.1, Hohsen Co.,) was assembled in an Ar-filled glove box. I have extracted lithium ion from the sample at a constant current of 0.01 C up to x = 0.12, 0.09 and 0.06 of $Li_xNi_{0.874}Co_{0.090}Al_{0.036}O_2$ at 25 °C. After the termination of lithium extraction, I immediately took the working electrode out of the cell in Ar-filled glove box to avoid the local cell reaction between the electrode material and the current via the electrolyte. Thereafter I washed the working electrode in DMC (Kishida Chemical Co., Ltd.) and then dried in Ar atmosphere.

2.2.2 X-ray diffraction measurement

The working electrode was set in a sealed holder (Rigaku Co., Ltd.,) with beryllium window in an Ar-filled glove box, which was then mounted on an X-ray diffractometer (Ultima-IV, Rigaku Co., Ltd.) for XRD measurement. The XRD measurement conditions was shown in Table 2.1. The diffracted X-ray was measured for 2θ values from 15 ° to 75 ° at a rate of 2 ° min^{-1} with 0.04 ° step width by using CuKα radiation. The X-ray tube voltage and current were set to 40 kV and 40 mA, respectively.

I analyzed the XRD profiles by the Rietveld method using RIEVEC code. The Rietveld analysis has been carried out assuming co-existence of two phases (H2 + H3 phases), both of which belong to $R\bar{3}m$ symmetry. Nickel (cobalt and aluminum) ions were placed at the 3*b* site and oxide ion at the 6*c* site in hexagonal axis, and the contribution of lithium has been ignored. The mole fractions of H2 and H3 phase were calculated from the scale factors and equation 2.1.

$$M_p = \frac{S_p (ZV)_p}{\sum_{i=1}^{n} S_i (ZV)_i} \qquad \text{(Equation 2.1)}$$

M: mole fraction

S: scale factor

Z: number of formulae in unit cell

V: cell volume

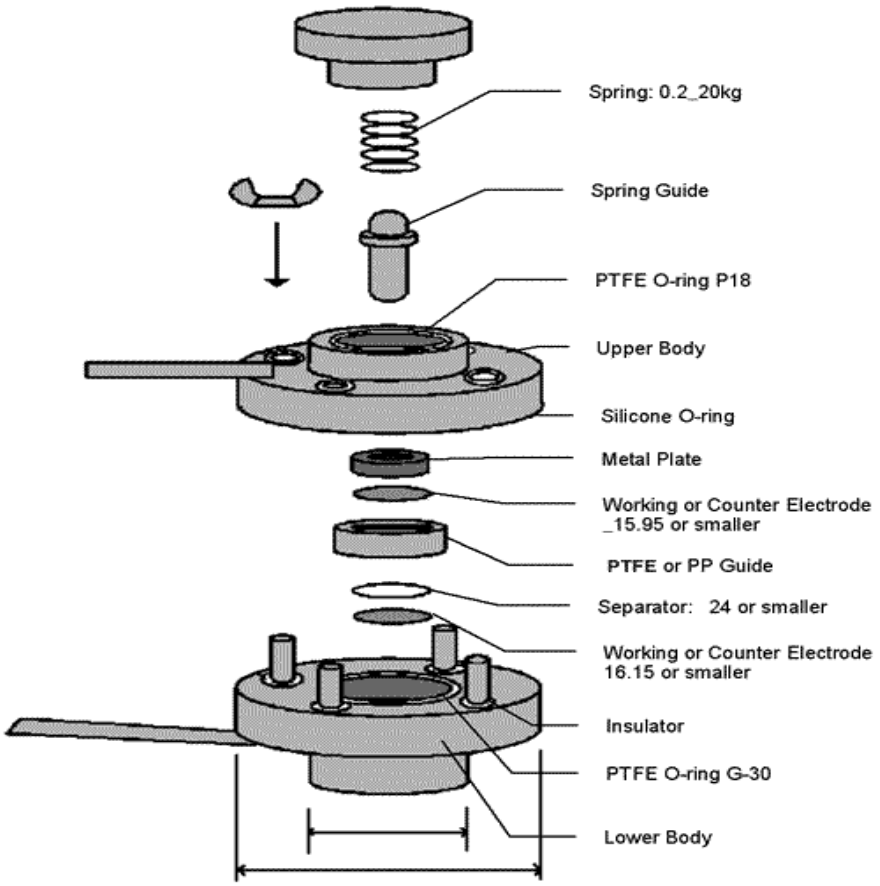

Figure 2.1 Schematic diagram of two electrode type metal cell.

Table 2.1 XRD measurement conditions.

X-ray diffractometer	Ultima IV (RIGAKU)
Source radiation	CuKα
Tube voltage / current	40 kV / 40 mA
method	$2\theta / \theta$
step width	0.04 °
speed	2 ° / min
Angle range	15 ° ≦ 2θ ≦ 75 °

2.3 Results and Discussion

Lithium ions were electrochemically extracted from Co-9.0 NCA to achieve the amount of lithium as x = 0.12, 0.09 and 0.06 for $Li_xNi_{0.874}Co_{0.090}Al_{0.036}O_2$ at a constant current rate of 0.01 C. The charge curve of Co-9.0 NCA appears to show a little gradient at the higher potential region as given in Figure 2.2, which is distinct from $LiNiO_2$ without cobalt doping in terms of potential plateau. Figures 2.3, 2.5 and 2.7 show the X-ray diffraction patterns for x = 0.12, 0.09 and 0.06 of Co-9.0 NCA at various relaxation times after the termination of lithium extraction, respectively. The 003 peaks for x = 0.12, 0.09 and 0.06 of Co-9.0 NAC are shown in Figures 2.4, 2.6 and 2.8. For x = 0.12, the 003 peaks shifts toward higher 2θ direction with relaxation time, while it does toward lower 2θ for x = 0.06 and peaks shift seems not occur for x = 0.09. The measured and the Rietveld fitted diffraction profiles of x = 0.12, 0.09 and 0.06 with 0 hour and 100 hours of relaxation are exemplified in Figures 2.9, 2.10 and 2.11, showing fairly good agreement to the yield with a sufficiently low R_{wp} value. I examined the refinements assuming two types of models: the two-phase coexistence (H2 and H3 phases), and single H2 phase model. The value of R_{wp} at 0 hour and 100 hours after the end of charging for single H2 phase model and the two-phase coexistence model obtained from the Rietveld analysis are shown in Table 2.2. It can be known that the lower R_{wp} value was achieved assuming single H2 phase only for x = 0.12. On the other hand, two phases model provided lower R_{wp} value for x = 0.09 and 0.06. Therefore, I think that single H2 phase is remained after the lithium extraction up to x = 0.12, and H3 phase appears at x = 0.09 and 0.06. The selected structural parameters of x = 0.12, 0.09 and 0.06 after refinements are listed in Tables 2.3, 2.4 and 2.5, respectively for the 0 hour and 100 hours of relaxed data.

Figures 2.12 and 2.13 represent the relaxation time dependence of a-lattice and c-lattice

parameters for H2 and H3 phases of Co-9.0 NCA, respectively. For all the composition of lithium ions, the variation of *a*-length is rather small in the present range of *x*, while the *c*-length varies with the lithium content *x*. Assuming that *c*-length is essentially attributed by the lithium concentration, lithium amount of H2 phase for $x = 0.12$ is a little smaller than that for $x = 0.09$, which might be due to the formation of H3 phase with smaller lithium concentration for $x = 0.09$. Nevertheless, H2 phase of $x = 0.06$ possesses smaller *c*-length as compared with those for $x = 0.12$ or 0.09. As for H3 phase, highly lithium extracted sample ($x = 0.06$) shows the smaller *c*-axis. Comparing with the previous study of $LiNiO_2$ and Co-3.1 NCA, *c*-axis in the small lithium region is relatively what for Co-9.0 NCA, which would help the lithium diffusion in the lithium layer, resulting in the smaller relaxation time.

Figure 2.14 shows the mole fraction of H3 phase including previous study $LiNiO_2$ and Co-3.1 NCA, and the present study Co-9.0 NCA. In Co-9.0 NCA, even for $x = 0.06$, H2 phase is still predominant and the molar ratio of H2 phase slightly increases with the relaxation time up to 100 hours. This indicates that small amount of H3 phase turns into H2 during the relaxation. Phase change from H3 to H2 during the relaxation is very small in the present system (Co-9.0 NCA) as almost constant mole fraction. Namely larger amount of Co substitution into $LiNiO_2$ enable the rapid phase change presumably due to the larger *c*-length in H3 phase, allowing the phase ratio of H2 / H3 nearly equilibrium during charging. This also improves the cycle performance in higher potential region.

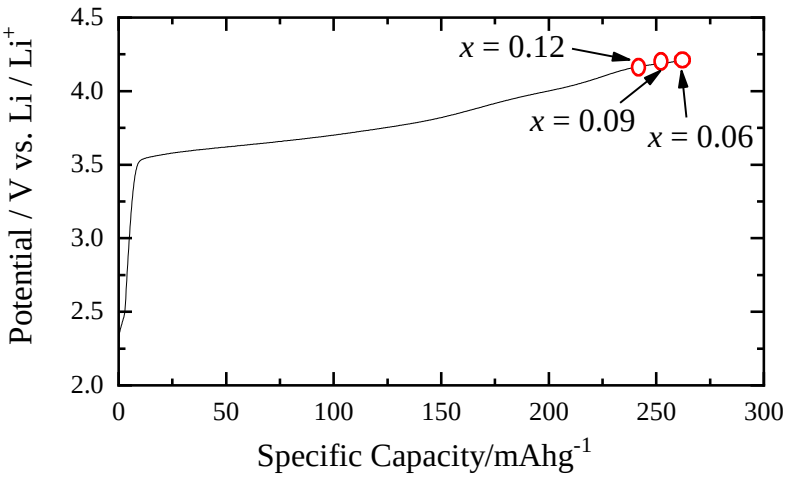

Figure 2.2 Charge curve of $Li_xNi_{0.874}Co_{0.090}Al_{0.036}O_2$ after lithium extraction up to x = 0.12, 0.09 and 0.06.

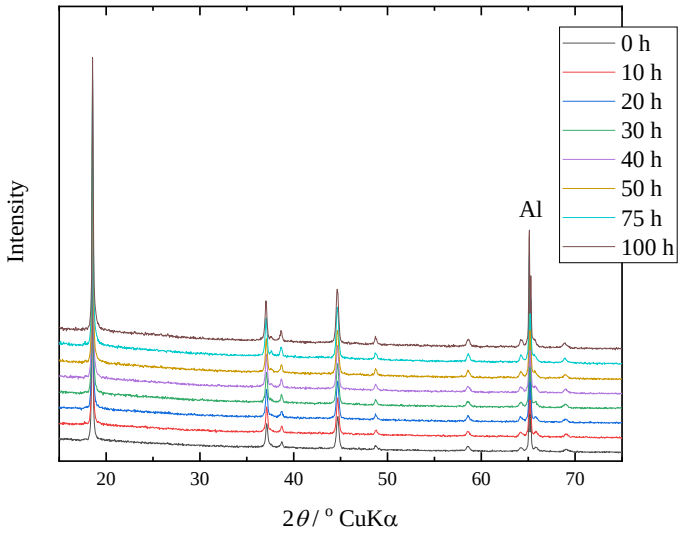

Figure 2.3 XRD pattern of $Li_{0.12}Ni_{0.874}Co_{0.090}Al_{0.036}O_2$.

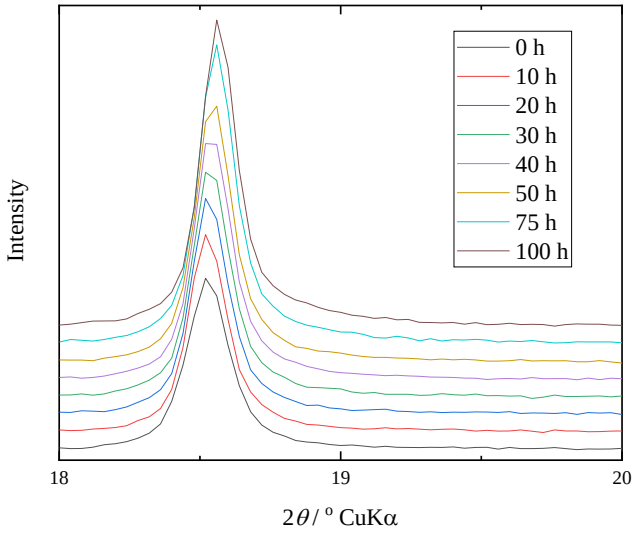

Figure 2.4 003 peaks of $Li_{0.12}Ni_{0.874}Co_{0.090}Al_{0.036}O_2$ ($2\theta = 18° \sim 20°$).

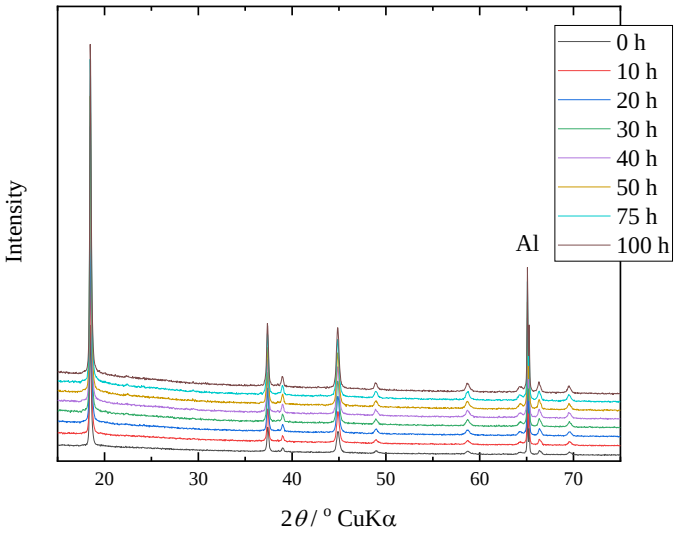

Figure 2.5 XRD patterns of $Li_{0.09}Ni_{0.874}Co_{0.090}Al_{0.036}O_2$.

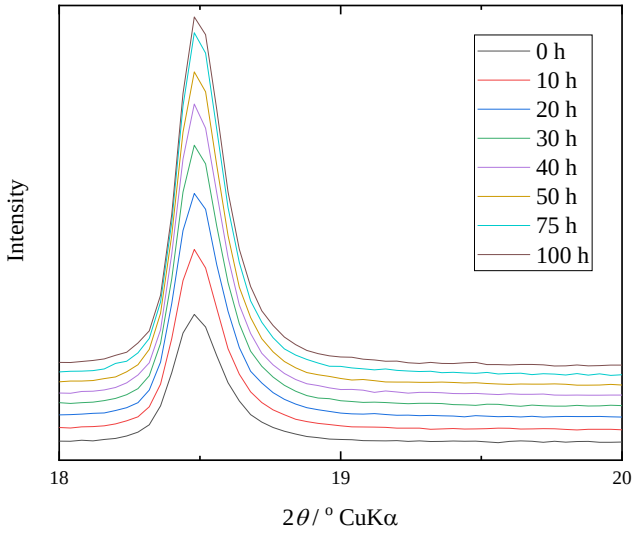

Figure 2.6 003 peaks of $Li_{0.09}Ni_{0.874}Co_{0.090}Al_{0.036}O_2$ ($2\theta = 18° \sim 20°$).

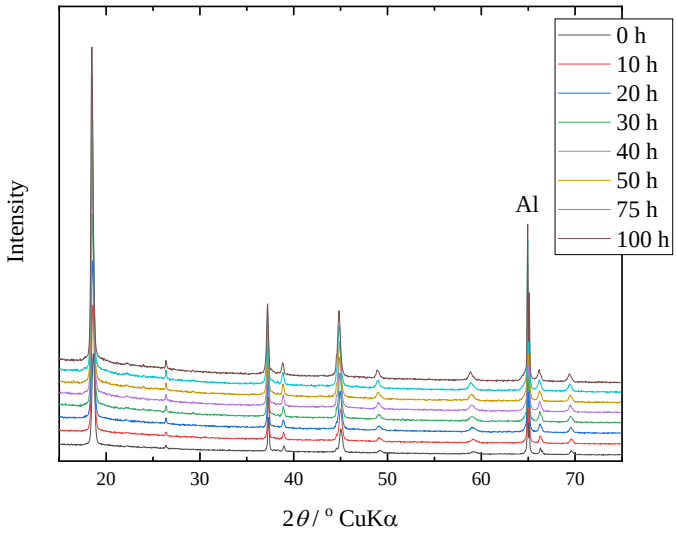

Figure 2.7 XRD patterns of $Li_{0.06}Ni_{0.874}Co_{0.090}Al_{0.036}O_2$.

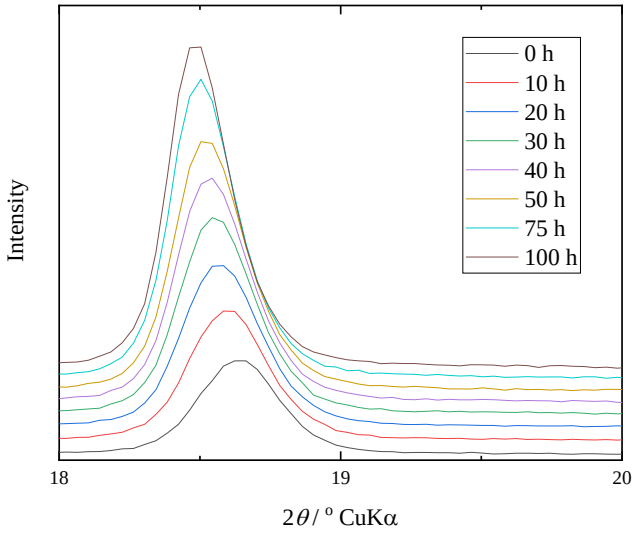

Figure 2.8 003 peaks of $Li_{0.06}Ni_{0.874}Co_{0.090}Al_{0.036}O_2$ ($2\theta = 18° \sim 20°$).

Table 2.2 Summary of R_{wp} for single phase and two-phase coexistence (H2+H3 phase) for each sample ($Li_xNi_{0.874}Co_{0.090}Al_{0.036}O_2$).

x		0.12		0.09		0.06	
Relaxation time / h		0	100	0	100	0	100
R_{wp}	Single phase	3.703	3.495	3.822	3.337	5.689	8.425
	H2 + H3 phase	4.228	4.032	3.550	2.708	5.223	2.981

Table 2.3 Refined structure parameters of $Li_{0.12}Ni_{0.874}Co_{0.090}Al_{0.036}O_2$ for initial state and after 100 h of relaxation.

			0 h	100 h
H2 phase	Lattice constant	a (Å)	2.8345(1)	2.8427(1)
		c (Å)	14.3738(2)	14.3621(4)
	z		0.235(1)	0.236(4)
Confidence factor		R_F (%)	2.68	4.459
		R_B (%)	3.012	5.004
Overall confidence factor		R_{wp} (%)	3.703	3.495
		GOF	1.206	1.448

Table 2.4 Refined structure parameters of $Li_{0.09}Ni_{0.874}Co_{0.090}Al_{0.036}O_2$ for initial state and after 100 h of relaxation.

			0 h	100 h
H2 phase	Lattice constant	*a* (Å)	2.8172 (1)	2.8204(5)
		c (Å)	14.4315(1)	14.4300(0)
		z	0.232(1)	0.227(1)
	Mole fraction		0.82(9)	0.86(6)
	Confidence factor	R_F (%)	2.282	2.103
		R_B (%)	2.185	1.504
H3 phase	Lattice constant	*a* (Å)	2.8136(1)	2.8180(4)
		c (Å)	14.3312(1)	13.3115(1)
		z	0.256(2)	0.246(3)
	Mole fraction		0.17(1)	0.13(4)
	Confidence factor	R_F (%)	3.944	2.933
		R_B (%)	5.750	3.610
Overall confidence factor		R_{wp} (%)	3.550	2.708
		GOF	1.321	1.537

Table 2.5 Refined structure parameters of $Li_{0.06}Ni_{0.874}Co_{0.090}Al_{0.036}O_2$ for initial state and after 100 h of relaxation.

			0 h	100 h
H2 phase	Lattice constant	a (Å)	2.8234(1)	2.8268(4)
		c (Å)	14.2609(1)	14.3261(3)
	Mole fraction		0.79(3)	0.86(2)
	z		0.230(4)	0.235(2)
	Confidence factor	R_F (%)	6.097	1.622
		R_B (%)	3.794	1.157
H3 phase	Lattice constant	a (Å)	2.8253(2)	2.8255(3)
		c (Å)	14.1475(1)	14.2098(1)
	z		0.242(1)	0.219(5)
	Mole fraction		0.20(7)	0.13(8)
	Confidence factor	R_F (%)	4.350	2.781
		R_B (%)	6.855	3.207
Overall confidence factor		R_{wp} (%)	5.223	2.981
		GOF	1.831	1.609

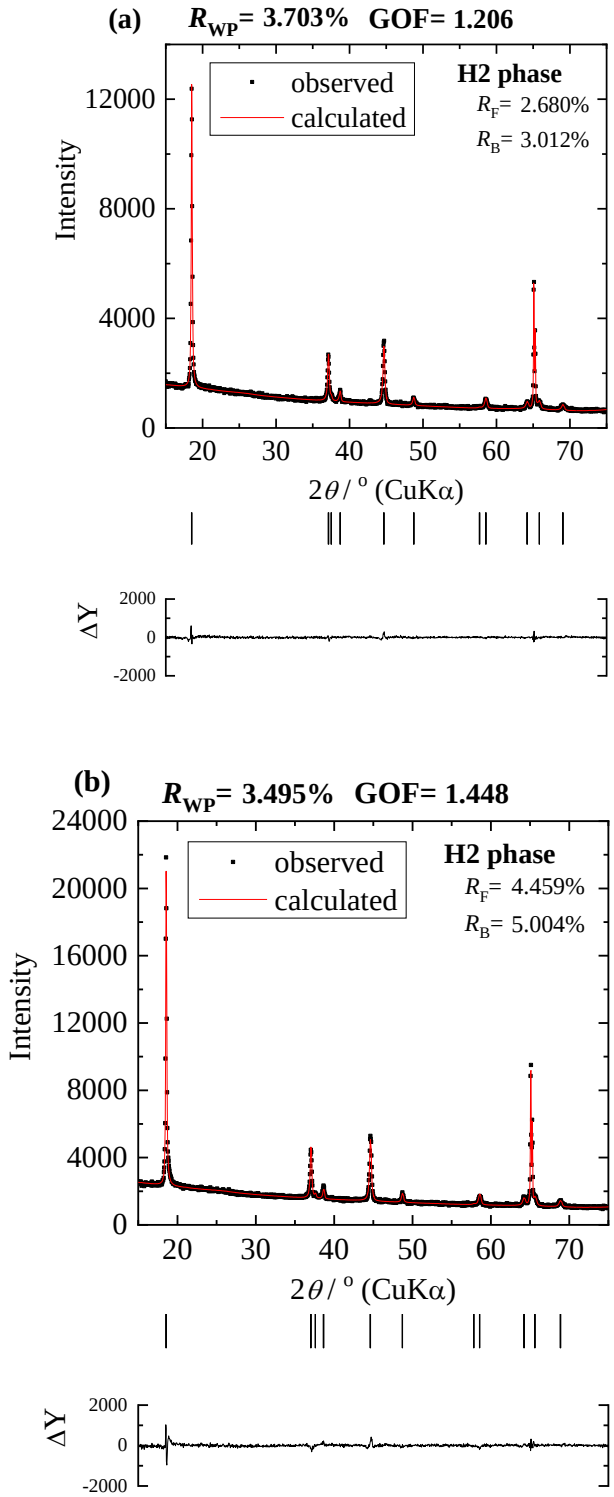

Figure 2.9 Observed and Rietveld fitted diffraction pattern of $Li_xNi_{0.874}Co_{0.090}Al_{0.036}O_2$ (x = 0.12) after (a) 0 h and (b) 100 h of relaxation.

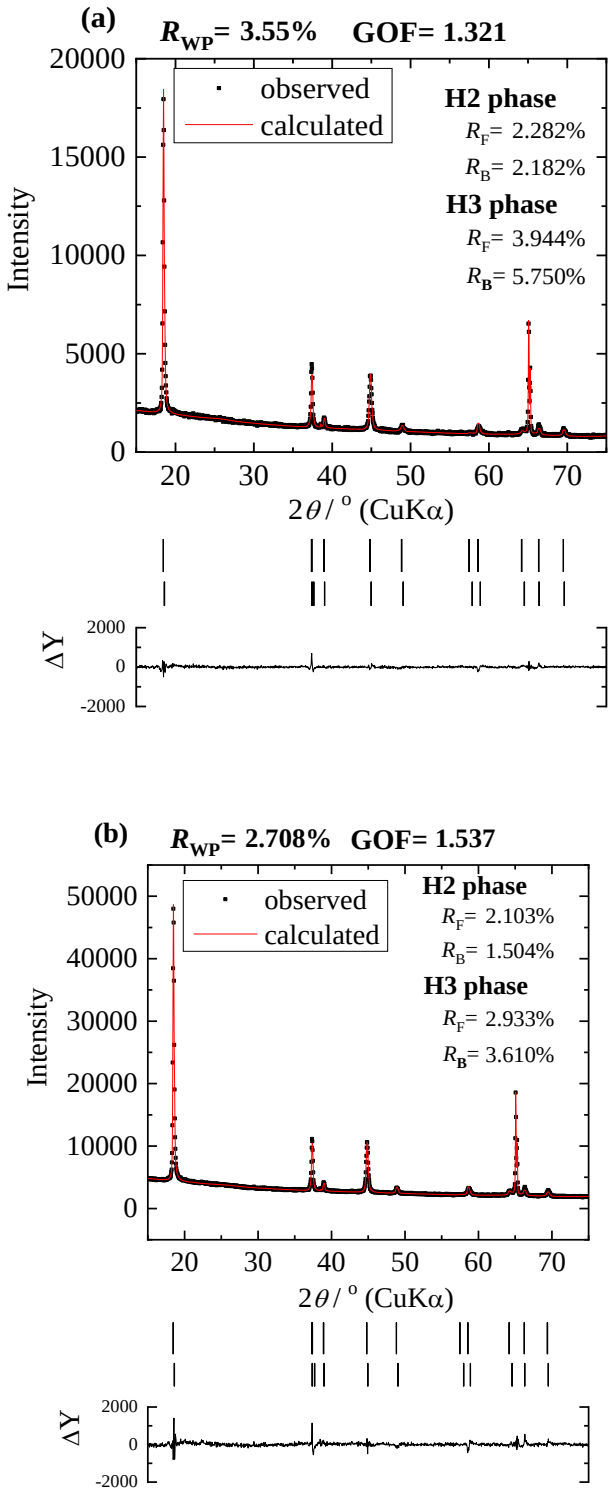

Figure 2.10 Observed and Rietveld fitted diffraction pattern of $Li_xNi_{0.874}Co_{0.090}Al_{0.036}O_2$ (x = 0.09) after (a) 0 h and (b) 100 h of relaxation.

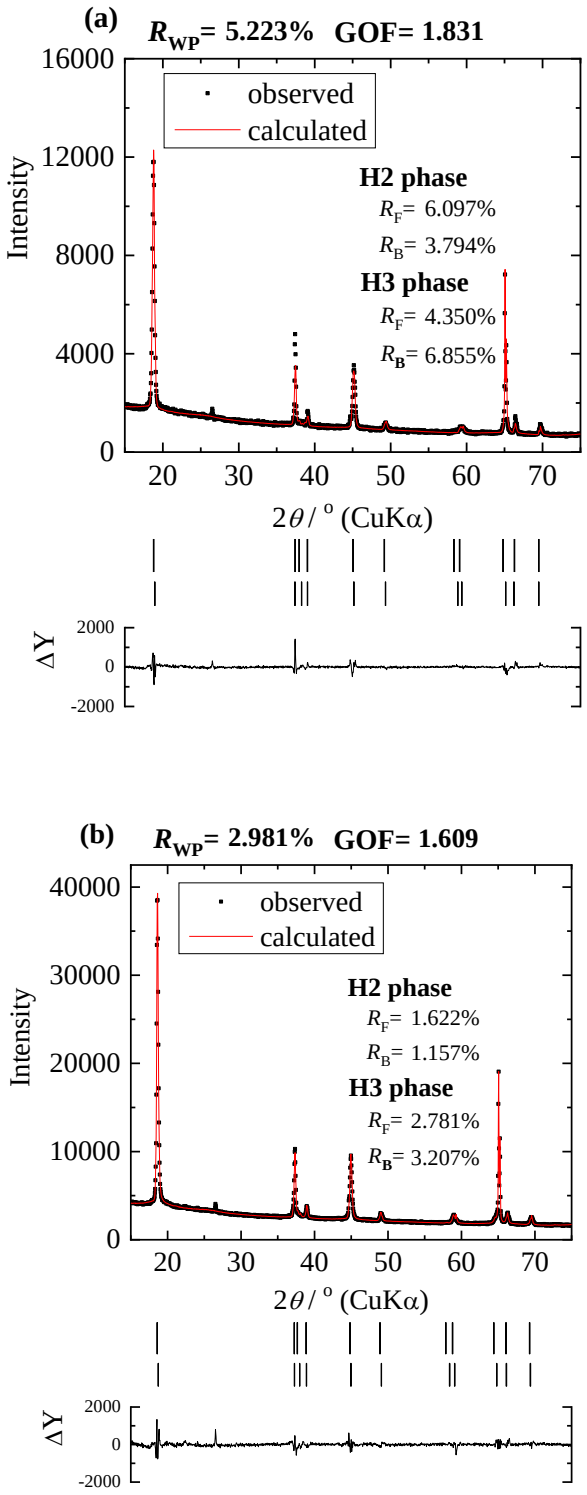

Figure 2.10 Observed and Rietveld fitted diffraction pattern of $Li_xNi_{0.874}Co_{0.090}Al_{0.036}O_2$ (x = 0.06) after (a) 0 h and (b) 100 h of relaxation.

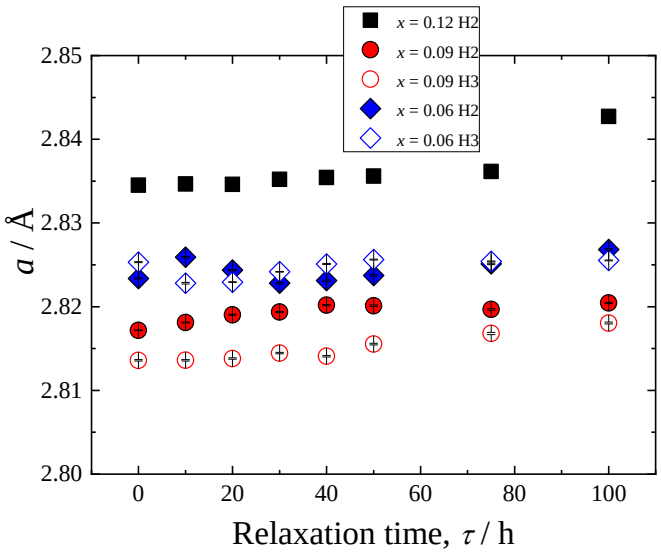

Figure 2.12 Change in lattice parameters of the *a*-axis of $Li_xNi_{0.874}Co_{0.090}Al_{0.036}O_2$ with relaxation time (x = 0.12, 0.09 and 0.06).

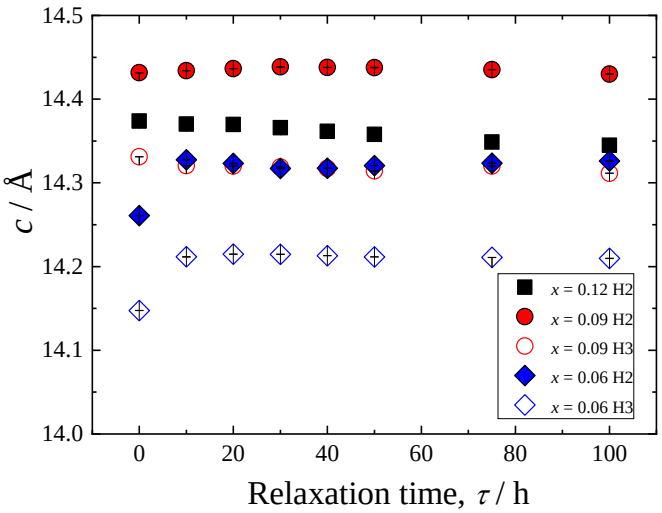

Figure 2.13 Change in lattice parameters of the *c*-axis of $Li_xNi_{0.874}Co_{0.090}Al_{0.036}O_2$ with relaxation time (x = 0.12, 0.09 and 0.06).

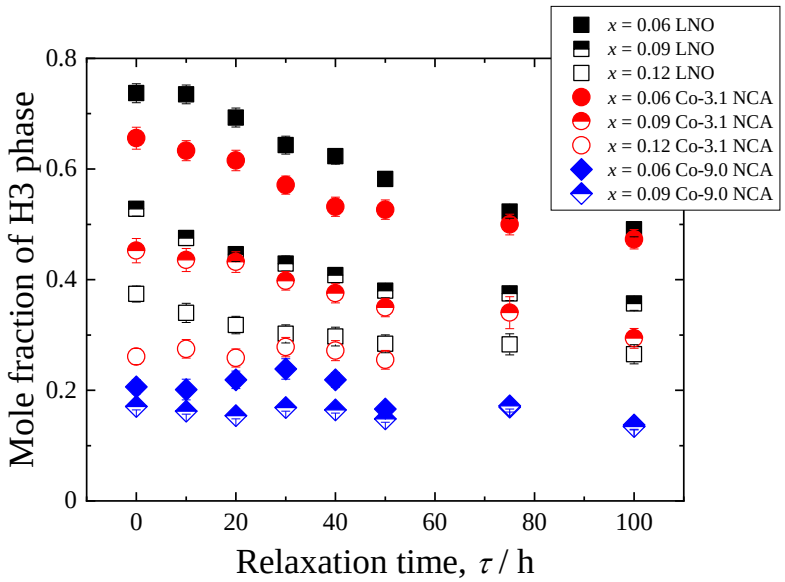

Figure 2.14 Calculated mole fraction changes of H3 phase for Li_xNiO_2 (LNO), $Li_xNi_{0.933}Co_{0.031}Al_{0.036}O_2$ (Co-3.1 NCA) and $Li_xNi_{0.874}Co_{0.090}Al_{0.036}O_2$ (Co-9.0 NCA) (x = 0.12, 0.06 and 0.06).

2.4 Conclusion

In chapter 2, I have carried out the relaxation analysis on Co-9.0 NCA to study the structural variability at the deeply lithium extracted region for $0.06 \leq x \leq 0.12$, and compared with the previous study $LiNiO_2$ and Co-3.1 NCA. Single H2 phase is remained after the lithium extraction up to $x = 0.12$, although H3 phase appears after the extraction to $x = 0.09$. Nevertheless, H2 phase is predominant for $x = 0.09$ and 0.06, and even small amount of H3 phase turns into the H2 during relaxation. Comparing with the $LiNiO_2$ and Co-3.1 NCA, it is found that larger amount of Co substitution reduce the mole fraction of H3 phase and allow the phase ratio of H2 / H3 nearly equilibrium during charging to make a better cycle performance.

Reference

[1] C. S. Yoon, M. J. Choi, D. W. Jun, Q. Zhang, P. Kaghazchi, K. H. Kim, and Y. K. Sun, *Chem. Mater*., **30**, 1808 (2018).

[2] E. Flores, N. Vonruti, P. Novak, U. Aschauer, and E. J. Berg, *Chem. Mater*., **30**, 4694 (2018).

[3] T. Ohzuku, A. Ueda, and M. Nagayama, *J. Electrochem. Soc*., **140**, 1862 (1993).

[4] H. Y. Li, N. Zhang, J. Li, and J. R. Dahn, *J. Electrochem. Soc*., **165**, A2985 (2018).

[5] H. B. Xie, K. Du, G. R. Hu, J. G. Duan, Z. D. Peng, Z. J. Zhang, and Y. B. Cao, *J. Mater. Chem. A*, **3**, 20236 (2015).

[6] Y. L. Lin, M. Q. Xu, Y. Y. Tian, W. Z. Fan, L. Y, and W. S. Li, *Mater. Chem. Phys*., **211**, 200 (2018).

[7] T. Tamura, S. Takai, T. Yabutsuka, and T. Yao, *J. Electrochem. Soc*., **164**, A1514 (2017).

Chapter 3 Structural Relaxation of $Li_xNi_{0.815}Co_{0.149}Al_{0.036}O_2$ after lithium extraction up to high voltage region ($0.06 \leq x \leq 0.12$) at 0.01 C

3.1 Introduction

It has been reported that $LiNi_{1-a-b}Co_aAl_bO_2$ (NCA) show a better cycle performance and good temperature stability, which is extensively used in electric vehicles.[1-3] However, the transition of H2-H3 phases still occurs in the high voltage regions as LNO.[4-7] While *a*-axis decreases with lithium extraction in NCA, *c*-axis increase slightly at H2 phase followed by decreasing at H3.[6] In the high voltage region, large differences in the *c*-length between H2 and H3 phases restrict the reversible reactions to degrade the capacity and cycle performance. Sun *et al*. have reported that the Ni-rich cathodes is considered to have the most severe H2-H3 phase transition, leading to the generation of an extensive crack network in the entire secondary particles.[8] Some papers have reported that the magnitude of the H2-H3 transformation increase when the Ni content exceeds 80%, and form a wide crack network along the grain boundaries which provide channels for electrolyte penetration into the particle interior. Consequently, the permeated electrolyte reacts with the exposed reactive Ni^{4+} to form an insulating NiO-like rock-salt layer and other electrolyte oxidation products, accelerating the loss of capacity and the increase of impedance.[8,9]

It is important to investigate the mechanism of the phase transformation in the high potential regions to use the LIBs with a capacity of more than 200 $mAh \cdot g^{-1}$. As well as the phase transition phenomena, structural difference between the kinetic and equilibrium states should be argued for the degeneration process of electrode. Our group have thus focused on the transient state from kinetically favorable toward equilibrium structures during relaxation time, and investigated the structural variation by using X-ray diffraction

accompanied by the Rietveld analysis. Our group named this technique as “Relaxation Analysis” and applied to various electrode materials.

In recent years, the structural relaxation analyses were carried out on $LiNi_{0.933}Co_{0.031}Al_{0.036}O_2$ (Co-3.1 NCA)[10] and $LiNi_{0.874}Co_{0.090}Al_{0.036}O_2$ (Co-9.0 NCA).[11,12] It was found that change in *c*-axis becomes small during the relaxation time and the formation of H3 phase is restricted with increasing cobalt content. In the present study, to clarify the contribution of cobalt substitution, we carried out the relaxation analysis on $LiNi_{0.815}Co_{0.149}Al_{0.036}O_2$ (Co-14.9 NCA). The results are compared with the previous Co-3.1 NCA and Co-9.0 NCA.

3.2 Experiment

3.2.1 Electrochemical lithium extraction

Cathode materials of $LiNi_{0.815}Co_{0.149}Al_{0.036}O_2$ (Co-14.9 NCA) have been supplied from Sumitomo Metal Mining Co., Ltd. The working electrode was prepared by mixing the cathode materials (Co-14.9 NCA) with Acetylene Black (AB) and PVdF power with the weight ratio of 80:10:10, and spreading the mixture on Al foil with a small amount of NMP. After drying the working electrode at 60 °C for 4 hours and 120 °C for 24 hours, a two-electrode metal cell (Hohsen Co.) was assembled in an Ar-filled glove box. I employed lithium metal and 1 $mol \cdot dm^{-3}$ $LiPF_6$ in a mixture of ethylene carbonate (EC) and dimethyl carbonate (DMC) solution (2:1 v / v, Kishida chemical Co., Ltd) as a counter electrode and electrolyte, respectively. Lithium ion was extracted from the Co-14.9 NCA at a constant current of 0.01 C to x = 0.12, 0.09 and 0.06 for $Li_xNi_{0.815}Co_{0.149}Al_{0.036}O_2$ at 25 °C. To avoid the local cell reaction between the electrode material and the current collector via the electrolyte, I immediately took the working electrode out of the cell in an Ar-filled glove box after the termination of lithium extraction. The working electrode was then washed in in DMC (Kishida Chemical Co., Ltd.) and then dried in Ar atmosphere.

3.2.2 X-ray diffraction measurement

I set the working electrode in a sealed holder (Rigaku Co., Ltd) with beryllium window in an Ar-filled glove box and installed in an XRD diffractometer (Ultima-IV, Rigaku Corp., Ltd.) for XRD experiments. The XRD measurements were carried out from 15° to 75° in 2θ at rate of 2° min^{-1} with 0.04 step width by using CuKα radiation. The X-ray tube voltage and current were set to 40 kV and 40 mA, respectively.

The XRD data were analyzed by the Rietveld method using RIEVEC code. The Rietveld analysis were made assuming single H2 phase and the two phases (H2 and H3 phases) co-existing, both of which belong to $R\bar{3}m$ symmetry. For the structure refinement, nickel (cobalt and aluminum) and oxide ions were placed at the 3*b* and 6*c* sites, respectively in hexagonal axis, and the contribution of lithium has been ignored.

3.3 Result and Discussion

To achieve the amount of lithium as x = 0.12, 0.09 and 0.06 for $Li_xNi_{0.815}Co_{0.149}Al_{0.036}O_2$ (Co-14.9 NCA), lithium ions were electrochemically extracted from Co-14.9 NCA at a constant current rate of 0.01 C. Figure 3.1 shows the charge curve of Co-14.9 NCA, where in remains a little gradient even at high potential region compared to previous $LiNiO_2$. Figures 3.2, 3.4 and 3.6 show X-ray diffraction patterns for x = 0.12, 0.09 and 0.06 of Co-14.9 NCA at various relaxation time after the termination of lithium extraction, respectively. The 003 peaks for x = 0.12, 0.09 and 0.06 was shown in Figures 3.3, 3.5 and 3.7, respectively. In comparison with x = 0.12 or 0.09, 003 peaks of x = 0.06 appears at higher diffraction angle as observed in the inset, and the amount of peak shift during the relaxation is larger. Figures 3.8, 3.9 and 3.10 exemplified the measured and the Rietveld fitted diffraction profiled of x = 0.12, 0.09 and 0.06 with 0 hour and 100 hours of relaxation, and providing fairly good agreement to yield a sufficiently low R_{wp} value. To compare the phases of the samples, a preliminary refinement was made assuming a single H2 phase model and two-phase coexisting model (H2+H3 phases) to compare the reliability factors. And table 3.1 shows the value of R_{wp} at 0 hour and 100 hours after the end of charging for single H2 phase model and the two-phase coexistence model obtained from the Rietveld analysis. For all the Co-14.9 NCA sample, the H2 single phase model was adopted because the R_{wp} was smaller when refined based on the H2 single phase model. The selected structural parameters after refinements are listed in Tables 3.2, 3.3 and 3.4, respectively for the 0 hour and 100 hours of relaxed data.

The relaxation time dependence of a-lattice and c-lattice parameters for single H2 phase of Co-14.9 NCA are shown in Figures 3.11 and 3.12, respectively. For all the samples, the a-length remains almost constant in the present range of x. On the other hand,

the *c*-length increase within 40 hours after the termination of lithium extraction to saturate up to 100 hours of relaxation, although the data for $x = 0.09$ does not represent such a tendency. Figure 3.13 shows the variation of lithium (d_{Li}) and nickel (d_{Ni}) interlayer distance, respectively with the relaxation time by using the refined oxide ion position. In $x = 0.06$, due to the smaller lithium content as well as higher valence of transition metal ions, and the ionic radius of transition metal ions decreased. As a result, both d_{Li} and d_{Ni} values are smaller than those of $x = 0.09$ or 0.12, which allows the smaller *c*-axis as shown in Figure 3.12. As for the relaxation behavior, lithium migration would enhance the lithium interlayer distance during charging, resulting in the shrinkage of d_{Li} during the relaxation toward the equilibrium values. On the other hand, increase in d_{Ni} at the relaxation time might be due to the contribution of d_{Li} or redistribution of charges in Co and Ni ions. The relaxation behavior of these two interlayer distance would give rise to the variation of *c*-length in Figure 3.12.

Figure 3.14 summarizes the observed phases in our relaxation study including previous data of LNO, Co-3.1 NCA and Co-9.0 NCA. It is clearly seen that cobalt substitution restricts the formation of H3 phase, e.g. H3 phase does not appear even at $x = 0.06$ for Co-14.9 NCA. In addition, cobalt substitution also appears to reduce the change in mole fraction during the relaxation. Figure 3.15 (a) exhibits the mole fraction of H3 phase for $x = 0.06$ of NCAs at 0 hour and 100 hours of relaxation, which is plotted versus cobalt content. For smaller cobalt concentration as LNO or Co-3.1 NCA, mole fraction of H3 phase apparently decrease from the initial one during 100 hours of relaxation, while mole fraction varies small for highly cobalt substituted samples. The difference in mole fraction of H3 phase between 0 hour and 100 hours of relaxation are plotted in Figure 3.15 (b). For all the lithium concentration *x*, the difference in mole fraction ($M_{0h} - M_{100h}$) decrease

with the cobalt content in NCAs, although H3 phase does not appear for Co-14.9 NCA, *i.e.* $M_{0h} - M_{100h}$ retains zero at $a = 14.9$.

Therefore, larger cobalt substitution or smaller nickel content in the Ni-rich NCA would restrict the formation of insulating rock salt layers such as NiO allowing the faster structural change into the equilibrium state during charging to stabilize H2 phase rather than H3. This would result in the improvement of long term cycle performance.

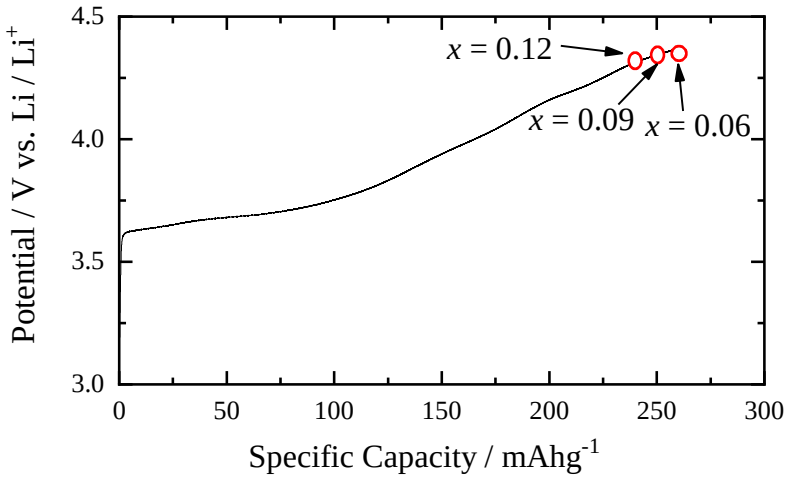

Figure 3.1 Charge curve of $Li_xNi_{0.815}Co_{0.149}Al_{0.036}O_2$ after lithium extraction up to x = 0.12, 0.09 and 0.06.

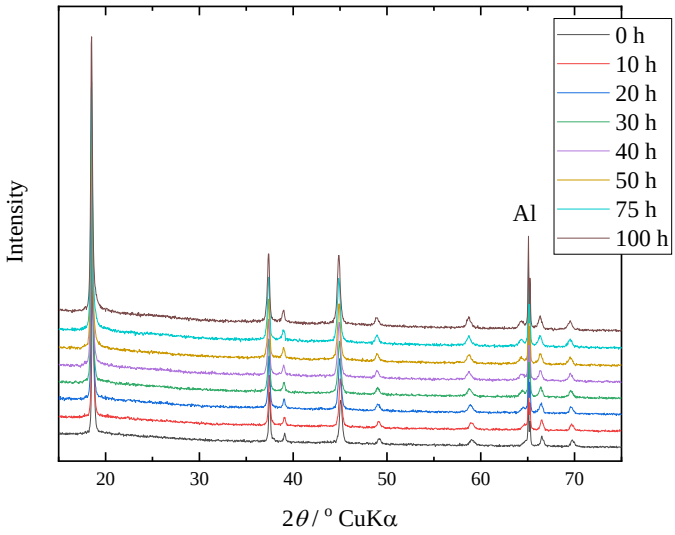

Figure 3.2 XRD parten of $Li_{0.12}Ni_{0.815}Co_{0.149}Al_{0.036}O_2$.

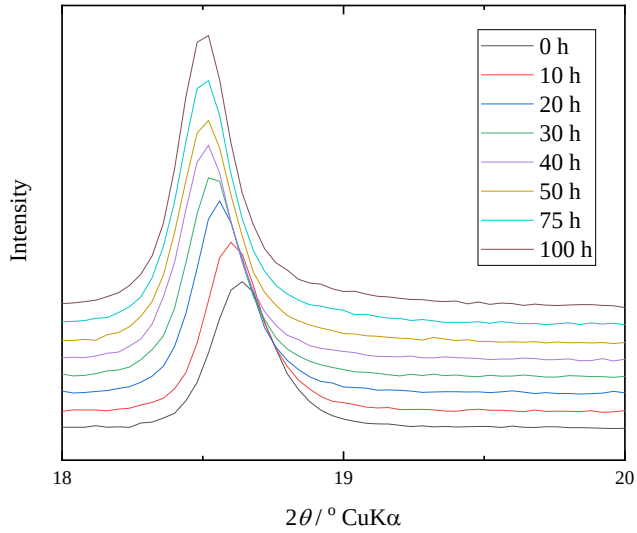

Figure 3.3 003 peaks of $Li_{0.12}Ni_{0.815}Co_{0.149}Al_{0.036}O_2$ ($2\theta = 18° \sim 20°$).

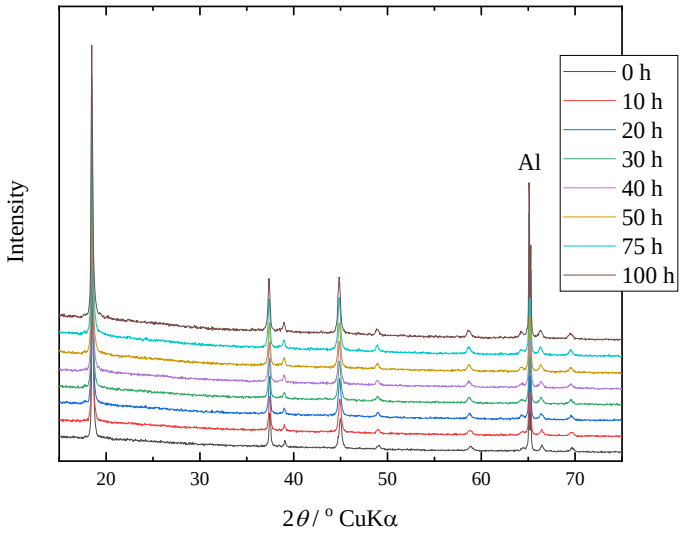

Figure 3.4 XRD parten of $Li_{0.09}Ni_{0.815}Co_{0.149}Al_{0.036}O_2$.

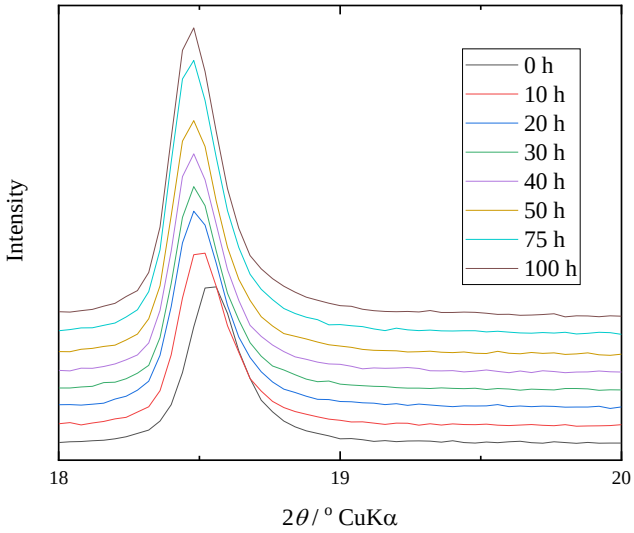

Figure 3.5 003 peaks of $Li_{0.09}Ni_{0.815}Co_{0.149}Al_{0.036}O_2$ ($2\theta = 18° \sim 20°$).

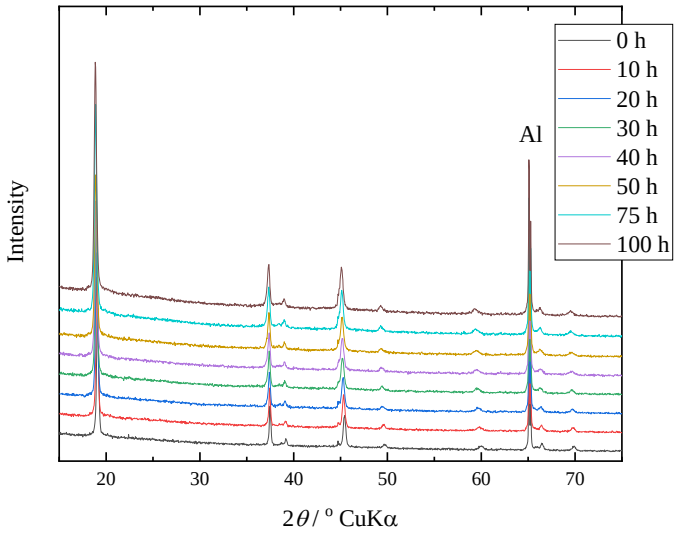

Figure 3.6 XRD parten of $Li_{0.06}Ni_{0.815}Co_{0.149}Al_{0.036}O_2$.

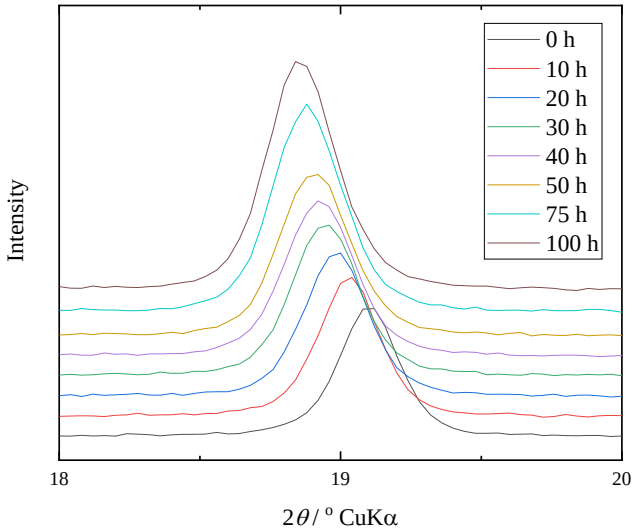

Figure 3.7 003 peaks of $Li_{0.06}Ni_{0.815}Co_{0.149}Al_{0.036}O_2$ ($2\theta = 18° \sim 20°$).

Table 3.1 Summary of R_{wp} for single phase and two phase coexistence for each sample ($Li_xNi_{0.815}Co_{0.149}Al_{0.036}O_2$).

x		0.12		0.09		0.06	
Relaxation time / h		0	100	0	100	0	100
R_{wp}	Single phase	4.320	2.771	4.032	2.887	4.220	3.064
	H2 + H3 phase	4.684	3.583	4.034	3.192	5.014	3.177

Table 3.2 Refined structure parameters of $Li_{0.12}Ni_{0.815}Co_{0.149}Al_{0.036}O_2$ for initial state and after 100 h of relaxation.

			0 h	100 h
H2 phase	Lattice constant	a (Å)	2.8158(3)	2.8198(1)
		c (Å)	14.3145(2)	14.4120(4)
	z		0.238(4)	0.236(4)
Confidence factor		R_F (%)	4.371	3.599
		R_B (%)	4.940	3.809
Overall confidence factor		R_{wp} (%)	4.320	2.771
		GOF	1.608	1.343

Table 3.3 Refined structure parameters of $Li_{0.09}Ni_{0.815}Co_{0.149}Al_{0.036}O_2$ for initial state and after 100 h of relaxation.

			0 h	100 h
H2 phase	Lattice constant	*a* (Å)	2.8137 (2)	2.8144(1)
		c (Å)	14.4063(2)	14.3836(4)
	z		0.231(6)	0.233(1)
Confidence factor		R_F (%)	3.675	2.958
		R_B (%)	3.419	2.734
Overall confidence factor		R_{wp} (%)	4.032	2.887
		GOF	1.309	1.209

Table 3.4 Refined structure parameters of $Li_{0.06}Ni_{0.815}Co_{0.149}Al_{0.036}O_2$ for initial state and after 100 h of relaxation.

			0 h	100 h
H2 phase	Lattice constant	*a* (Å)	2.8117(2)	2.8176(1)
		c (Å)	13.9447(2)	14.0701 (4)
	z		0.235(3)	0.232(5)
Confidence factor		R_F (%)	4.011	2.562
		R_B (%)	3.776	2.044
Overall confidence factor		R_{wp} (%)	4.220	3.064
		GOF	1.307	1.244

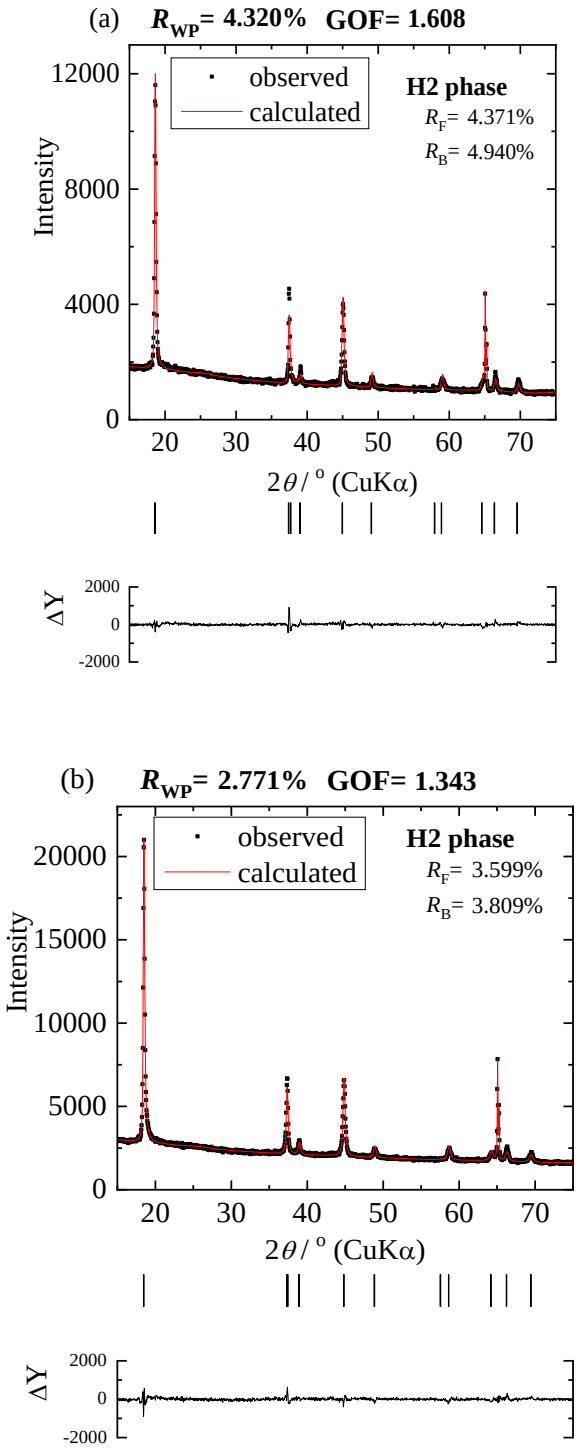

Figure 3.8 Observed and Rietveld fitted diffraction pattern of $Li_xNi_{0.815}Co_{0.149}Al_{0.036}O_2$ (x = 0.12) after (a) 0 h and (b) 100 h of relaxation.

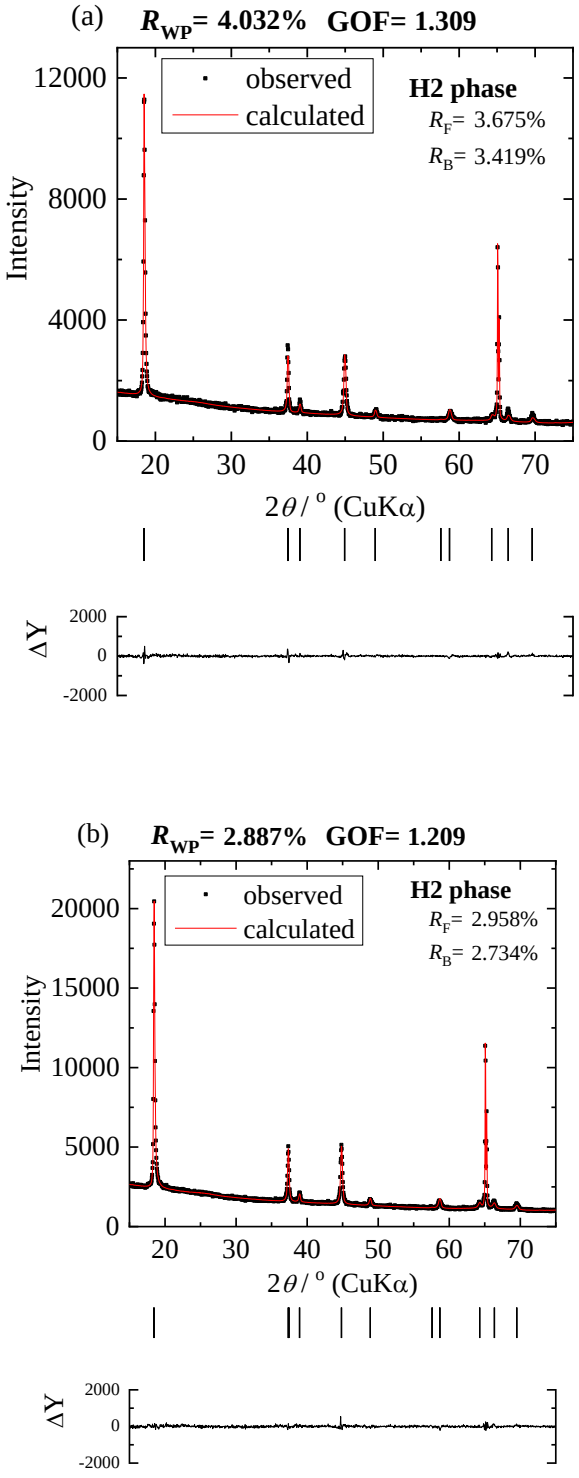

Figure 3.9 Observed and Rietveld fitted diffraction pattern of $Li_xNi_{0.815}Co_{0.149}Al_{0.036}O_2$ (x = 0.09) after (a) 0 h and (b) 100 h of relaxation.

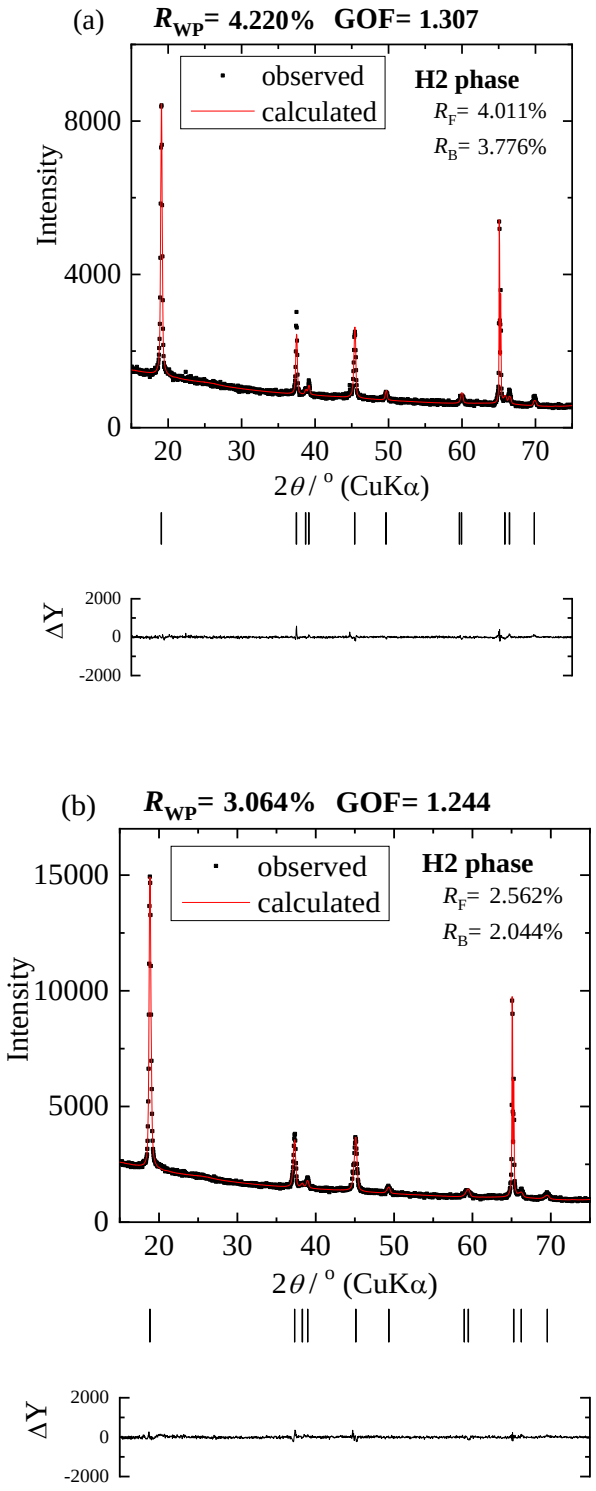

Figure 3.10 Observed and Rietveld fitted diffraction pattern of $Li_xNi_{0.815}Co_{0.149}Al_{0.036}O_2$ (x = 0.06) after (a) 0 h and (b) 100 h of relaxation.

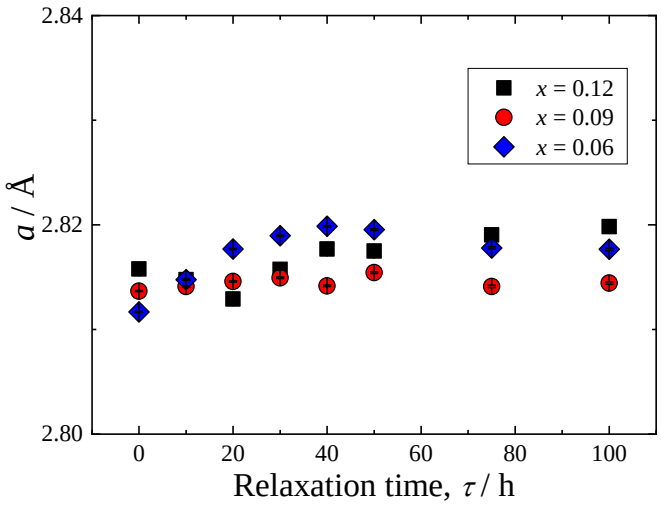

Figure 3.11 Change in lattice parameters of the *a*-axis of $Li_xNi_{0.815}Co_{0.149}Al_{0.036}O_2$ with relaxation time (x = 0.12, 0.09 and 0.06).

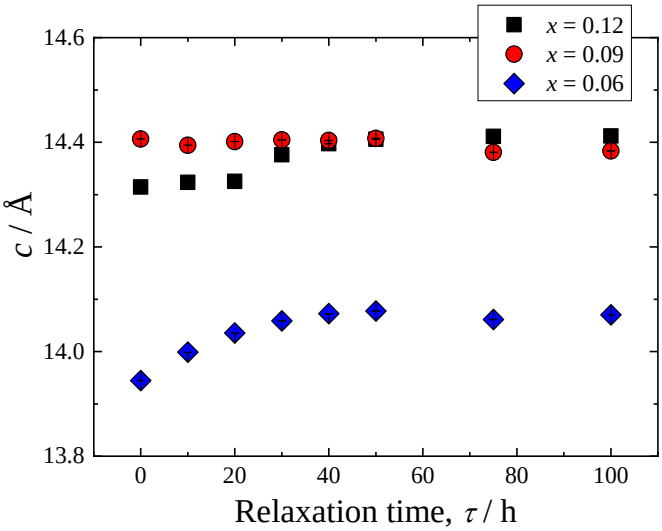

Figure 3.12 Change in lattice parameters of the *c*-axis of $Li_xNi_{0.815}Co_{0.149}Al_{0.036}O_2$ with relaxation time (x = 0.12, 0.09 and 0.06).

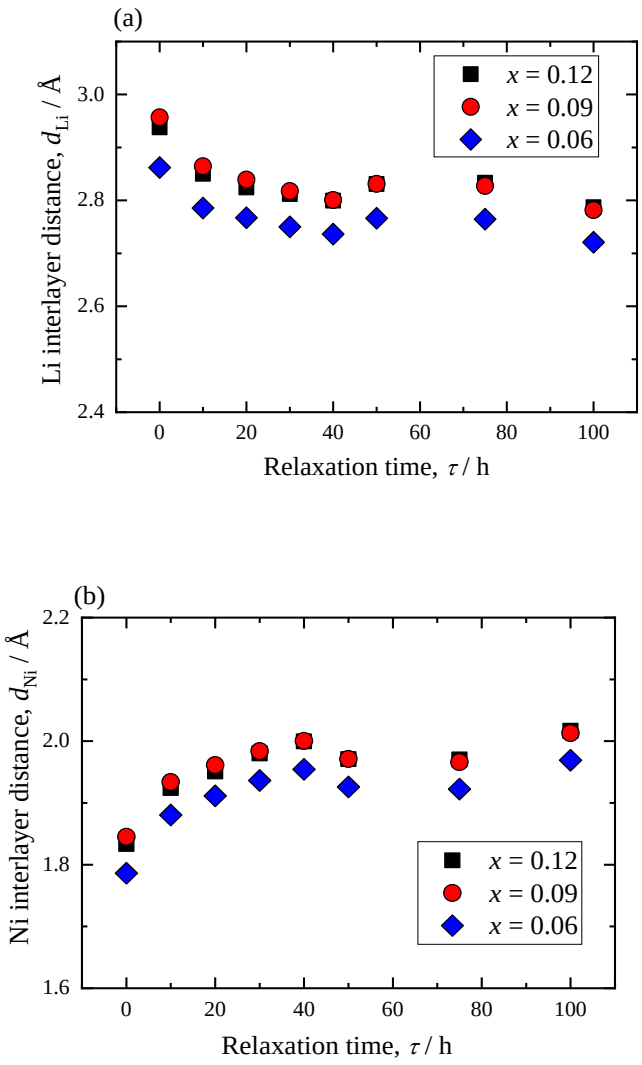

Figure 3.13 (a) Lithium and (b) nickel interlayer distance of $Li_xNi_{0.815}Co_{0.149}Al_{0.036}O_2$ plotted versus relaxation time (x = 0.12, 0.09 and 0.06).

	$x = 0.12$	$x = 0.09$	$x = 0.06$
Li_xNiO_2	H2+H3	H2+H3	H2+H3
Co-3.1 NCA	H2+H3	H2+H3	H2+H3
Co-9.0 NCA	H2	H2+H3	H2+H3
Co-14.9NCA	H2	H2	H2

Figure 3.14 Observed phase during the relaxation analysis at various lithium extraction amount for LNO and NCAs.

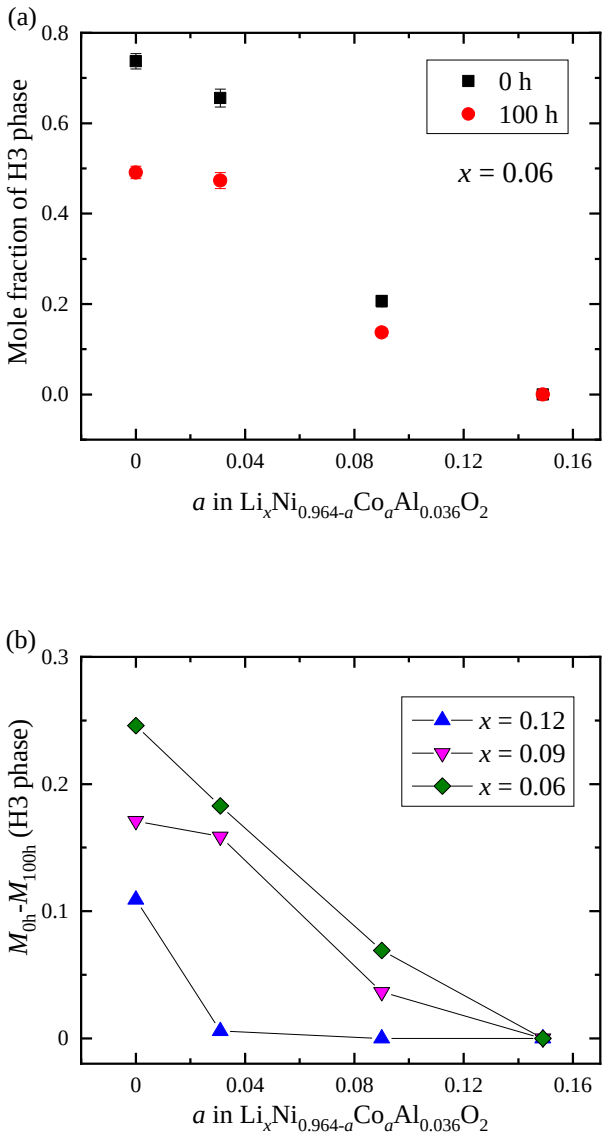

Figure 3.15 (a) Mole fraction of H3 phase for x = 0.06 of LNO and NCAs after 0 h and 100 h of relaxation. (b) The difference in mole fraction between 0 h and 100 h of relaxation plotted versus cobalt content.

3.4 Conclusion

In chapter 3, I have carried out the relaxation analysis on Co-14.9 NCA to study the structural variation at the deeply lithium extracted region for $0.06 \leq x \leq 0.12$, which were then compared with previous $LiNiO_2$, Co-3.1 NCA and Co-9.0 NCA system. In the present chapter, single H2 phase is remained at all the lithium concentration. It was found that c-length increases with relaxation time especially for highly lithium extracted Co-14.9 NCA. Concerning with the previous relaxation studies, larger amount of Co substitution reduces the mole fraction of H3 phase and allow the H2 / H3 phase ratio nearly the equilibrium during charging. Elucidating the structural relaxation properties of NCAs after lithium extraction up to highly potential region would enable the design of practical LIBs effective for the actual applications as electric vehicles.

Reference

[1] M. Li, J. Lu, Z.W. Chen, and K. Amind, *Adv. Mater*., **30**, 1800561 (2018).

[2] G. E. Blomgren, *J. Electrochem. Soc*., **164**, A5019 (2017).

[3] S. Hu, J. Wang, Y. Lu, L. Yang, L. Xiong, S. Zhao, L. Bai, C. Huang, C. Zhou, J. Zhu, W. Zhou, Y. Zhou, and Y. Yang, *Applied Surface Science*, **579**, 152183 (2022).

[4] G. Mao, F. Xiao, L. Zeng, R. Tang, J. Li, Q. Zhou, and Y. Wang, *J. Alloys and Compounds*, **892**, 162161 (2022).

[5] J. Duan, G. Hu, Y. Cao, C. Tan, C. Wu, K. D, and Z. Peng, *J. Power. Sources*. **326**, 322 (2016).

[6] K. Park, M. Choi, F. Maglia, S. Kim, K. Kim, C. Yoon, and Y. Sun, *Adv. Energy. Mater*., **8**, 1703612 (2018).

[7] M. M. Loghavi, H.M. Manesh, and R. Eqra, *J. Electroanal. Chem*., **848**, 113326 (2019).

[8] G.W. Nam, N.Y. Park, K.J. Park, J.J. Yang, J. Liu, C.S. Yoon, and Y.K. Sun, *ACS. Energy. Lett*., **4**, 2995 (2019).

[9] J.P. Pender, G. Jha, D.H. Youn, J.M. Ziegler, L. Andoni, E.J. Choi, A. Heller, B.S. Dunn, P. S. Weiss, R.M. Penner, and C.B. Mullins, *ACS Nano*., **14,** 1243 (2020).

[10] T. Tamura, S. Takai, T. Yabutsuka, and T. Yao, *J. Electrochem. Soc*., **164,** A1514 (2017).

[11] J. Kang, S. Takai, T. Yabutsuka, and T. Yao, *Materials*. **11,** 1299 (2018).

[12] J. Kang, S. Takai, T. Yabutsuka, and T. Yao, *J. Electrochem. Soc*., **166**, A5153 (2019).

Chapter 4 Structural Relaxation of $Li_xNi_{0.8}Co_{0.1}Mn_{0.1}O_2$ after lithium extraction up to high voltage region ($0.06 \leq x \leq 0.12$) at 0.01 C

4.1 Introduction

To improve the electrochemical performance of $LiNiO_2$-based electrode materials, a lots of research have been carried out by substituting Ni with various types or transition metal (Co, Mn, Al, Fe, Mg).[1-3] Among them, $LiNi_{1-a-b}Co_aMn_bO_2$ (NCM) are promising cathode materials for the application to EVs due to its high specific capacity and high energy density.[4-6] $LiNi_{1/3}Co_{1/3}Mn_{1/3}O_2$ (NCM 333) was synthesized to successfully commercialize for LIBs due to high specific capacity, structural stability and excellent cycle life.[7] In recent years, Ni-rich NCMs such as $LiNi_{0.5}Co_{0.2}Mn_{0.3}O_2$ (NCM-523) attract great interest for excellent electrode performance and a high capacity for long time use. In this system, Co and Mn contribute to the improvement of electric conductivity and structural stability, respectively.[8] $LiNi_{0.8}Co_{0.1}Mn_{0.1}O_2$ (NCM-811) has been also investigated for its larger capacity mainly focused on the application of EVs or power storage systems.[9] However, it is difficult to commercialize due to the possible reaction between highly oxidizing Ni^{4+} and electrolyte to form NiO-like rock salt type layer. The rock salt layer is thought to increase the charge transfer resistance leading capacity fade. Further severe is for exceeding 80% of Ni content.[10]

Our group have investigated the structural variation after the termination of charging / discharging for a lot of cathode or anode materials of LIBs by means of X-ray diffraction coupled with the Rietveld analysis. The information of structural change toward the equilibrium state would provide valuable information of structural stability at the charging or discharging process. Since the structural variation from kinetically favorable state toward thermodynamically equilibrium state is investigated, we refer this

methodology as Relaxation analysis.

In recent years, our group have carried out the structural relaxation analysis on $LiNiO_2$ and NCAs.[11-14] It was found that the larger amount of Co substitution in NCA reduces the mole fraction of H3 phase and allow the H2-H3 phase ration nearly the equilibrium bring relaxation time. In the present study, to clarify the contribution of cobalt substitution in NCM system, I carried out relaxation analysis on $LiNi_{0.8}Co_{0.1}Mn_{0.1}O_2$ after the lithium extraction up to high voltage region. The present study results are also compared with the previous study $LiNiO_2$.

4.2 Experiment

4.2.1 Electrochemical lithium extraction

The working electrode was prepared by mixing the cathode active material ($LiNiO_2$, Sumitomo), acetylene black (AB) and PVdF with the weight ratio of 80:10:10 to spread on Al foil with a small amount of NMP. A two-electrode type metal cell (Hohsen Co.,) was assembled in an Ar-filled glove box after drying the working electrode at 60 °C for 4 hours and 120 °C for 24 hours. Lithium metal and 1 $mol \cdot dm^{-3}$ $LiPF_6$ in a mixture of ethylene carbonate (EC) and dimethyl carbonate (DMC) solution (2:1 v / v, Kishida Chemical Co., Ltd) was used for counter electrode and electrolyte, respectively. I have extracted lithium ion from the NCM-811 at a constant current rate of 0.01 C up to x = 0.12, 0.09 and 0.06 for $Li_xNi_{0.8}Co_{0.1}Mn_{0.1}O_2$ at 25 °C. In the present study, the lithium content (x = 0.12, 0.09 and 0.06) was determined from the charged capacity. Just after terminating the lithium extraction, I separated the working electrode out of the half cell in Ar-filled glove box to prevent the local cell reaction between electrode and current collector. Then, I washed the working electrode in DMC (Kishida Chemical Co., Ltd.) followed by drying in Ar atmosphere.

4.2.2 X-ray diffraction measurement

The obtained working electrode was set in a sealed holder (Rigaku Co., Ltd.) with beryllium in an Ar-filled glove box to mount in an XRD diffractometer ((Ultima-IV, Rigaku Co., Ltd.) for XRD experiments. The XRD experiments were performed from 15 ° to 75 ° in 2θ at rate of 2 ° min^{-1} with 0.04 ° step width by using CuKα radiation. The X-ray tube voltage and current were operated at 40 kV and 40 mA, respectively. The data collection has been made every 10 hours step to evaluate the structural variation during the relaxation time.

I analyzed the XRD data by the Rietveld refinement using RIEVEC code. I carried out the Rietveld analysis assuming the two phase co-existing (H2 and H3), both of which belong to $R\bar{3}m$ symmetry. For the structure refinement, Nickel (Cobalt and Manganese) and oxide ions were placed at 3*b* and 6*c* sites, respectively in hexagonal axis ignoring the contribution of lithium.

4.3 Result and Discussion

Figure 4.1 represents the charge curve of NCM-811, showing higher charging potential compared to the previously reported $LiNiO_2$ of Co-3.1 NCA. After charging to x = 0.12, 0.09 and 0.06 for $Li_xNi_{0.8}Co_{0.1}Mn_{0.1}O_2$ as depicted by arrows, relaxation analyses have been carried out. The obtained X-ray diffraction patterns for x = 0.12, 0.09 and 0.06 for NCM-811 after various relaxation time are plotted in Figures 4.2, 4.4 and 4.6, respectively. The 003 peaks (2θ = 18° to 20°) for x = 0.12, 0.09 and 0.06 for NCM-811are shown in Figures 4.3, 4.5 and 4.7. The peaks observed around 18.5° and 19.5° are ascribed to 003 reflections of H2 and H3 phases, respectively. While 003 peaks of H3 phase appear to shift toward lower 2θ direction with relaxation time for all the samples, those of H2 phase dose not. It is also found that, with extracting lithium ions or decreasing x, relative intensity of 003_{H2} diffraction peak diminishes. In addition, peak shifts of 003_{H3} become gentle with reducing x or deeply lithium extraction. Just after the termination of lithium extraction to x = 0.12, slight shoulder is observed at the lower angle side of 003_{H3} peak. This would be due to the intermediate structure between H2 and H3, which rapidly transforms into H2 and H3 phases. For highly extracted compositions up to x = 0.09 or 0.06, such a shoulder did not appear, since H3 phase is supposed to be favorable even just after the termination of charging. For all the diffraction patterns, the Rietveld refinements have been carried out assuming coexistence of H2 and H3 phase. Figure 4.8, 4.9 and 4.10 shows the Rietveld refinement for x = 0.12, 0.09 and 0.06 after 0 hour and 50 hours of relaxation, resulting in good agreement of the measured and refined patterns with sufficiently R_{wp} value.

Mole fraction of H3 phase, lattice parameters and fractional coordinates (0 0 z) of oxide ion site are listed in Tables 4.1, 4.2 and 4.3 for x = 0.12, 0.09 and 0.06 for 0 hour and 50

hours. Figure 4.11 exhibits the relaxation time dependence of mole fraction of H3 phase, the remains from the unity being that of H2. As the general trend, it is observed that the lower lithium concentration possesses the higher H3 mole fraction. Moreover, the molar ratio of H3 phase gradually decrease with the relaxation time for x = 0.09 and 0.06, while it does not for x = 0.12. Namely, it is supposed that the H3 phase is excessively created during the deeper lithium extraction, then it turns back into H2 at the relaxation. Such a transformation behavior during the relaxation has also been observed for previously studied LNO or Ni-rich NCA (Co-3.1 NCA) system as plotted in Figure 4.12. However, the mole fraction of H3 phase in LNO or Co-3.1 NCA are lower than that of NCM. Moreover, deeply lithium extracted samples in Co-3.1 NCA or LNO exhibit apparent transition from H3 to H2 phases.

Figures 4.13 and 4.14 shows the relaxation time dependence of *a*-lattice and *c*-lattice parameters, respectively for H2 and H3 phases. All the samples exhibit the similar *a*-length regardless of the lithium concentration even for H2 and H3 phase, which slightly increase with the relaxation time. On the other hand, H3 phase possesses distinctly smaller *c*-length compared to H2 phase, although the data of H2 phase are a little scattered presumably due to the much smaller peak intensity. As for the relaxation behavior of H3 phase, the *c*-length gradually increases during the relaxation. Assuming that a part of H3 phase transformed into H2 as described above, the remaining H3 phase should include fewer lithium ions to decrease the *c*-length, which is not consistent to the result in Figure 4.14. To clarify this phenomenon, we focused on the variation of interlayer distances consisting of the *c*-axis.

Figure 4.15 plots the relaxation time dependence of lithium and nickel interlayer distances (d_{Li} and d_{Ni},) of H3 phase calculated using the refined oxide ion positions. It is

observed that the lithium interlayer distance increases while the nickel interlayer slightly shrinks during the relaxation. Assuming that the excessively formed H3 phase transforms into H2 during the relaxations as described above, the remained H3 phase would include the smaller amount of lithium ions and the average valence of nickel ions in H3 phase should increase. Accordingly, the increase in repulsive force between the oxide ions in lithium interlayer and the decrease in size of nickel ions qualitatively explain the increases in d_{Li} accompanied by decrease in d_{Ni} during the relaxation. In such a highly lithium extracted region with smaller lithium concentration as 6 to 12% of lithium ion occupancy, smaller variation in concentration of lithium ions, which shield the repulsive force between oxide ions, would attribute largely to d_{Li} rather than d_{Ni}. Consequently, *c*-length consisting of d_{Li} and d_{Ni} should slightly increase during the relaxation.

The relaxation variation of *c*-parameter for LNO and Co-3.1 NCA are comparatively plotted in Figure 4.16. In LNO, the difference in *c*-length between H2 and H3 phases keep approximately 0.8 Å during the relaxation, while the difference is much smaller in Co-3.1 NCA. I have assumed that the large difference in *c*-length between H2 and H3 phases suppress the phase change between H2 and H3, resulting in the larger change in mole fraction at the relaxation. In the case of NCM, the relaxation behavior of *c*-length is rather similar to LNO in comparison with Co-3.1 NCA. In terms of the result of change in mole fraction during the relaxation in Figure 4.12, NCM is thought to rapidly achieve the equilibrium structure in comparison with Co-3.1 NCA or LNO. Accordingly, rapid phase change would contribute to the improvement of cycle performance in NCM, while Co-3.1 NCA improves by means of the closer lattice parameters between H2 and H3 phases.

In summary, NCM forms larger amount of H3 phase at the highly lithium extracted region in comparison with LNO or Co-3.1 NCA. Nevertheless, rapid phase change

facilitates the achievement of equilibrium structure for NCM, allowing smaller amount of structural change during the relaxation. Further discussion should be made based on the first principal calculation for the improved phase change properties of NCM.

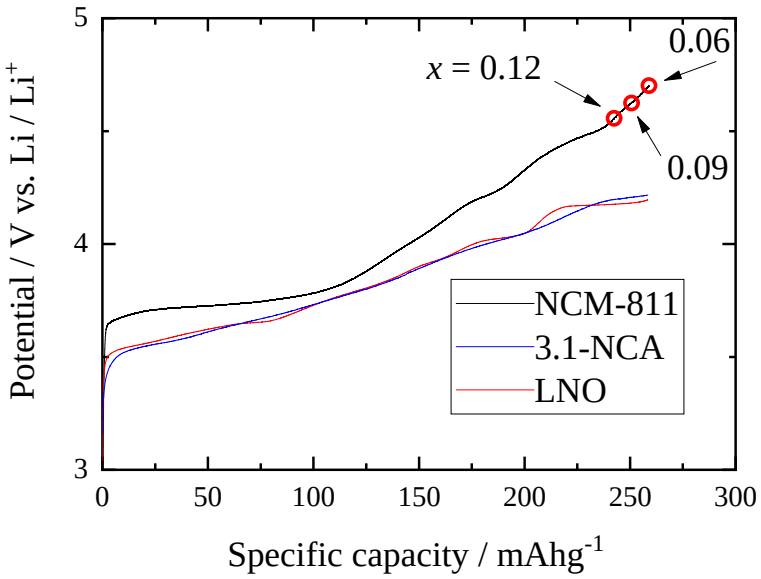

Figure 4.1 Charge curve of $Li_xNi_{0.8}Co_{0.1}Mn_{0.1}O_2$ after lithium extraction up to x = 0.12, 0.09 and 0.06.

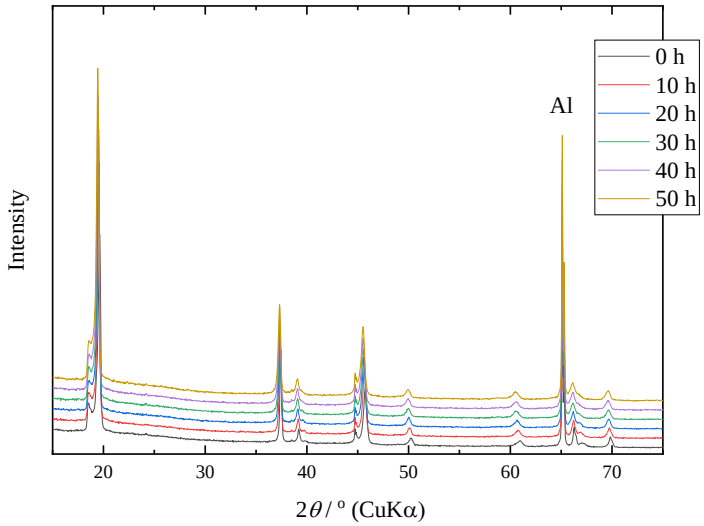

Figure 4.2 XRD pattern of $Li_{0.12}Ni_{0.8}Co_{0.1}Mn_{0.1}O_2$.

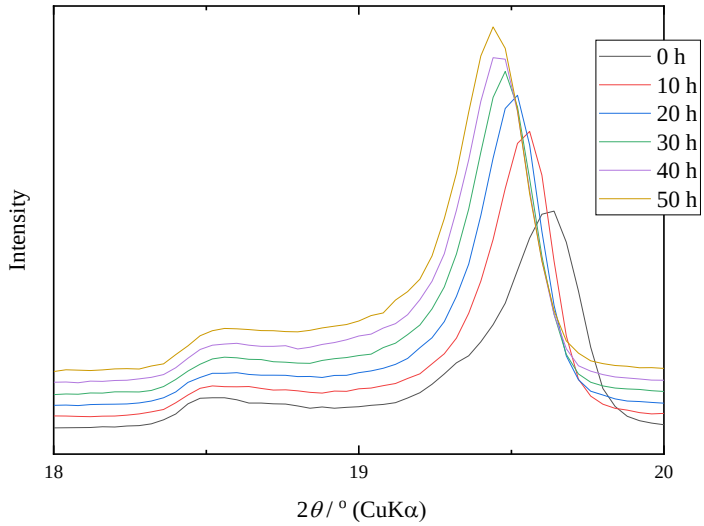

Figure 4.3 003 peaks of $Li_{0.12}Ni_{0.8}Co_{0.1}Mn_{0.1}O_2$ ($2\theta = 18° \sim 20°$).

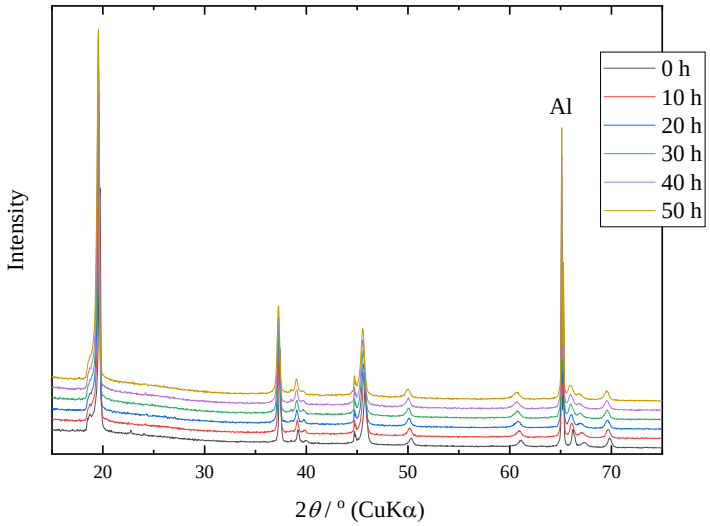

Figure 4.4 XRD pattern of $Li_{0.09}Ni_{0.8}Co_{0.1}Mn_{0.1}O_2$.

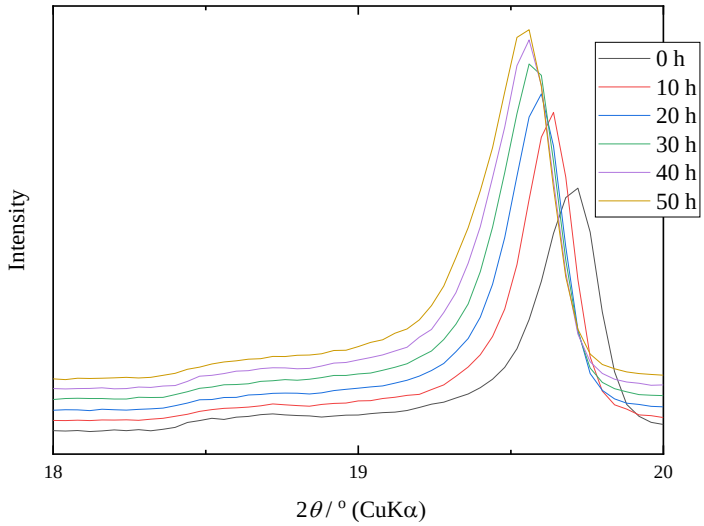

Figure 4.5 003 peaks of $Li_{0.09}Ni_{0.8}Co_{0.1}Mn_{0.1}O_2$ ($2\theta = 18° \sim 20°$).

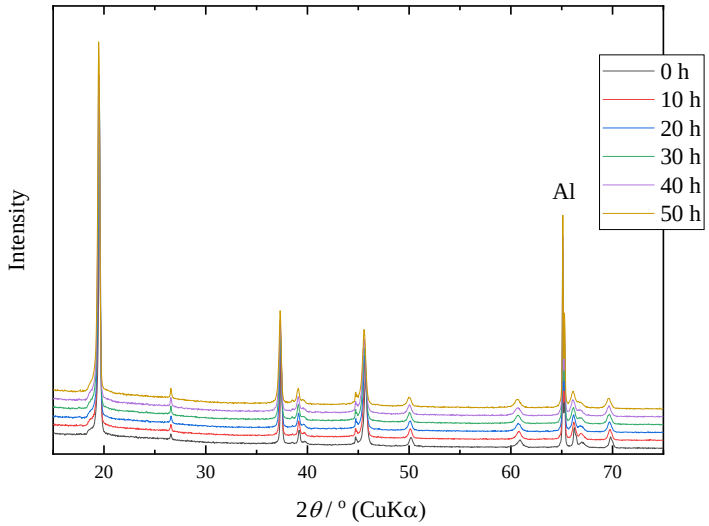

Figure 4.6 XRD pattern of $Li_{0.06}Ni_{0.8}Co_{0.1}Mn_{0.1}O_2$.

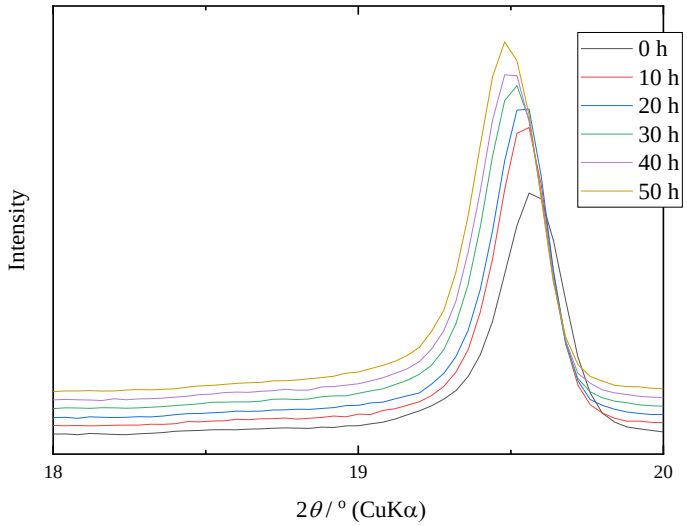

Figure 4.7 003 peaks of $Li_{0.06}Ni_{0.8}Co_{0.1}Mn_{0.1}O_2$ ($2\theta = 18° \sim 20°$).

Table 4.1 Refined structure parameters of $Li_{0.12}Ni_{0.8}Co_{0.1}Mn_{0.1}O_2$ for initial state and after 50 h of relaxation.

			0 h	50 h
H2 phase	Lattice constant	*a* (Å)	2.8129(5)	2.8242(3)
		c (Å)	14.423(1)	14.459(1)
	z		0.233(6)	0.236(3)
	Mole fraction		0.24(9)	0.23(6)
	Confidence factor	R_F (%)	4.476	1.673
		R_B (%)	4.681	2.262
H3 phase	Lattice constant	*a* (Å)	2.8136(1)	2.8180(4)
		c (Å)	14.3312(1)	13.3115(1)
	z		0.256(2)	0.246(3)
	Mole fraction		0.17(1)	0.13(4)
	Confidence factor	R_F (%)	5.813	2.754
		R_B (%)	4.970	2.744
Overall confidence factor		R_{wp} (%)	8.132	4.861
		GOF	3.387	2.326

Table 4.2 Refined structure parameters of $Li_{0.09}Ni_{0.8}Co_{0.1}Mn_{0.1}O_2$ for initial state and after 50 h of relaxation.

			0 h	50 h
H2 phase	Lattice constant	*a* (Å)	2.8172 (1)	2.8204(5)
		c (Å)	14.4315(1)	14.4300(0)
	z		0.232(1)	0.227(1)
	Mole fraction		0.82(9)	0.86(6)
	Confidence factor	R_F (%)	3.373	2.174
		R_B (%)	4.804	3.354
H3 phase	Lattice constant	*a* (Å)	2.8136(1)	2.8180(4)
		c (Å)	14.3312(1)	13.3115(1)
	z		0.256(2)	0.246(3)
	Mole fraction		0.17(1)	0.13(4)
	Confidence factor	R_F (%)	5.135	4.538
		R_B (%)	5.572	3.660
Overall confidence factor		R_{wp} (%)	8.775	7.250
		GOF	2.554	2.452

Table 4.3 Refined structure parameters of $Li_{0.06}Ni_{0.8}Co_{0.1}Mn_{0.1}O_2$ for initial state and after 50 h of relaxation.

			0 h	50 h
H2 phase	Lattice constant	*a* (Å)	2.8234(1)	2.8268(4)
		c (Å)	14.2609(1)	14.3261(3)
	Mole fraction		0.79(3)	0.86(2)
	z		0.230(4)	0.235(2)
	Confidence factor	R_F (%)	2.225	0.486
		R_B (%)	3.688	0.868
H3 phase	Lattice constant	*a* (Å)	2.8253(2)	2.8255(3)
		c (Å)	14.1475(1)	14.2098(1)
	z		0.242(1)	0.219(5)
	Mole fraction		0.20(7)	0.13(8)
	Confidence factor	R_F (%)	6.171	3.275
		R_B (%)	7.181	4.276
Overall confidence factor		R_{wp} (%)	7.630	6.582
		GOF	2.314	2.291

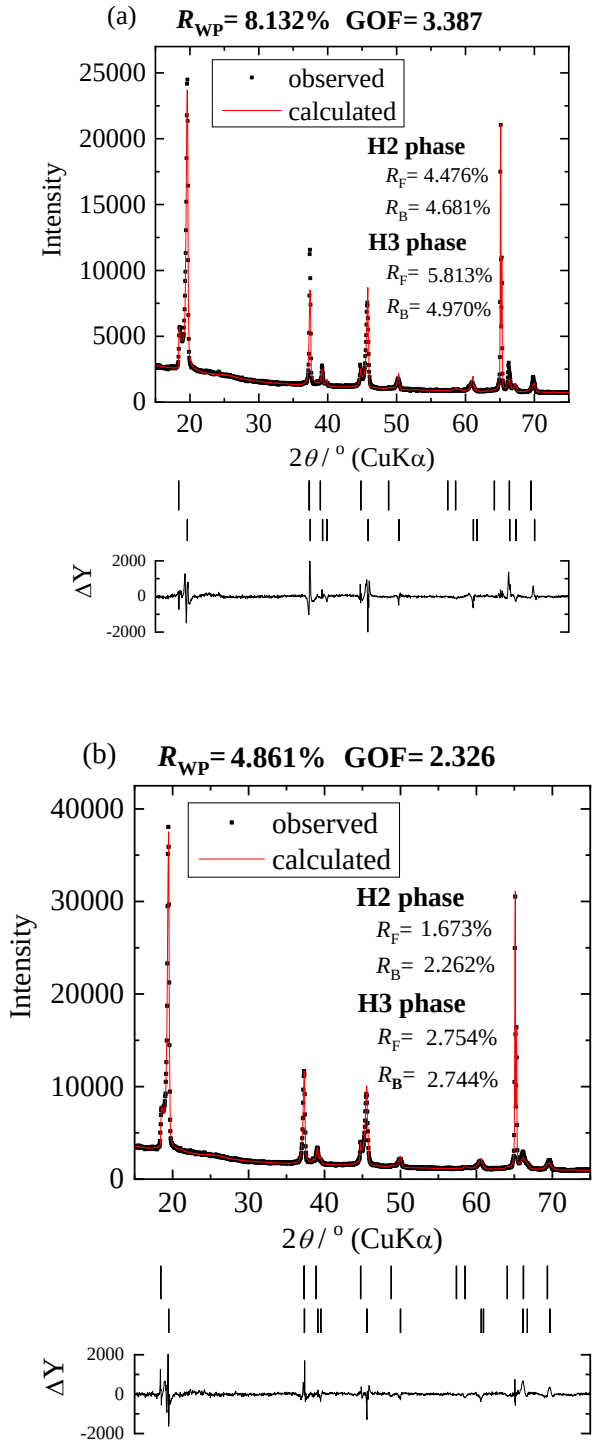

Figure 4.8 Observed and Rietveld fitted diffraction pattern of $Li_xNi_{0.8}Co_{0.1}Mn_{0.1}O_2$ (x = 0.12) after (a) 0 h and (b) 50 h of relaxation.

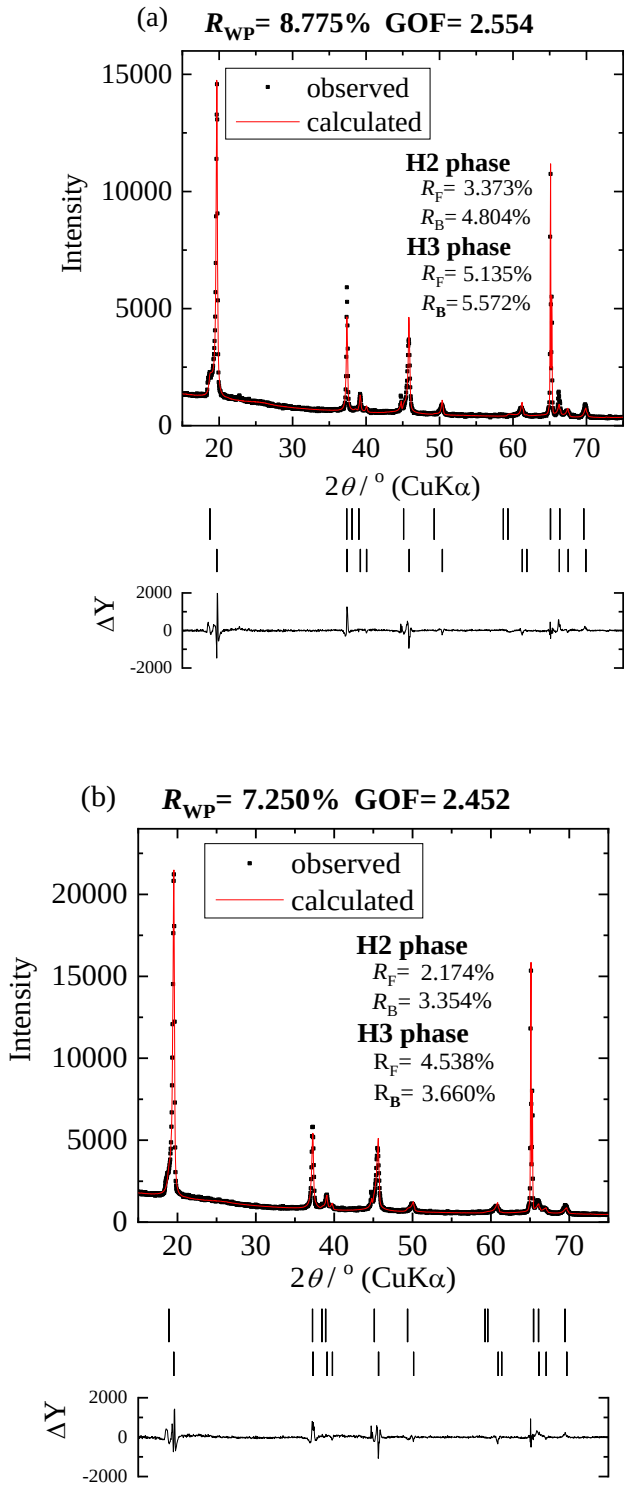

Figure 4.9 Observed and Rietveld fitted diffraction pattern of $Li_xNi_{0.8}Co_{0.1}Mn_{0.1}O_2$ (x = 0.09) after (a) 0 h and (b) 50 h of relaxation.

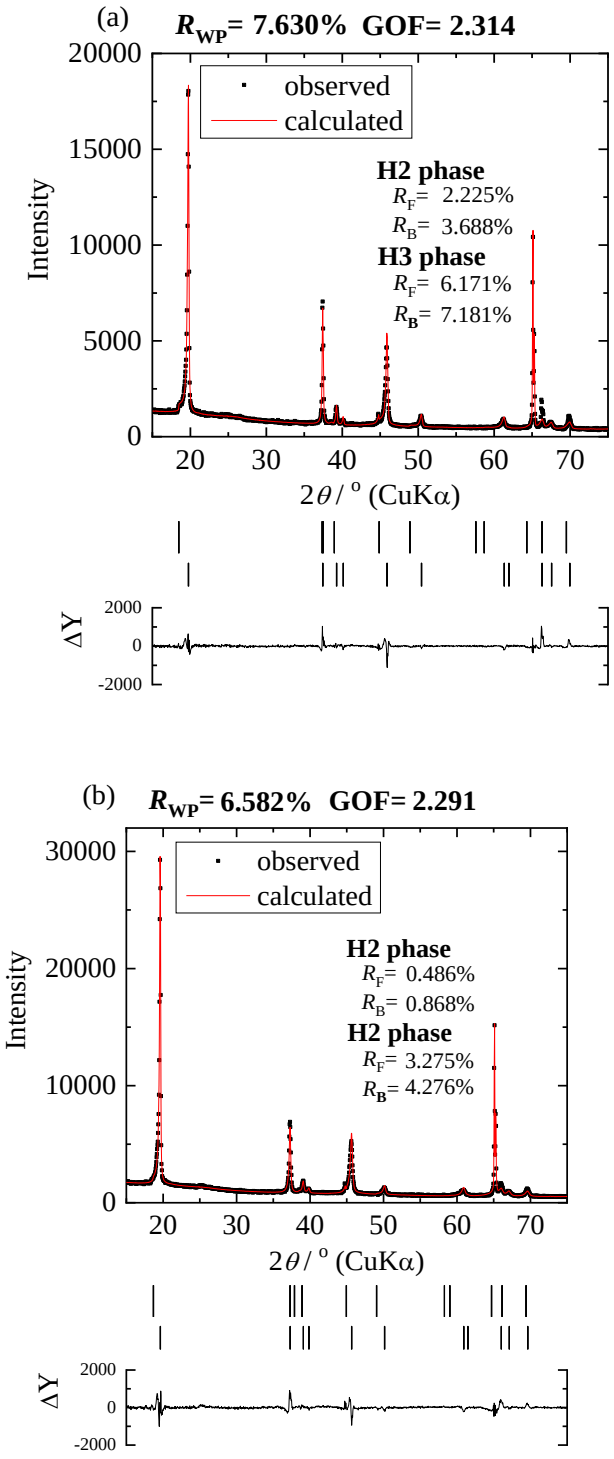

Figure 4.10 Observed and Rietveld fitted diffraction pattern of $Li_xNi_{0.8}Co_{0.1}Mn_{0.1}O_2$ (x = 0.06) after (a) 0 h and (b) 50 h of relaxation.

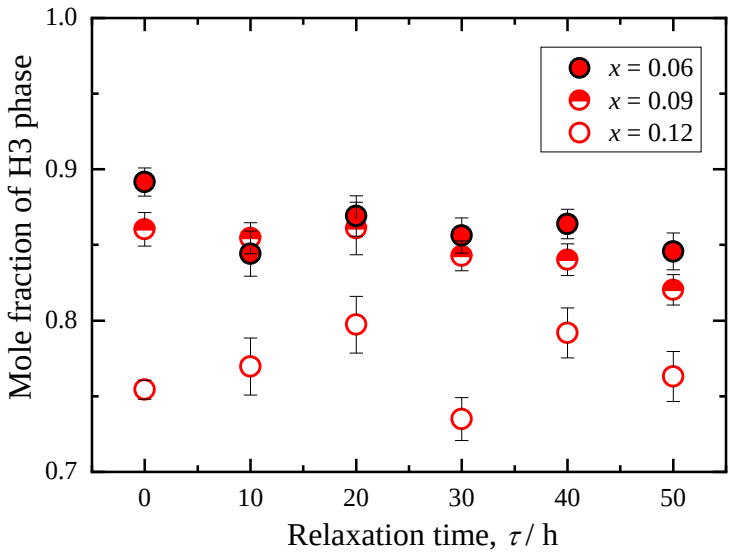

Figure 4.11 Calculated mole fraction changes of H3 phase for $Li_xNi_{0.8}Co_{0.1}Mn_{0.1}O_2$ (x = 0.12, 0.09 and 0.06).

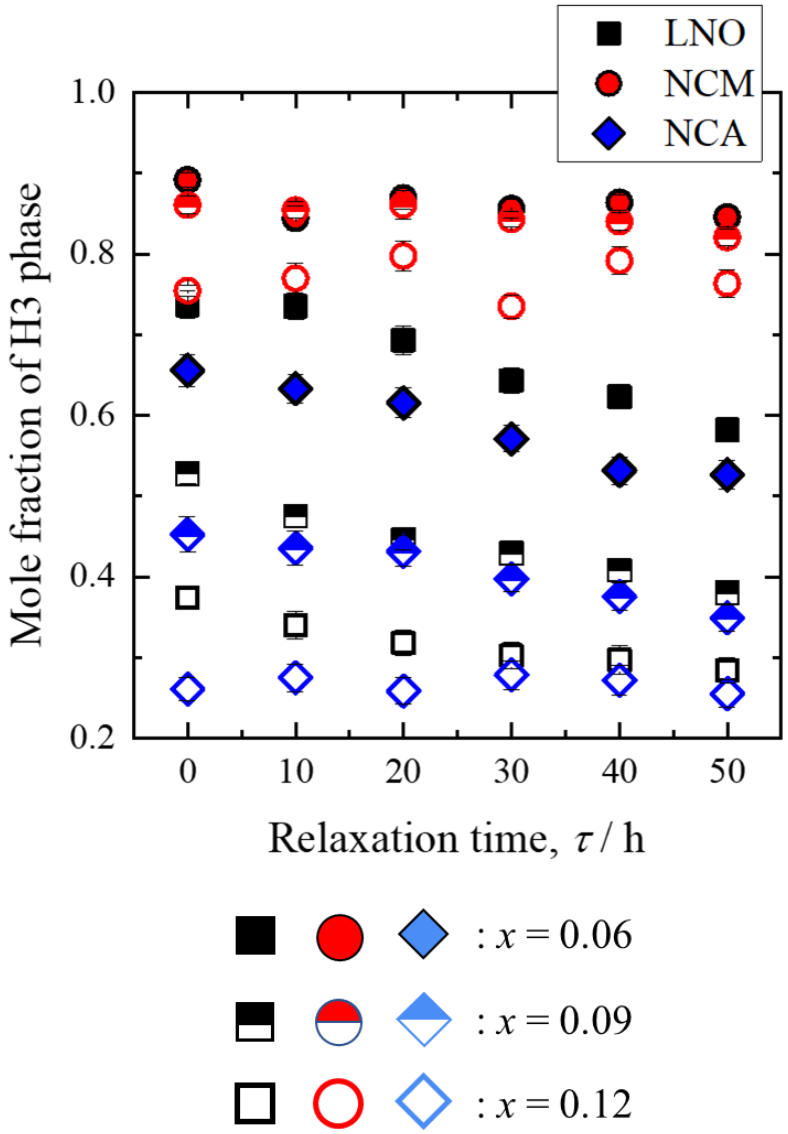

Figure 4.12 Calculated mole fraction changes of H3 phase for Li_xNiO_2, $Li_xNi_{0.933}Co_{0.031}Al_{0.036}O_2$ and $Li_xNi_{0.8}Co_{0.1}Mn_{0.1}O_2$.

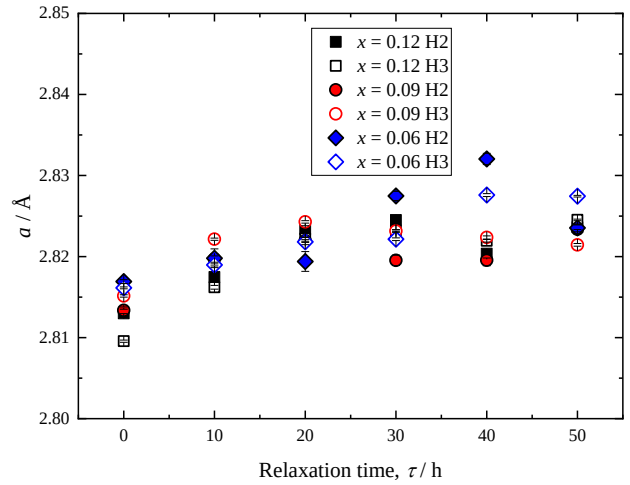

Figure 4.13 Change in lattice parameters of the *a*-axis of $Li_xNi_{0.8}Co_{0.1}Mn_{0.1}O_2$ with relaxation time (x = 0.12, 0.09 and 0.06).

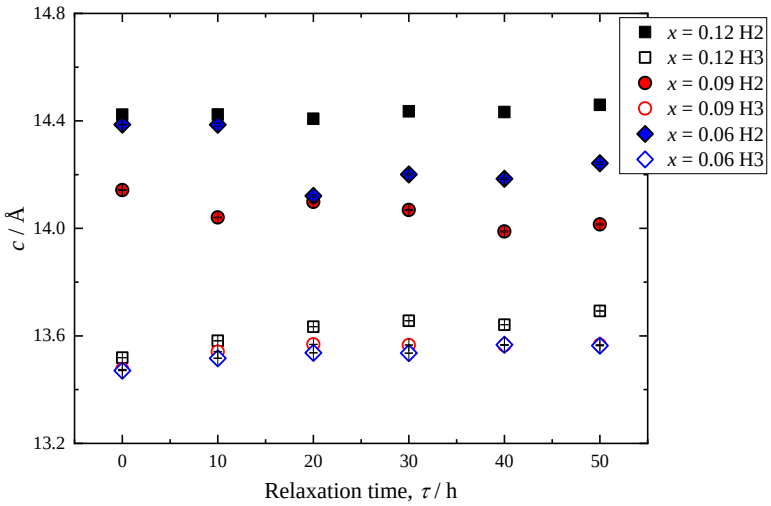

Figure 4.14 Change in lattice parameters of the *c*-axis of $Li_xNi_{0.8}Co_{0.1}Mn_{0.1}O_2$ with relaxation time (x = 0.12, 0.09 and 0.06).

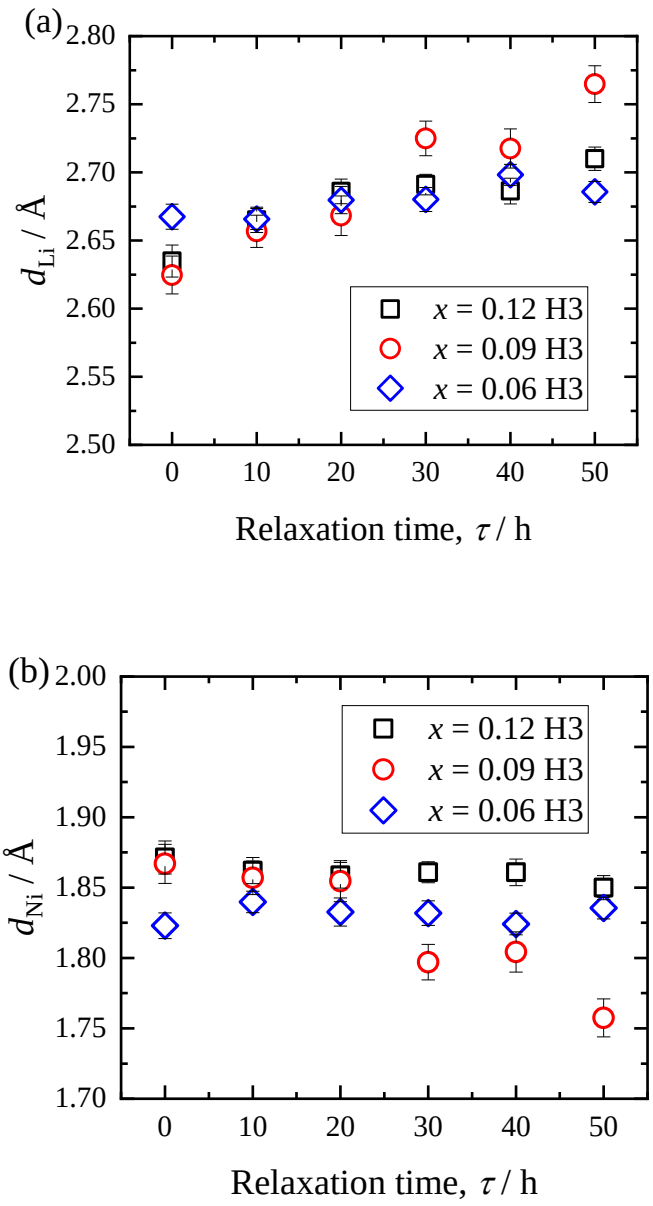

Figure 4.15 Lithium and nickel interlayer distance of $Li_xNi_{0.8}Co_{0.1}Mn_{0.1}O_2$ plotted versus relaxation time (x = 0.12, 0.09 and 0.06).

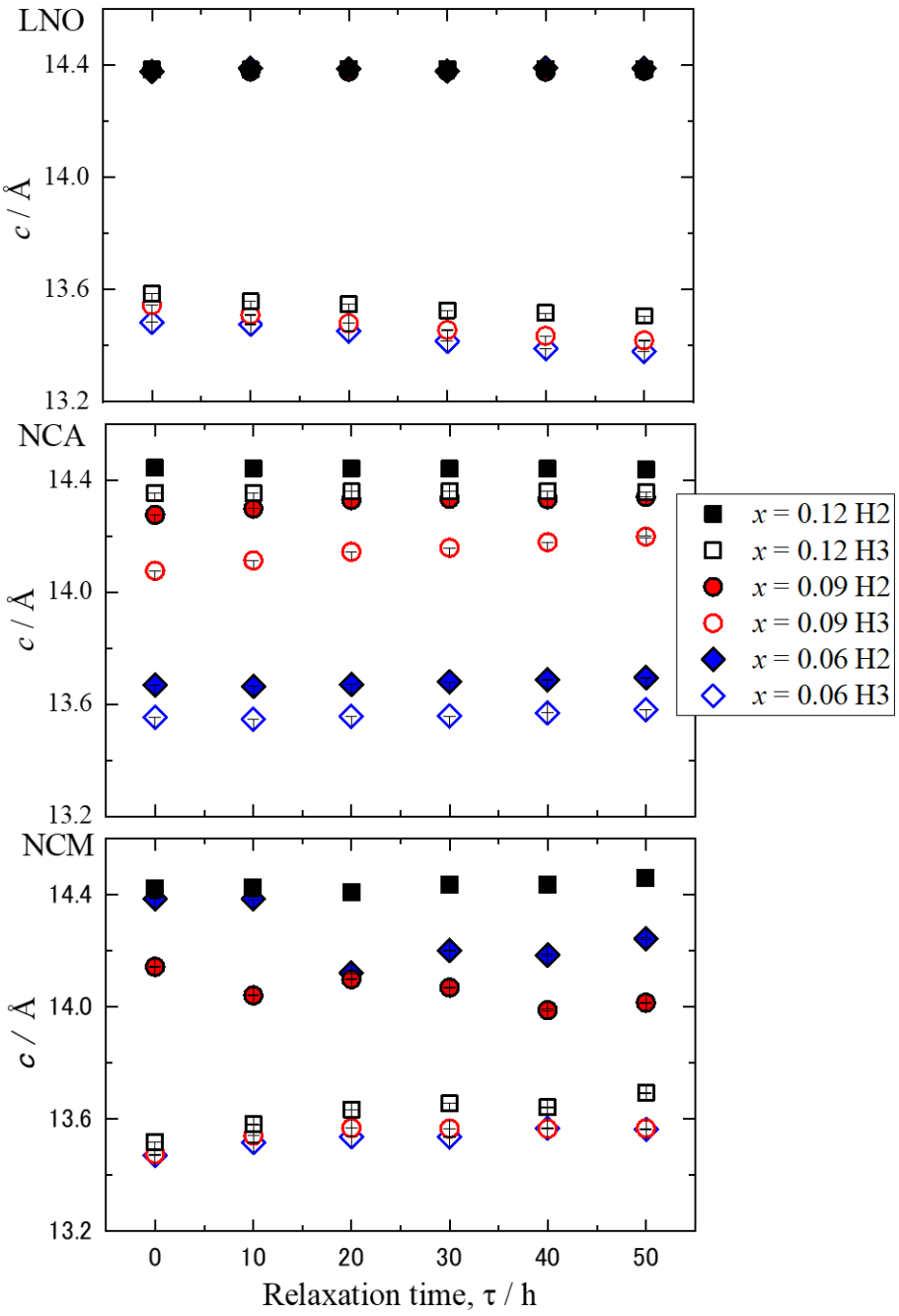

Figure 4.16 Change in c-axis of H2 and H3 phase of Li_xNiO_2, $Li_xNi_{0.933}Co_{0.031}Al_{0.036}O_2$ and $Li_xNi_{0.8}Co_{0.1}Mn_{0.1}O_2$ with relaxation time (x = 0.12, 0.09 and 0.06).

4. 4 Conclusion

I have carried out the relaxation analysis on NCM-811 to study the structural variation at the deeply lithium extracted region for $0.06 \leq x \leq 0.12$, the results of which were then compared with previous $LiNiO_2$ and Co-3.1 NCA. Just after the termination of lithium extraction, the coexistence of H2 and H3 phases was detected for all the lithium concentrations, and it is also found that excessively formed H3 phase partly transforms into H2 during the relaxation as the $LiNiO_2$ and Co-3.1 NCA. The variation of mole fraction from H3 to H2 phases during the relaxation is smaller than that of $LiNiO_2$ or Co-3.1 NCA. This indicates that NCM-811 easily follows the equilibrium state during the charging, despite of relatively large change in *c*-length between H2 and H3 phases.

It is reported that the surface deterioration as well as particle cracking degrade the cycle performance. Even though, after resolving these problems by surface modification or development of electrolytes, relatively higher potential region would be utilized to exploit energy density. I believe the present structural relaxation study would provide valuable information for the use of higher potential region.

Reference

[1] C. Delams, I. Saadoune, and A. Rougier, *J. Power Sources*, **44**, 595 (1993).

[2] H. Arai, S. Okada, Y. Sakurai, and J. Yamaki, *J. Electrochem. Soc*., **144**, 3117 (1997).

[3] Z. Lu, D. D. MacNeil, and J. R. Dahn, *Electrochem. Solid State Lett*., **4**, A191 (2001).

[4] F. Schipper, E. Erickson, C. Erk, J. Shin, F. Chesneau, and D. Aurbach, *J. Electrochem. Soc*., **164**, A6220 (2017).

[5] J. Xu, F. Lin, M. Doeff, and W. Tong, *J. Mater. Chem. A*, **5**, 874 (2017).

[6] J. Kim, H. Lee, H. Cha, M. Yoon, M. Park, and J. Cho, *Adv. Energy Mater*., **8**, 1702028 (2018).

[7] T. Ohzuku, and Y. Makimura, *Chem. Lett*., **30**, 642 (2001).

[8] N. Voronina, Y. Sun, and S. Myung, ACS. Energy Lett., *ACS. Energy Lett*., **5**, 1814 (2020).

[9] S. Gao, Y. Cheng, and M. Shirpour, *ACS. Appl. Mater. Interfaces*, **11**, 982 (2019).

[10] J. Pender, G. Jha, D. H. Youn, J. M. Ziegler, I. Andoni, E. J. Choi, A. Heller, B. S. Dunn, P. S. Weiss, R. M. Penner, and C. B. Mullins, *ACS Nana*., **14**, 1243 (2020).

[11] T. Tamura, S. Takai, T. Yabutsuka, and T. Yao, *J. Electrochem. Soc*., **164**, A1514 (2017).

[12] J. Kang, S. Takai, T. Yabutsuka, and T. Yao, *Materials*. **11**, 1299 (2018).

[13] J. Kang, S. Takai, T. Yabutsuka, and T. Yao, *J. Electrochem. Soc*., **166**, A5153 (2019).

[14] J. Kang, S. Takai, T. Yabutsuka, and T. Yao, *J. Eletroanalytical. Chem*., **878**, 114566 (2020).

Chapter 5 Structural Relaxation of $Li_xNi_{0.8}Co_{0.1}Mn_{0.1}O_2$ and $Li_xNi_{0.35}Co_{0.35}Mn_{0.30}O_2$ after lithium extraction up to high voltage region ($0.06 \leq x \leq 0.12$) at 0.1 C

5.1 Introduction

$LiNi_{1-a-b}Co_aMn_bO_2$ (NCM) are regarded as a promising cathode material due to their relatively low cost, high capacity and excellent cycle performance.[1-4] In NCM systems, nickel contribute to a high capacity and increase energy density of batteries, while cobalt and manganese provide electrical conductivity and structural stability, respectively.[5] Among NCM based cathode materials, nickel-rich NCM have been attracted a great deal of attention because their capacity increases with Ni content.[6] However, increasing the Ni content in Ni-rich systems has a negative impact on capacity degradation, which prevent large scale commercialization.[6-7] To solve these problems, many experimental methods have been explored, such as surface coating,[8] making singly crystal particles,[9,10] and core shell / concentration gradient structures.[11,12]

In the present study, to clarify the contribution of cobalt substitution in NCM system, I carried out relaxation analysis on $LiNi_{0.8}Co_{0.1}Mn_{0.1}O_2$ and $LiNi_{0.35}Co_{0.35}Mn_{0.30}O_2$ after the lithium extraction up to high voltage region at 0.1 C. To clarify the relationship between the structural change in the relaxation time and the current density, we also compared the results of the NCM-811 charged to the high potential region at 0.1 C and 0.01 C.[13]

5.2 Experiment

5.2.1 Electrochemical lithium extraction

$LiNi_{0.8}Co_{0.1}Mn_{0.1}O_2$ (NCM-811) and $LiNi_{0.35}Co_{0.35}Mn_{0.30}O_2$ (NCM-353530) from Sumitomo Metal Mining Co., Ltd. Were used as cathode materials. To make the electrode slurries, we mixed the 80 wt% cathode active materials (NCM-811 and NCM-353530), 10 wt% Acetylene Black (AB) and 10 wt% poly-vinylidene fluoride (PVdF). The slurries were spread on Al foil with a small amount of NMP and dried at 60 °C for 4 hours and 120 °C for 24 hours. To perform the electrochemical tests, a two-electrode metal cell (Hohsen Co.,) was assembled using lithium metal as a counter electrode and 1 $mol \cdot dm^{-3}$ $LiPF_6$ in a mixture of ethylene carbonate (EC) and dimethyl carbonate (DMC) solution (2:1 v / v, Kishida Chemical Corp., Ltd.) as electrolyte in an Ar-filled glove box. Lithium ion was electrochemically extracted from the $Li_xNi_{0.8}Co_{0.1}Mn_{0.1}O_2$ and $Li_xNi_{0.35}Co_{0.35}Mn_{0.30}O_2$ at a constant current of 0.1 C to achieve the compositions of x = 0.12, 0.09 and 0.06 at 25 °C. To avoid the local cell reaction between electrode and current collector, I separated the working electrode out of the half cell in Ar-filled glove box after the termination of lithium extraction. The working electrode was washed in DMC (Kishida Chemical Co., Ltd) and then dried in glove box.

5.2.2 X-ray diffraction measurement

The working electrode was set in a sealed holder (Rigaku Co., Ltd) with beryllium window in an Ar-filled glove box to avoid the reaction between the electrode and the air. Then the sealed holder was mounted on a XRD diffractometer (Ultima-IV, Rigaku Corp., Ltd.) for XRD measurement by using CuKα radiation (40 kv and 40 mA) with a scanning speed of 2 ° min^{-1} with 0.04 ° step from 15 ° to 75 ° in 2θ. The data collection was performed every 10 hours from 0 hour to 50 hours after the termination of lithium extraction to measure the structural variation during the relaxation time.

The Rietveld refinement of XRD profiles was carried our using RIEVEC program, which assuming the single phase and two phase co-existing (H2 and H3), both of which belong to $R\bar{3}m$ symmetry. Nickel (cobalt and manganese) and oxide ions were placed at the 3*b* and 6*c* sites, respectively in hexagonal axis, and the contribution of lithium was ignored.

5.3 Result and Discussion

Figure 5.1 represents the charge curve of NCM-811 and NCM-353530. In the intermediate region, NCM-353530 showed a higher voltage than NCM-811, but at the end of charging, NCM-353530 showed a similar voltage with NCM-811. I carried out the relaxation time analyses after charging to $x = 0.12$, 0.09 and 0.06 for $Li_xNi_{0.8}Co_{0.1}Mn_{0.1}O_2$ and $Li_xNi_{0.35}Co_{0.35}Mn_{0.30}O_2$. Figures 5.2, 5.4 and 5.6 show the X-ray diffraction patterns for $x = 0.12$, 0.09 and 0.06 of NCM-811 after various relaxation time. The 003 peaks (2θ = 18° to 20°) for $x = 0.12$, 0.09 and 0.06 for NCM-811are shown in Figures 5.3, 5.5 and 5.7. Two peaks were observed in NCN-811, which are considered to have appeared as two-phase coexistence of the H2 and H3 phases during the relaxation process. The peaks observed around 18.5 ° and 19.5 ° are attributed to 003 reflections of the H2 and H3 phase, respectively. In all samples, the 003 peaks of H3 phase appear to shift toward the lower 2θ direction with relaxation time, while that of the H2 phase dose not. It was also found that the relative intensity of the diffraction peak of 003_{H2} was reduced when the lithium ion was extracted, or x was reduced.

The obtained X-ray diffraction patterns for $x = 0.12$, 0.09 and 0.06 for NCM-353530 after various relaxation time are plotted in Figures 5.8, 5.10 and 5.12, respectively. And the Figures 5.9, 5.11 and 5.13 shows the 003 peaks (2θ = 18° to 20°) for $x = 0.12$, 0.09 and 0.06 for NCM-353530. In NCM-353530, the 003 peaks were observed as only one, and it suggests that only a single phase appeared in the relaxation times. Rietveld refinement was performed on all the diffraction patterns of NCM-811 and NCM-353530 assuming two-phase coexistence (H2 and H3 phases) and single phase, respectively. Figures 5.14, 5.15 and 5.16 show the result of the Rietveld refinement for $x = 0.12$, 0.09 and 0.06 for NCM-811 after 0 hour and 50 hours, with a sufficiently low R_{wp} value that

the measured and refined patterns are in good agreement. The result of the Rietveld refinement for x = 0.12, 0.09 and 0.06 for NCM-353530 after 0 hour and 50 hours were showed in Figures 5.17, 5.18 and 5.19, respectively. Tables 5.1, 5.2 and 5.3 show the mole fraction of the H2 phase and H3 phase, lattice parameters and fractional coordinates of oxide ion sites (0 0 z) for the initial data (0 h) and final data (after 50 h of relaxation) of NCM-811. And the refined structure parameters for NCM-353530 were listed in Tables 5.4, 5.5 and 5.6.

Figure 5.20 shows the relaxation time dependence of the mole fraction of the H3 phase for NCM-811 and NCM-353530. It was found that NCM-811 has a two phase coexistence of the H2 and H3 phases with a mole fraction pf about 1 : 9, while NCM-353530 has a single phase. Assuming that the single phase of NCM-353530 is the H2 phase, the H3 phase will be 0. In NCM-811, the sample with lithium extraction up to x = 0.06 showed a slight decrease in the mole fraction of the H3 phase with relaxation time and a tendency to change from the H3 to the H2 phase, but the majority of the sample remained in the H3 phase and there was no significant change in the mole fraction. The comparison of the change in mole fractions of NCM-811 and NCM-353530 during the relaxation process suggests that the appearance of the H3 phase is suppressed with increasing cobalt substitution in the NCM system. Such the contribution of cobalt was also observed in previous LNO and NCAs studies.

Figures 5.21 and 5.22 shows the relaxation time dependence of a-lattice and c-lattice parameters for NCM-811, respectively. The relaxation time dependence of a-axis and c-axis for NCM-353530 was plotted in Figure 5.23 and 5.24. NCM-811 and NCM-353530 showed no significant change in a-axis during the relaxation time. On the other hand, the H2 phase showed a shorter c-axis for the composition with lower lithium content or x in

NCM-811, but the *c*-axis of the H3 phase was relatively close for all composition. As for the relaxation behavior of the lattice parameter, a decrease in the *c*-axis of the H2 phase was observed in the early stage of relaxation in the sample desorbed to $x = 0.06$ in NCM-811, but the *c*-axis of the H3 phase was relatively close for all composition. As for the relaxation behavior of the lattice parameter, a decrease in the *c*-axis of the H2 phase was observed in the early stage of relaxation in the sample desorbed to $x = 0.06$ in NCM-811, but no significant change was observed in the other samples. This is because the composition dependence of the *c*-axis of the H2 phase is large than that of the H3 phase, it is considered to be susceptible to changes in lithium concentration. Nevertheless, the overall trend was that the *c*-axis decreased with relaxation time in the H2 phase and slightly increased in the H3 phase, especially at $x = 0.06$. From this, especially when lithium was extracted up to high potential, deviation from equilibrium mole fraction occurred, and structural change from the H3 phase to the H2 phase, which could not be followed during charging, occurred during relaxation process, and change in lattice parameter accompanying change in lithium concentration in each phase was observed.

For NCM-353530, which consists only for the H2 phase, a significant increase in the *c*-axis is observed for the $x = 0.06$ during the relaxation time, as shown in Figure 5.24. In this case, since no phase transition occurs, there is no delay in following the equilibrium mole fraction, but rather the excess extraction sample near the surface pushes down the overall *c*-axis and changes in toward a stable *c*-axis during relaxation time. Figure 5.25 plots the relaxation time dependence of the lithium and nickel interlayer distance (d_{Li} and d_{Ni}) of H3 phase for NCM-811 obtained by using the refined oxide ion positions. The lithium and nickel interlayers of H3 phase show no significant compositional dependence or relaxation time variation. The lithium and nickel interlayer distance of H2 phase for

NCM-353530 was plotted at Figure 5.26. The d_{Li} and d_{Ni} of x = 0.12 and 0.09 show no significant change during the relaxation time. On the other hand, that of x = 0.06 vary largely with the relaxation.

In order to clarify the relationship between the structural change in the relaxation time and current density, I compared the results of the NCM-811 changed to the high potential region at 0.1 C in this study with the result of NCM-811 charged at 0.01 C in the past. The charge curve of NCM-811 with lithium extracted at 0.1 C and 0.01 C are shown in Figure 5.27. The charge curve of 0.1 C initially showed a larger overvoltage than that of 0.01 C, but there was no significant difference at the end of charge.

Figure 5.28 shows the variation in the mole fraction of the H3 phase during the relaxation time of NCM-811 charged to the high potential region at 0.1 C and 0.01 C. The sample extracted at 0.1 C shows a larger mole fraction of H3 phase than the sample extracted at 0.01 C. The samples charged at 0.1 C and 0.01 C do not show a significant difference in the change of the H3 phase mole fraction with relaxation time. Figure 5.29 shows the change in *c*-axis of the H3 phase at 0.1 C and 0.01 C during the relaxation time. The sample with lithium extracted at 0.1 C shows a larger *c*-axis than the sample at 0.01 C, but the change during the relaxation process is quite close. The relaxation time dependence of lithium and nickel interlayer distances of H3 phase was plotted in Figure 5.30, which calculated using the refined oxide ion positions and *c*-axis. It can be seen that the sample extracted at 0.01 C shows large Li interlayer distance and small Ni interlayer distance in the relaxation time. In the sample charged at 0.1 C, the H3 phase with low concentration is formed first because the lithium ion extracted from the part of the particle that is easy to be removed first. And the low Li concentration in the H3 phase results in a small Li interlayer distance and a large Ni interlayer distance because the Ni valence is

small, and the average ionic radius is large. Comparing the relaxation time change, the Li concentration in the H3 phase of the sample charged at 0.1 C is low, but the lithium moved slowly from the H2 phase to the H3 phase toward the equilibrium state during the relaxation time. This behavior is more pronounced that at 0.01 C, suggesting that the Li interlayer distance increases and the Ni interlayer distance decrease rapidly.

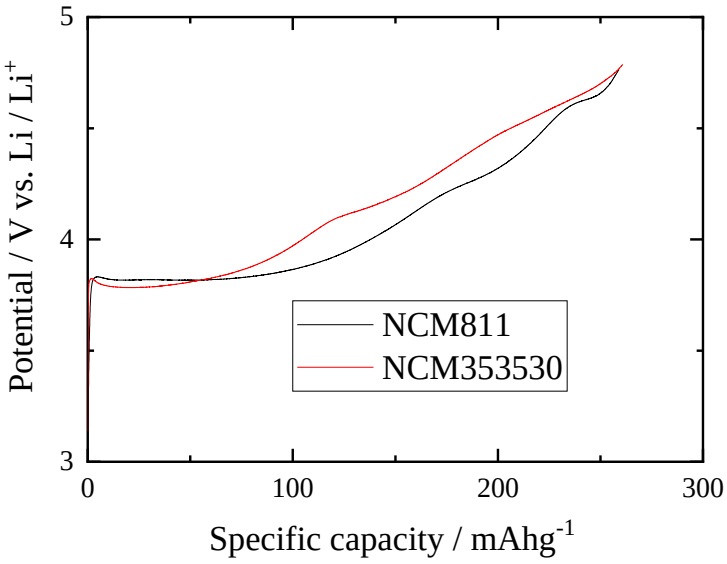

Figure 5.1 Charge curve of $Li_xNi_{0.8}Co_{0.1}Mn_{0.1}O_2$ and $Li_xNi_{0.35}Co_{0.35}Mn_{0.30}O_2$ after lithium extraction up to x = 0.12, 0.09 and 0.06.

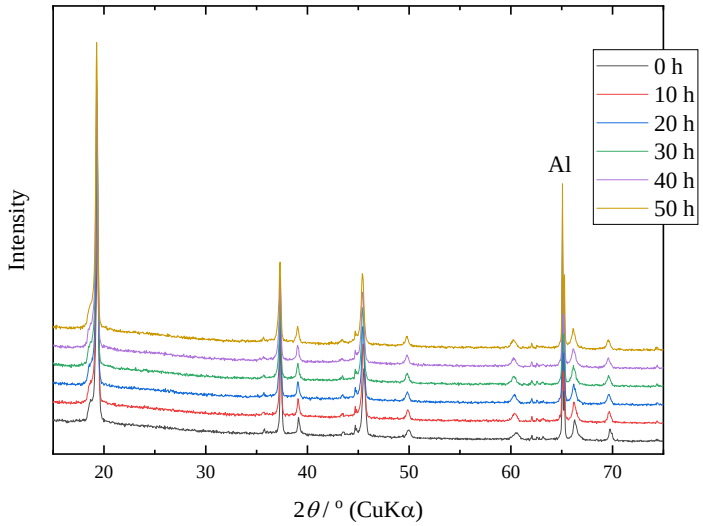

Figure 5.2 XRD parten of $Li_{0.12}Ni_{0.8}Co_{0.1}Mn_{0.1}O_2$.

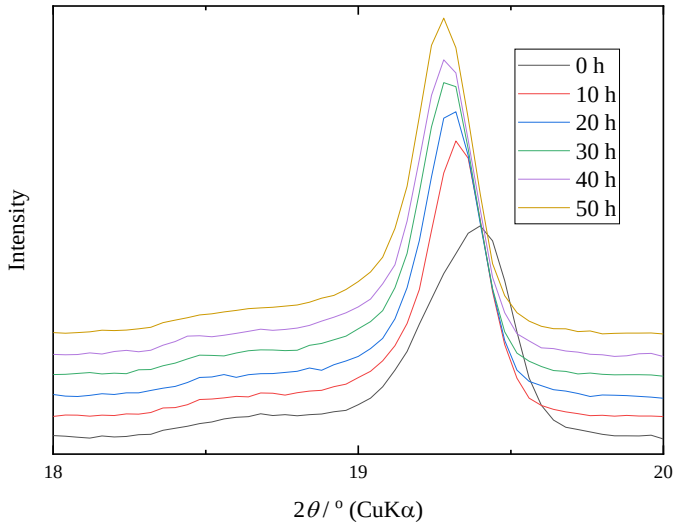

Figure 5.3 003 peaks of $Li_{0.12}Ni_{0.8}Co_{0.1}Mn_{0.1}O_2$ ($2\theta = 18° \sim 20°$).

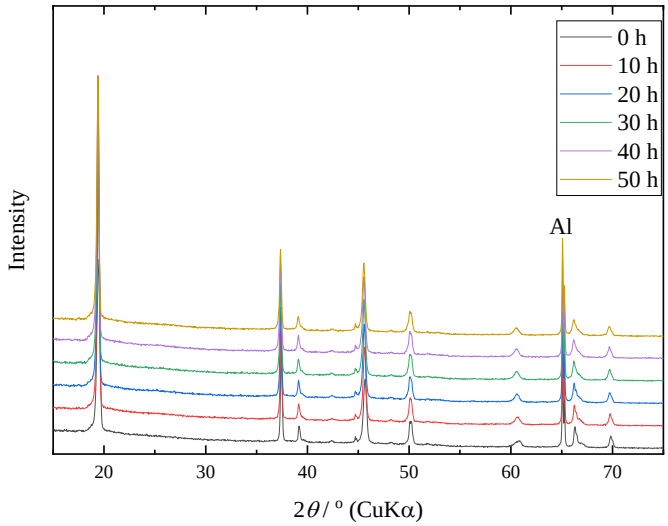

Figure 5.4 XRD parten of $Li_{0.09}Ni_{0.8}Co_{0.1}Mn_{0.1}O_2$.

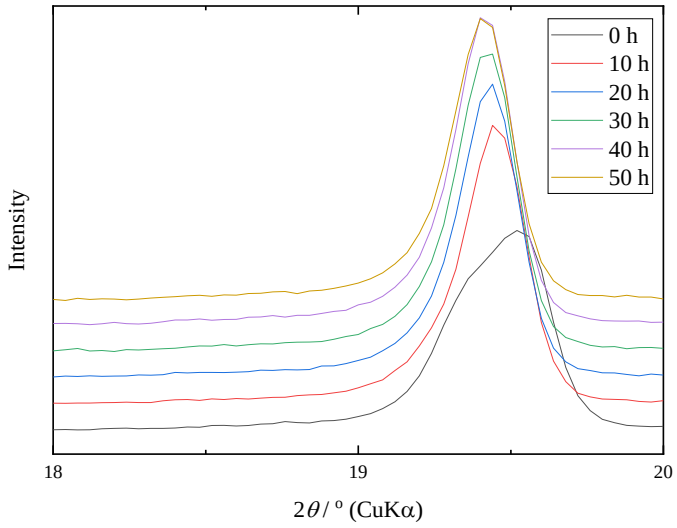

Figure 5.5 003 peaks of $Li_{0.09}Ni_{0.8}Co_{0.1}Mn_{0.1}O_2$ ($2\theta = 18° \sim 20°$).

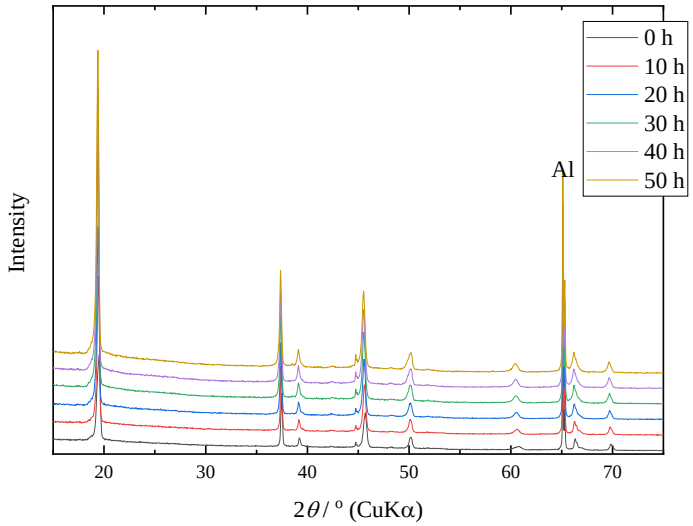

Figure 5.6 XRD parten of $Li_{0.06}Ni_{0.8}Co_{0.1}Mn_{0.1}O_2$.

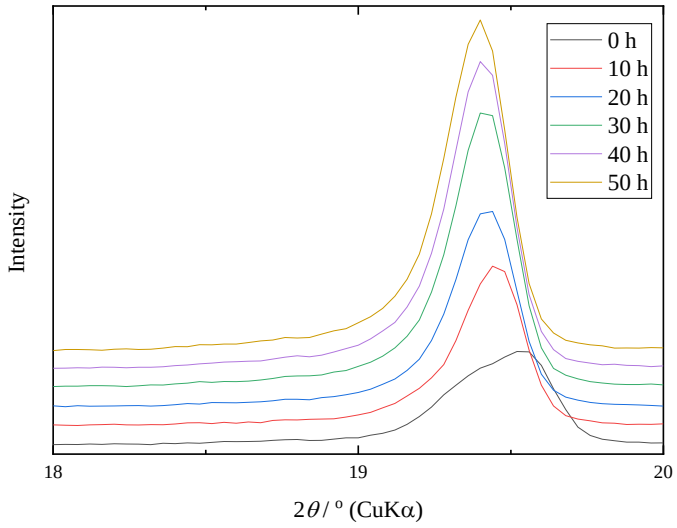

Figure 5.7 003 peaks of $Li_{0.06}Ni_{0.8}Co_{0.1}Mn_{0.1}O_2$ ($2\theta = 18° \sim 20°$).

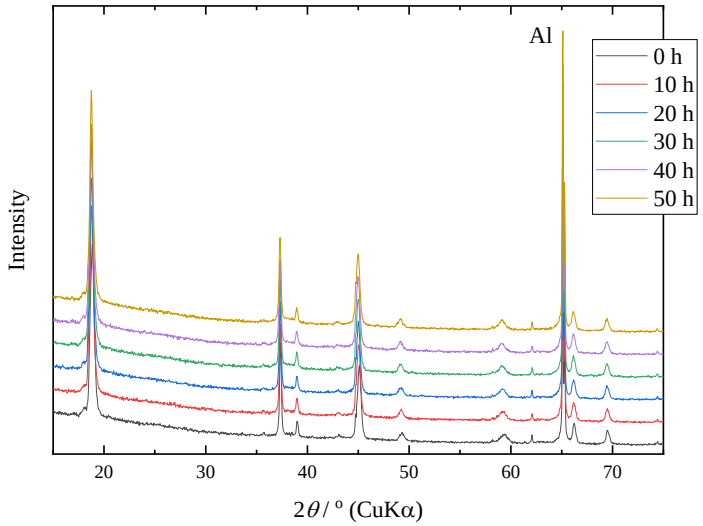

Figure 5.8 XRD parten of $Li_{0.12}Ni_{0.35}Co_{0.35}Mn_{0.30}O_2$.

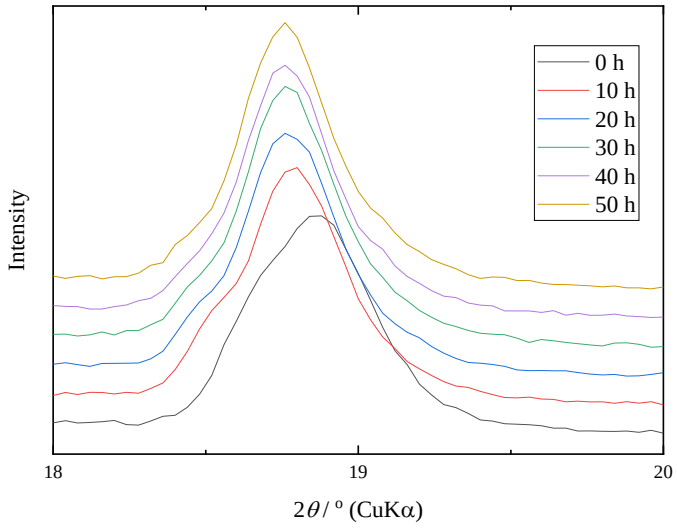

Figure 5.9 003 peaks of $Li_{012}Ni_{0.35}Co_{0.35}Mn_{0.30}O_2$ ($2\theta = 18° \sim 20°$).

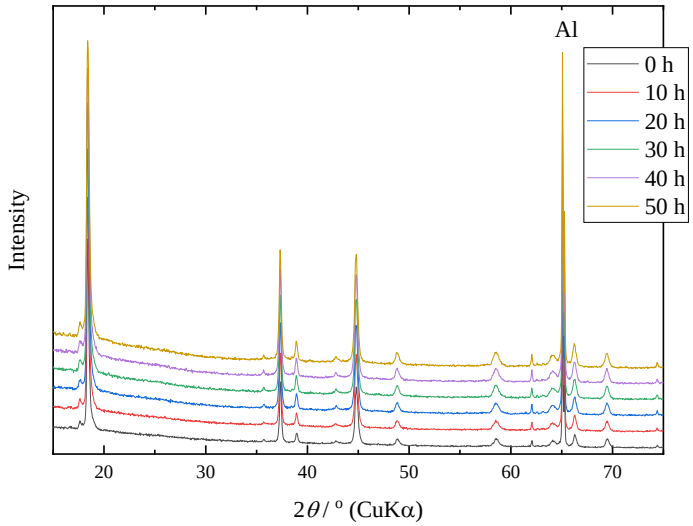

Figure 5.10 XRD parten of $Li_{0.09}Ni_{0.35}Co_{0.35}Mn_{0.30}O_2$.

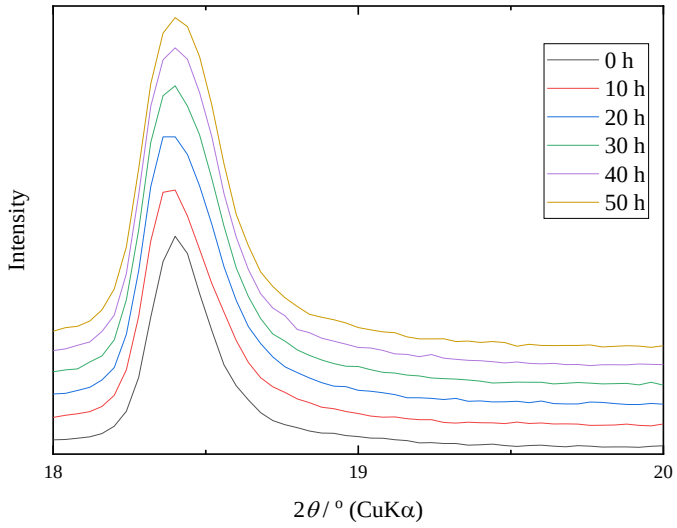

Figure 5.11 003 peaks of $Li_{0.09}Ni_{0.35}Co_{0.35}Mn_{0.30}O_2$ ($2\theta = 18° \sim 20°$).

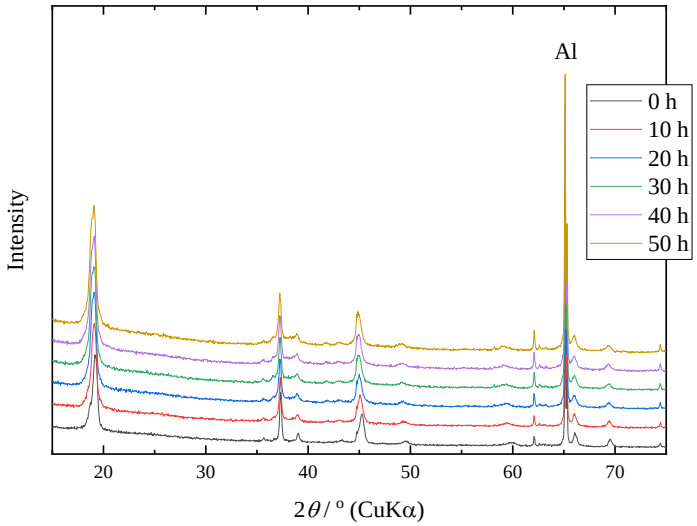

Figure 5.12 XRD parten of $Li_{0.06}Ni_{0.35}Co_{0.35}Mn_{0.30}O_2$.

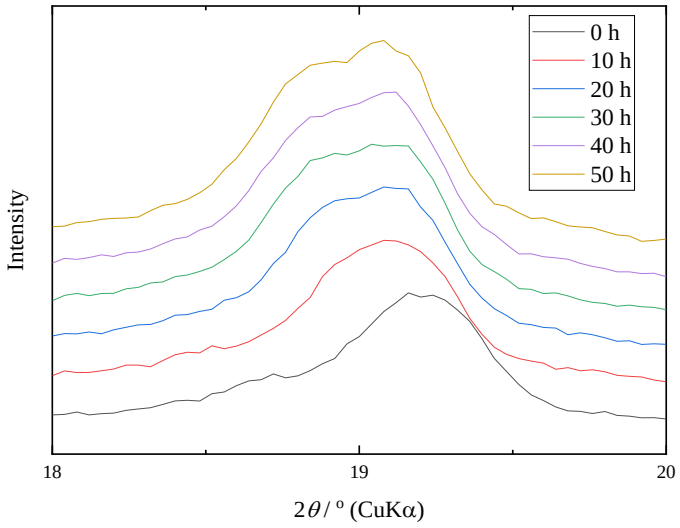

Figure 5.13 003 peaks of $Li_{0.06}Ni_{0.35}Co_{0.35}Mn_{0.30}O_2$ ($2\theta = 18° \sim 20°$).

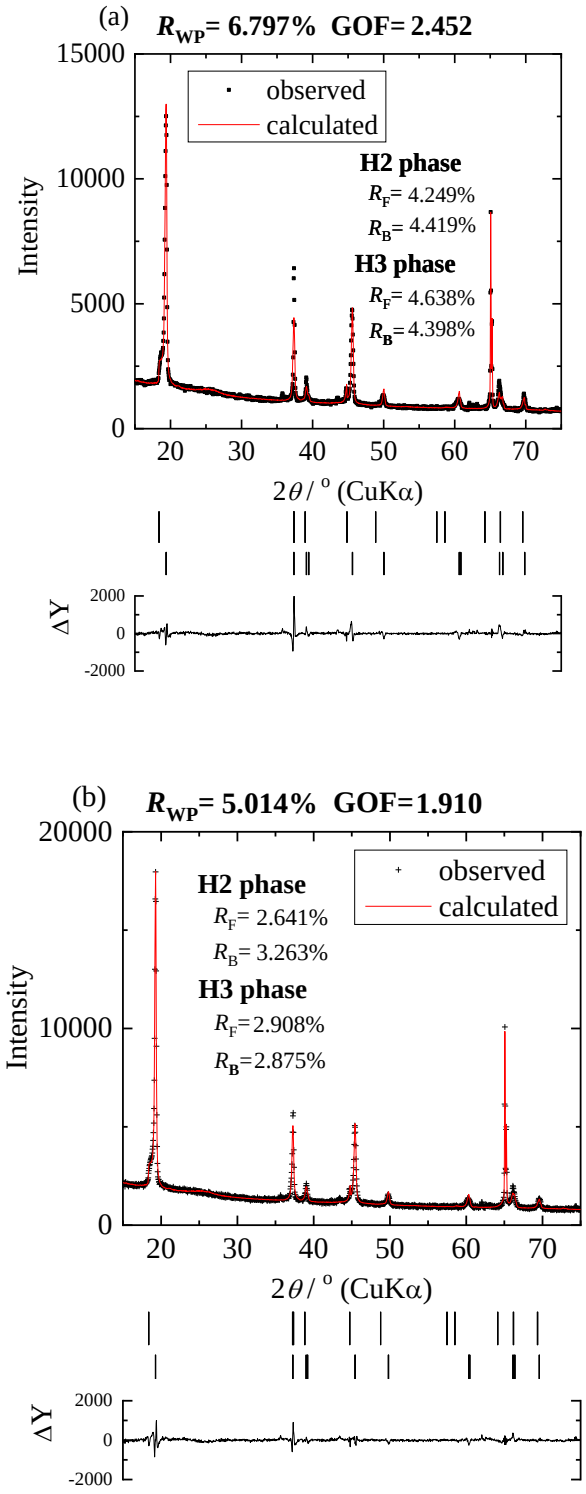

Figure 5.14 Observed and Rietveld fitted diffraction pattern of $Li_xNi_{0.8}Co_{0.1}Mn_{0.1}O_2$ (x = 0.12) after (a) 0 h and (b) 50 h of relaxation.

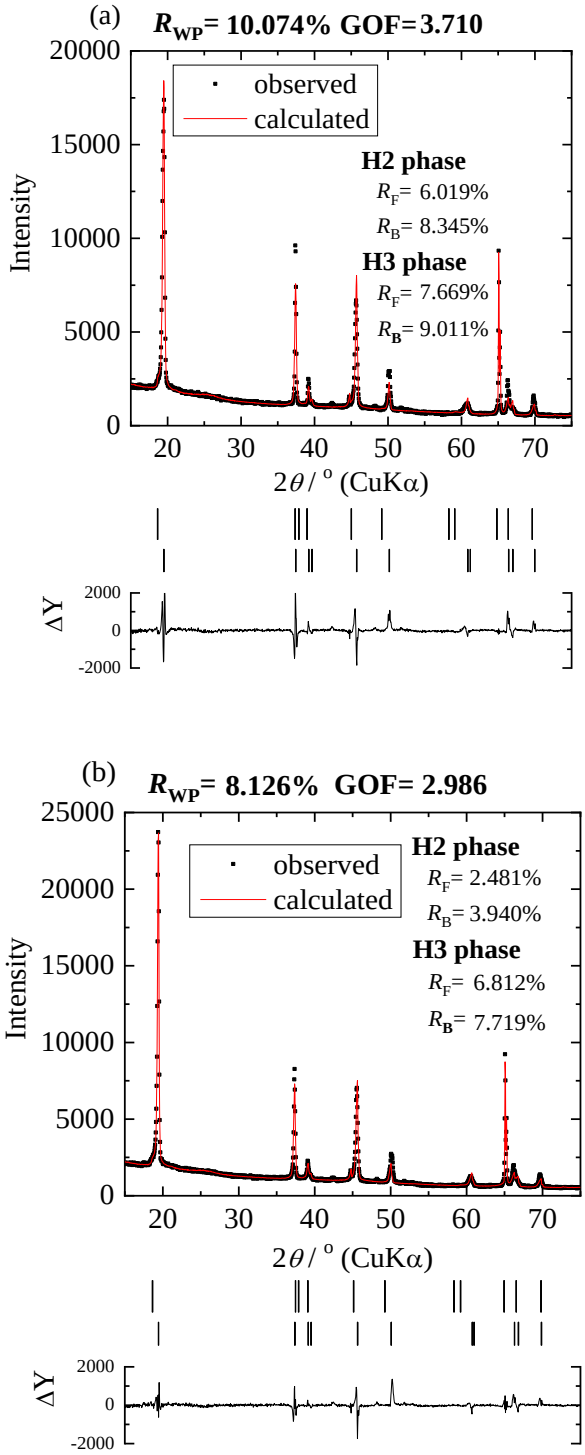

Figure 5.15 Observed and Rietveld fitted diffraction pattern of $Li_xNi_{0.8}Co_{0.1}Mn_{0.1}O_2$ (x = 0.09) after (a) 0 h and (b) 50 h of relaxation.

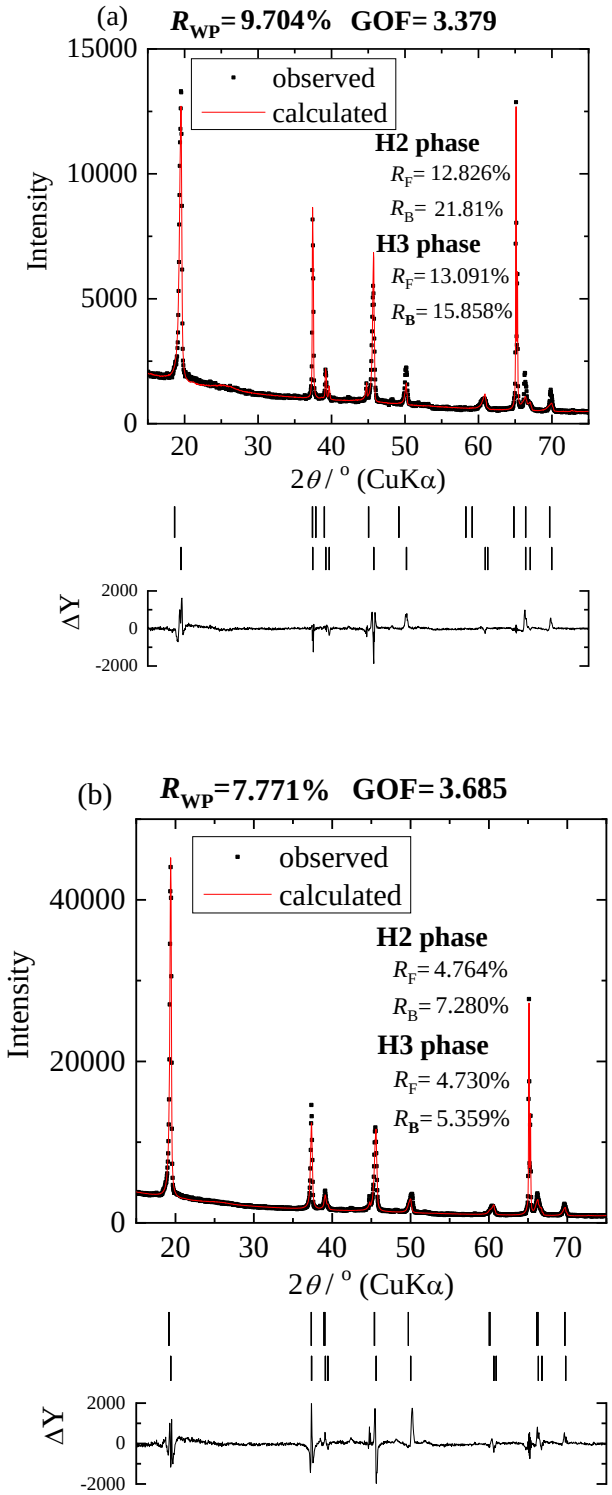

Figure 5.16 Observed and Rietveld fitted diffraction pattern of $Li_xNi_{0.8}Co_{0.1}Mn_{0.1}O_2$ (x = 0.06) after (a) 0 h and (b) 50 h of relaxation.

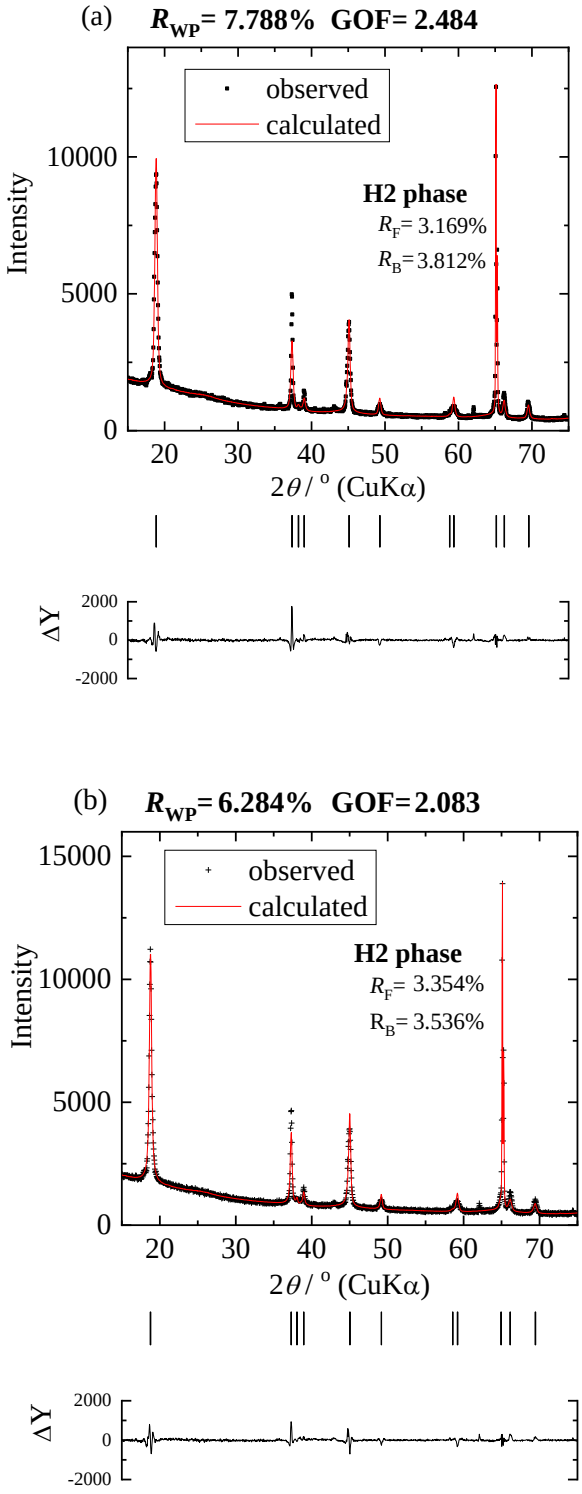

Figure 5.17 Observed and Rietveld fitted diffraction pattern of $Li_xNi_{0.35}Co_{0.35}Mn_{0.30}O_2$ (x = 0.12) after (a) 0 h and (b) 50 h of relaxation.

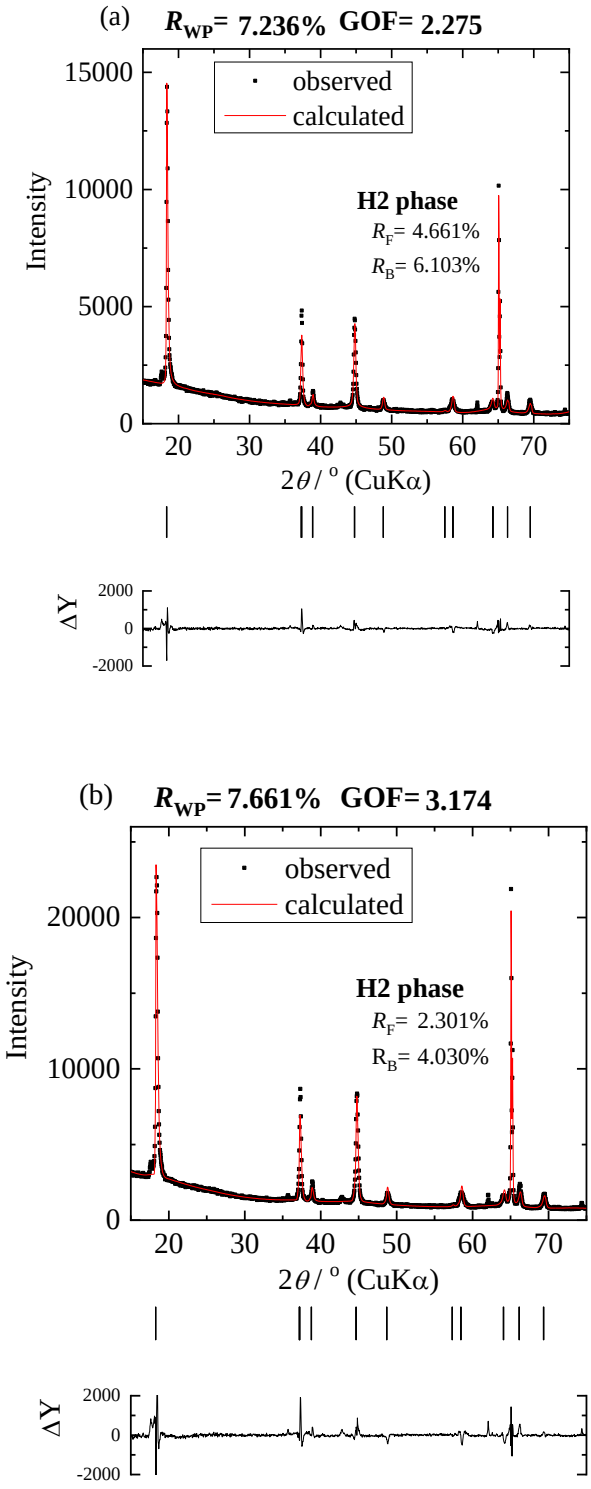

Figure 5.18 Observed and Rietveld fitted diffraction pattern of $Li_xNi_{0.35}Co_{0.35}Mn_{0.30}O_2$ (x = 0.09) after (a) 0 h and (b) 50 h of relaxation.

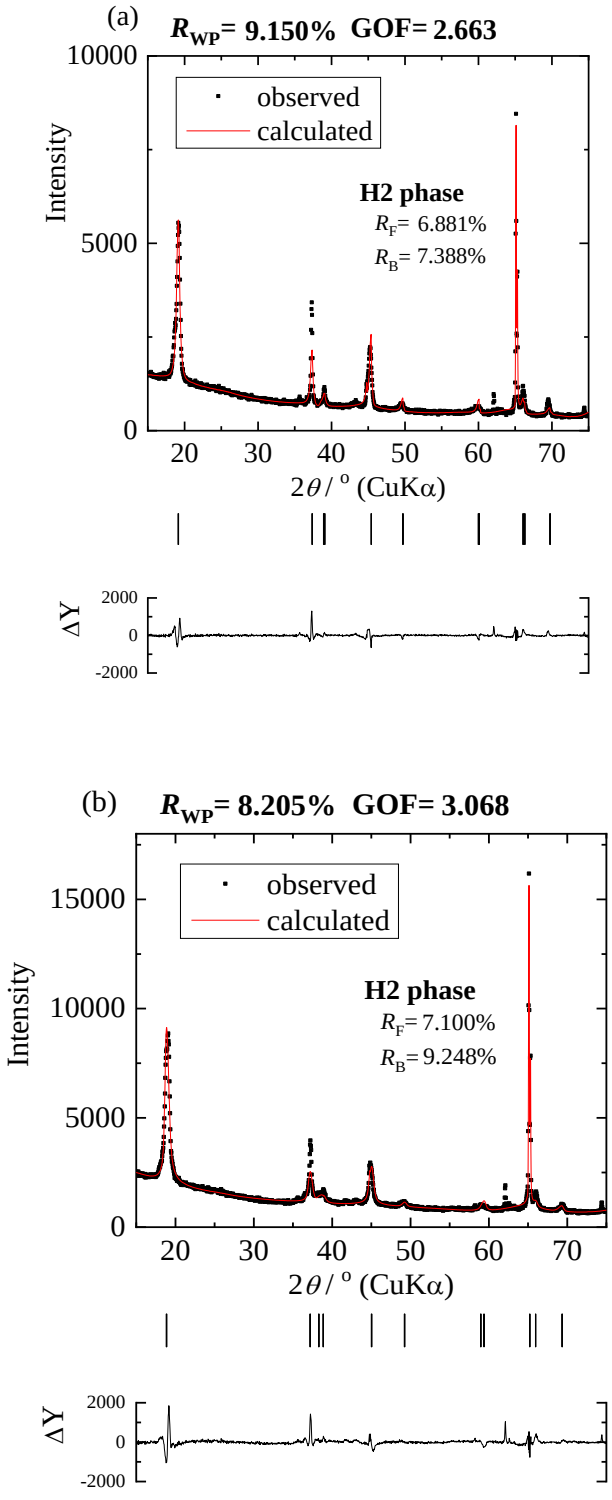

Figure 5.19 Observed and Rietveld fitted diffraction pattern of $Li_xNi_{0.35}Co_{0.35}Mn_{0.30}O_2$ (x = 0.06) after (a) 0 h and (b) 50 h of relaxation.

Table 5.1 Refined structure parameters of $Li_{0.12}Ni_{0.8}Co_{0.1}Mn_{0.1}O_2$ for initial state and after 50 h of relaxation.

			0 h	50 h
H2 phase	Lattice constant	*a* (Å)	2.8172 (1)	2.8204(5)
		c (Å)	14.4315(1)	14.4300(0)
	z		0.232(1)	0.227(1)
	Mole fraction		0.82(9)	0.86(6)
	Confidence factor	R_F (%)	4.249	2.641
		R_B (%)	4.419	3.263
H3 phase	Lattice constant	*a* (Å)	2.8136(1)	2.8180(4)
		c (Å)	14.3312(1)	13.3115(1)
	z		0.256(2)	0.246(3)
	Mole fraction		0.17(1)	0.13(4)
	Confidence factor	R_F (%)	4.638	2.908
		R_B (%)	4.398	2.875
Overall confidence factor		R_{wp} (%)	6.797	5.014
		GOF	2.452	1.910

Table 5.2 Refined structure parameters of $Li_{0.09}Ni_{0.8}Co_{0.1}Mn_{0.1}O_2$ for initial state and after 50 h of relaxation.

			0 h	50 h
H2 phase	Lattice constant	*a* (Å)	2.8172 (1)	2.8201(1)
		c (Å)	14.4315(1)	14.4377(1)
	z		0.232(1)	0.226(0)
	Mole fraction		0.82(9)	0.85(1)
	Confidence factor	R_F (%)	6.019	2.481
		R_B (%)	8.345	3.940
H3 phase	Lattice constant	*a* (Å)	2.8136(1)	2.8155(3)
		c (Å)	14.3312(1)	13.3142(1)
	z		0.256(2)	0.244(6)
	Mole fraction		0.17(1)	0.14(9)
	Confidence factor	R_F (%)	7.669	6.812
		R_B (%)	9.011	7.719
Overall confidence factor		R_{wp} (%)	10.074	8.126
		GOF	3.710	2.986

Table 5.3 Refined structure parameters of $Li_{0.06}Ni_{0.8}Co_{0.1}Mn_{0.1}O_2$ for initial state and after 50 h of relaxation.

			0 h	50 h
H2 phase	Lattice constant	*a* (Å)	2.8234(1)	2.8237(3)
		c (Å)	14.2609(1)	14.3206(3)
	Mole fraction		0.79(3)	0.83(1)
	z		0.230(4)	0.238(3)
	Confidence factor	R_F (%)	12.826	4.764
		R_B (%)	21.81	7.280
H3 phase	Lattice constant	*a* (Å)	2.8253(2)	2.8256(4)
		c (Å)	14.1475(1)	14.2116(1)
	z		0.242(1)	0.230(2)
	Mole fraction		0.20(7)	0.16(9)
	Confidence factor	R_F (%)	13.091	4.730
		R_B (%)	15.858	5.359
Overall confidence factor		R_{wp} (%)	9.704	7.771
		GOF	3.379	3.685

Table 5.4 Refined structure parameters of $Li_{0.12}Ni_{0.35}Co_{0.35}Mn_{0.30}O_2$ for initial state and after 50 h of relaxation.

			0 h	50 h
H2 phase	Lattice constant	a (Å)	2.8234(1)	2.8237(3)
		c (Å)	14.2609(1)	14.3206(3)
	Mole fraction		0.79(3)	0.83(1)
	z		0.230(4)	0.238(3)
	Confidence factor	R_F (%)	3.169	3.354
		R_B (%)	3.812	3.536
Overall confidence factor		R_{wp} (%)	7.788	6.284
		GOF	2.484	2.083

Table 5.5 Refined structure parameters of $Li_{0.09}Ni_{0.35}Co_{0.35}Mn_{0.30}O_2$ for initial state and after 50 h of relaxation.

			0 h	50 h
H2 phase	Lattice constant	a (Å)	2.8234(1)	2.8237(3)
		c (Å)	14.2609(1)	14.3206(3)
	Mole fraction		0.79(3)	0.83(1)
	z		0.230(4)	0.238(3)
	Confidence factor	R_F (%)	4.661	2.301
		R_B (%)	6.103	4.030
Overall confidence factor		R_{wp} (%)	7.236	7.661
		GOF	2.275	3.174

Table 5.6 Refined structure parameters of $Li_{0.06}Ni_{0.35}Co_{0.35}Mn_{0.30}O_2$ for initial state and after 50 h of relaxation.

			0 h	50 h
H2 phase	Lattice constant	a (Å)	2.8234(1)	2.8237(3)
		c (Å)	14.2609(1)	14.3206(3)
	Mole fraction		0.79(3)	0.83(1)
	z		0.230(4)	0.238(3)
	Confidence factor	R_F (%)	6.881	7.100
		R_B (%)	7.388	9.248
Overall confidence factor		R_{wp} (%)	9.150	8.205
		GOF	2.663	3.068

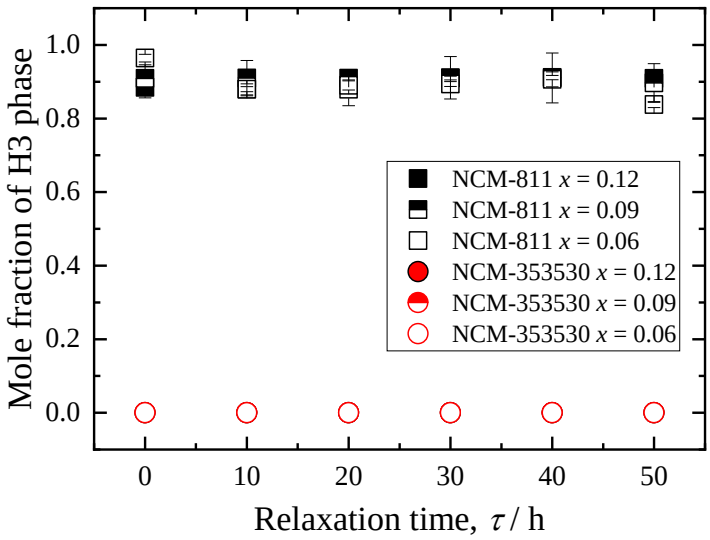

Figure 5.20 Calculated mole fraction changes of H3 phase for $Li_xNi_{0.8}Co_{0.1}Mn_{0.1}O_2$ and $Li_xNi_{0.35}Co_{0.35}Mn_{0.30}O_2$ (x = 0.12, 0.09 and 0.06).

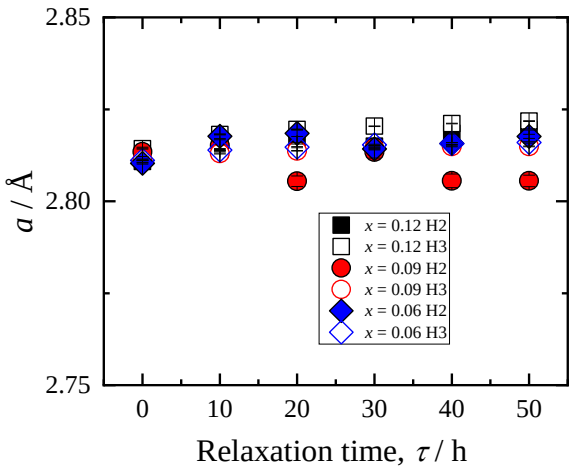

Figure 5.21 Change in lattice parameters of the *a*-axis of $Li_xNi_{0.8}Co_{0.1}Mn_{0.1}O_2$ with relaxation time (x = 0.12, 0.09 and 0.06).

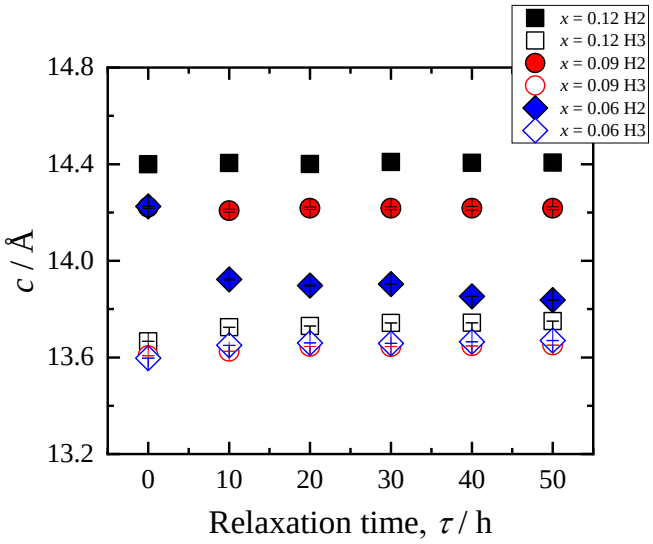

Figure 5.22 Change in lattice parameters of the *c*-axis of $Li_xNi_{0.8}Co_{0.1}Mn_{0.1}O_2$ with relaxation time (x = 0.12, 0.09 and 0.06).

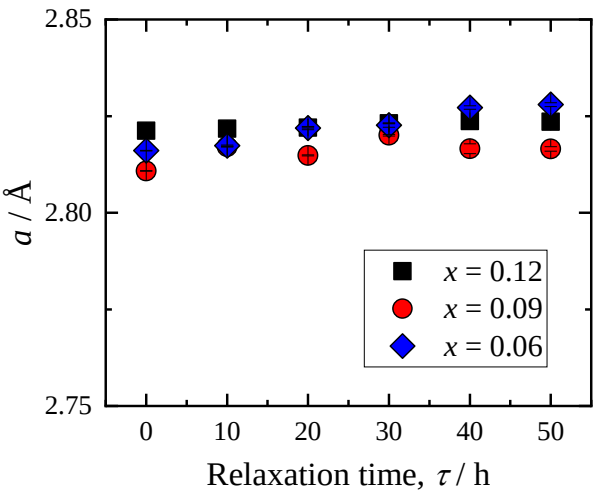

Figure 5.23 Change in lattice parameters of the *a*-axis of $Li_xNi_{0.35}Co_{0.35}Mn_{0.30}O_2$ with relaxation time (x = 0.12, 0.09 and 0.06).

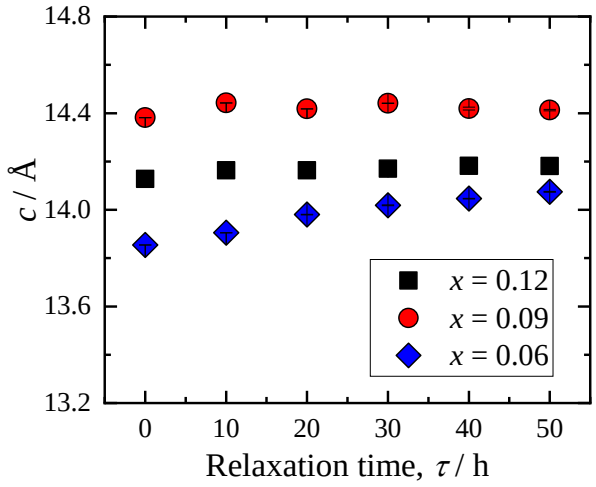

Figure 5.24 Change in lattice parameters of the *a*-axis of $Li_xNi_{0.35}Co_{0.35}Mn_{0.30}O_2$ with relaxation time (x = 0.12, 0.09 and 0.06).

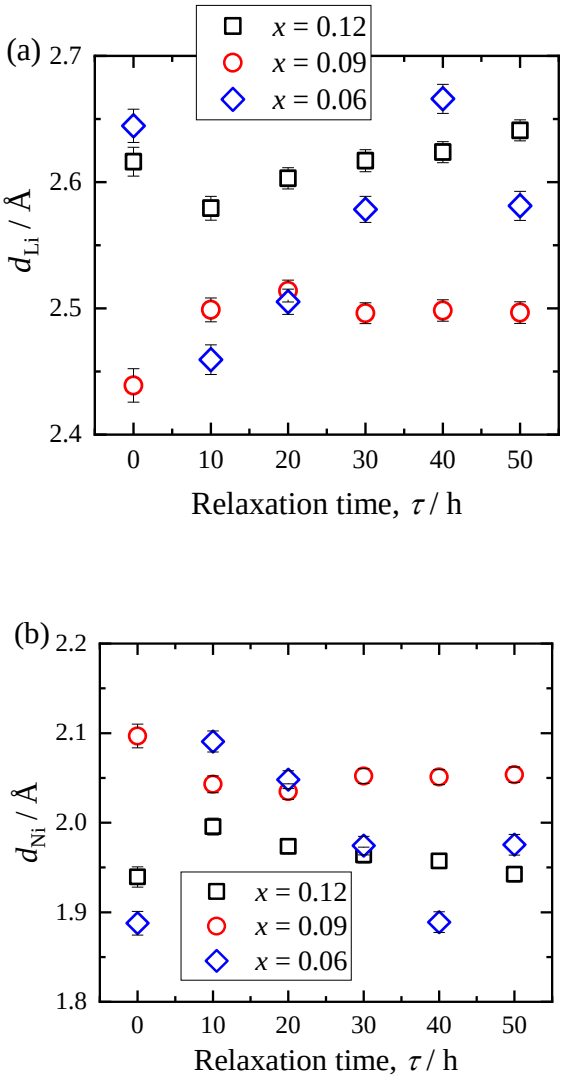

Figure 5.25 (a) Lithium and (b) nickel interlayer distance of $Li_xNi_{0.8}Co_{0.1}Mn_{0.1}O_2$ plotted versus relaxation time (x = 0.12, 0.09 and 0.06).

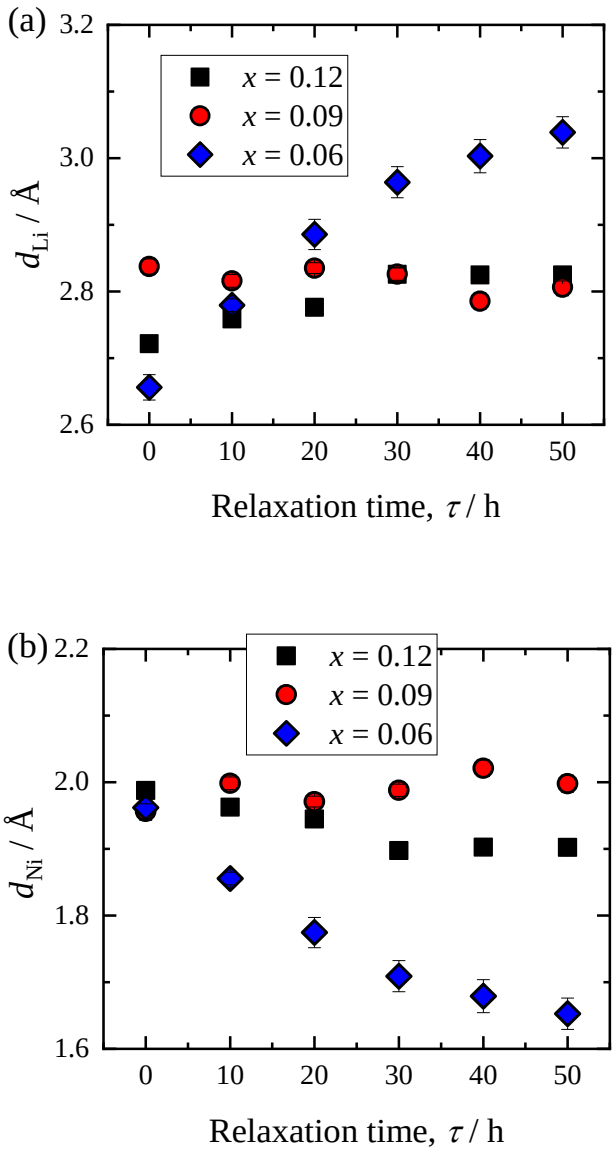

Figure 5.26 (a) Lithium and (b) nickel interlayer distance of $Li_xNi_{0.35}Co_{0.35}Mn_{0.30}O_2$ plotted versus relaxation time (x = 0.12, 0.09 and 0.06).

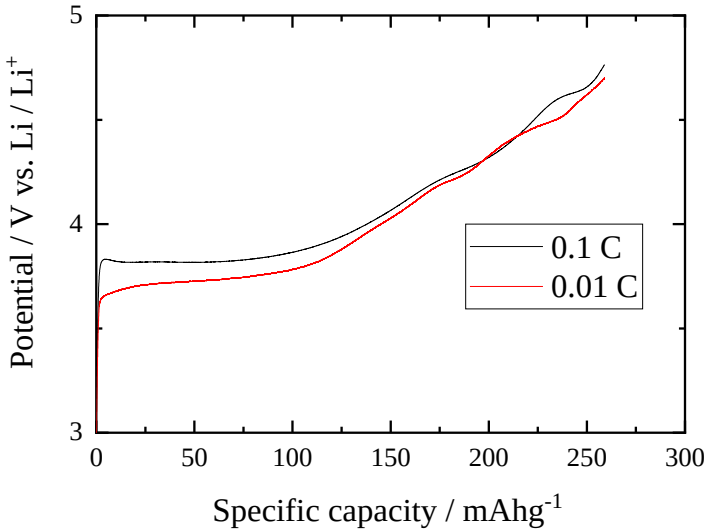

Figure 5.27 Charge curve of $Li_xNi_{0.8}Co_{0.1}Mn_{0.1}O_2$ after lithium extraction up to x = 0.12, 0.09 and 0.06 at 0.01 C and 0.1 C.

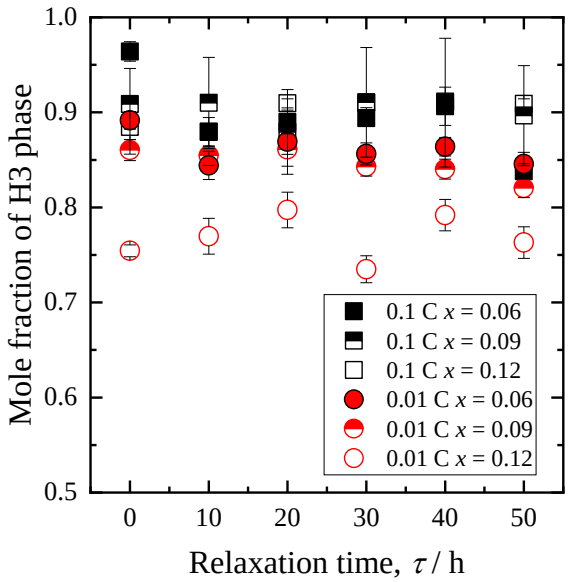

Figure 5.28 Calculated mole fraction changes of H3 phase for $Li_xNi_{0.8}Co_{0.1}Mn_{0.1}O_2$ (x = 0.12, 0.09 and 0.06).

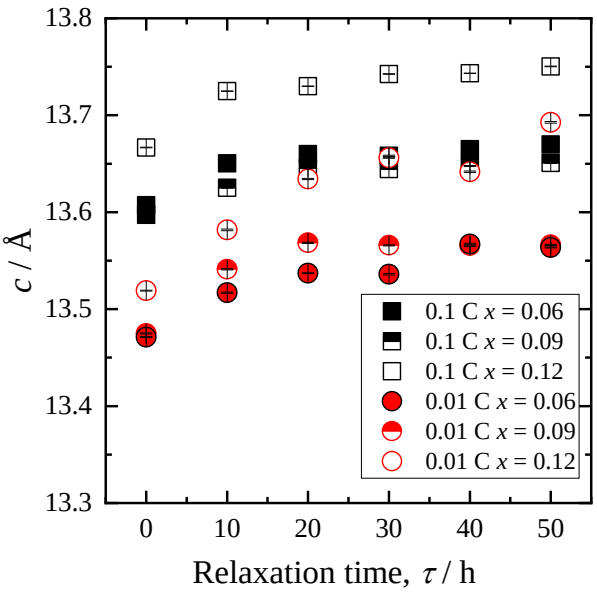

Figure 5.29 Change in lattice parameters of the *c*-axis of $Li_xNi_{0.8}Co_{0.1}Mn_{0.1}O_2$ with relaxation time at 0.01 C and 0.1 C (x = 0.12, 0.09 and 0.06).

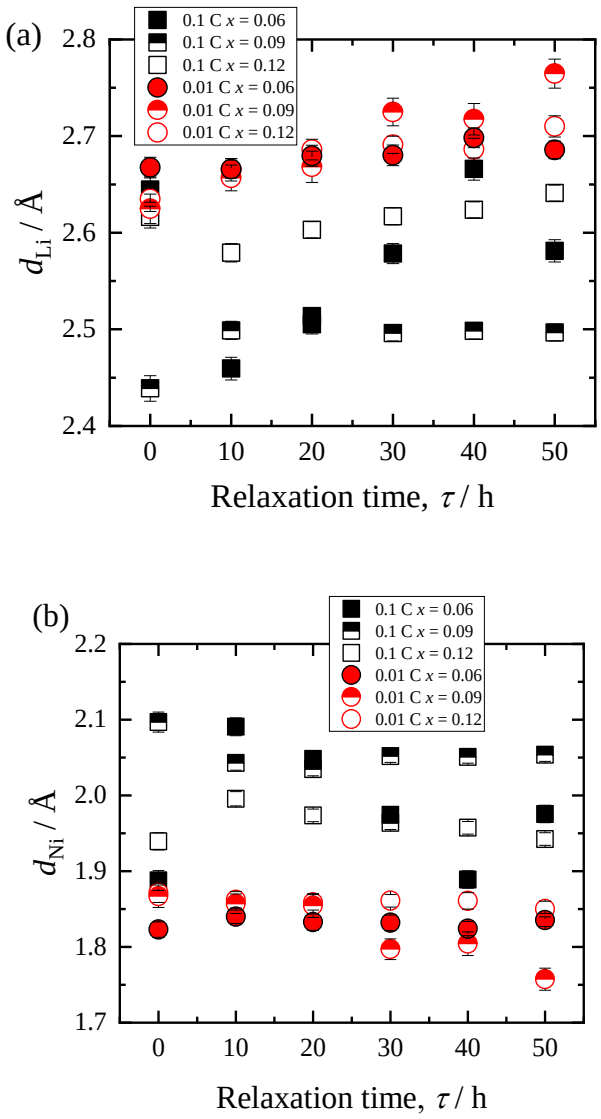

Figure 5.30 (a) Lithium and (b) nickel interlayer distance of $Li_xNi_{0.8}Co_{0.1}Mn_{0.1}O_2$ plotted versus relaxation time at 0.01 C and 0.1 C (x = 0.12, 0.09 and 0.06).

5. 4 Conclusion

The relaxation analyses were carried out on NCM-811 and NCM-353530 to study the structural variation at the deeply lithium extracted region for $0.06 \leq x \leq 0.12$ at 0.1 C. In NCM-811, 90 % of the H3 phase was observed immediately after lithium extraction, and no significant change during the relaxation time. On the other hand, NCM-353530 was observed as only single H2 phase. It is thought that appearance of H3 phase is suppressed when the substitution amount of Co is increased in the NCM cathode materials, which is the same as the NCA cathode materials. To investigate the effect of current density, the results of NCM-811 with lithium extraction at 0.01 C and 0.1 C were compared. Lithium extraction at 0.1 C showed a larger H3 phase and *c*-axis than that of the 0.1 C. And the change in the mole fraction and *c*-axis of H3 phase during the relaxation process was small for both 0.01 C and 0.1 C. The sample extraction with 0.01 C shows a larger Li interlayer distance and a smaller Ni interlayer distance during the relaxation. In the sample charged at 0.1 C, the H3 phase with low concentration is formed first because the lithium ion extracted from the part of the particle that is easy to be removed first. And the low Li concentration in the H3 phase results in a small Li interlayer distance and a large Ni interlayer distance because the Ni valence is small, and the average ionic radius is large. Comparing the relaxation time change, the Li concentration in the H3 phase of the sample charged at 0.1 C is low, but the lithium moved slowly from the H2 phase to the H3 phase toward the equilibrium state during the relaxation time. This behavior is more pronounced that at 0.01 C, suggesting that the Li interlayer distance increase and the Ni interlayer distance decrease rapidly.

Ni-rich NCM cathode materials are used in electric vehicles, but it is still difficult to use in the high potential region. It has been reported that surface deterioration and particle

cracking during the cycling in the high potential region can degrade the cycle performance. Even though, after resolving these problems by surface modification or development of electrolytes, relatively higher potential region would be utilized to exploit energy density. I believe the present structural relaxation study would provide valuable information for the use of higher potential region.

Reference

[1] T. Ohzuku, and Y. Makimura, *Chem. Lett*., **30**, 642 (2001).

[2] S. Gao, Y. Cheng, and M. Shirpour, *ACS. Appl. Mater. Interfaces*, **11**, 982 (2019).

[3] G. Qian, Y. Zhang, L. Li, R. Zhang, J. Xu, Z. Cheng, S. Xie, H. Wang, Q. Rao, Y. He, Y. Shen, L. Chen, M. Tang, and Z. Ma, *Energy Storage Materials*, **27**, 140 (2020).

[4] F. Wu, J. Dong, L. Chen, L. Bao, N. Li, D. Cao, Y. Lu, R. Xue, N. Liu, L. Wei, Z. Wang, S. Chen, and Y. Su, *Energy Storage Materials*, **41**, 495 (2021).

[5] N. Voronina, Y. K. Sun, and S. T. Myung, *ACS. Energy Lett*., **5**, 1814 (2020).

[6] H. Sun, H. Ryu, U. Kim, J. Weeks, A. Heller, and Y. Sun, *ACS Energy lett*., **5**, 1136 (2020)

[7] F. Wu, N. Liu, L. Chen, N. Li, J. Dong, Y. Lu, G. Tan, M. Xu, D. Cao, Y. Liu, Y. Chen, and Y. Su, *J. Energy Chem*., **62**, 351 (2021).

[8] F. Schipper, H. Bouzaglo, M. Dixit, E. M. Erickson, T. Weigel, M. Talianker, J. Grinblat, L. Burstein, M. Schmidt, J. Lampert, C. Erk, B. Markovsky, D. T. Major, and D. Aurbach, Angew. *Adv. Energy Mater*., **8**, 1701682 (2018).

[9] G. Qian, Y. Zhang, L. Li, R. Zhang, J. Xu, Z. Cheng, S. Xie, H. Wang, Q. Rao, Y. He, Y. Shen, L. Chen, M. Tang, and Z. Ma, *Energy Storage Mater*., **27**, 140 (2020).

[10] H. Li, J. Li, X. Ma, and J. R. Dahn, *J. Electrochem. Soc*., **165**, A1038 (2018).

[11] Y. Sun, S. Myung, M. Kim, J. Prakash, and K. Amine, *J. Am. Chem. Soc*., **127**, 13411 (2005).

[12] Y. Sun, D. Kim, H. Jung, S. Myung, and K. Amine, *Electrochimica Acta*, **55**, 8621 (2010).

[13] J. Kang, S. Takai, T. Yabutsuka, and T. Yao, *J. Electrochem. Soc*., **168**, 010518 (2021).

Chapter 6 General Summary

In the present study, the relaxation analysis was carried out on Co-9.0 NCA, Co-14.9 NCA, NCM-811 and NCM-353530 after lithium extraction up to high potential region (x = 0.12, 0.09 and 0.06).

In the chapter 2, I have carried out the relaxation analysis on $Li_xNi_{0.874}Co_{0.090}Al_{0.036}O_2$ (Co-9.0 NCA) after lithium extraction up to high voltage region (x = 0.12, 0.09 and 0.06). In the Co-9.0 NCA, single H2 phase is remained after the lithium extraction up to x = 0.12, although H3 phase appears after the extraction to x = 0.09 and 0.06. Nevertheless, H2 phase is predominant for x = 0.09 and 0.06 and the change in mole fraction was smaller during the relaxation process. On the other hand, in the previous study of $LiNiO_2$ and Co-3.1 NCA, all samples showed a larger H3 phase immediately after the end of charging, and mole fraction of H3 phase became smaller with relaxation time. Comparing with $LiNiO_2$ and Co-3.1 NCA, it is found that larger amount of Co substitution reduces the mole fraction of H3 phase and allow the phase ration of H2 / H3 nearly equilibrium during charging.

In the chapter 3, relaxation analysis was carried out on $Li_xNi_{0.815}Co_{0.149}Al_{0.036}O_2$ (Co-14.9 NCA) to study the structural variation at the high potential region (x = 0.12, 0.09 and 0.06). In the present study, H3 phase was not observed in all the lithium extraction amounts, and only H2 phase appeared. It can be thought that the H3 phase disappeared completely when the Co substitution was increased to 14.9 in NCA. Summarizing the result of previous $LiNiO_2$, Co-3.1 NCA, and Co-9.0 NCA, the formation of H3 phase is suppressed by Co substitution in NCA-based cathode materials. In addition, Co substitution reduces the change in the mole fractions of H2 and H3 phases during the relaxation process. In other words, increasing the amount of Co substitution in Ni-rich

NCAs accelerate the structural change to the equilibrium state during charging, and the H2 phase becomes more stable than the H3 phase.

In the chapter 4, structural variation was investigated during relaxation process after the lithium extraction from $Li_xNi_{0.8}Co_{0.1}Mn_{0.1}O_2$ (NCM-811) to high voltage region (x = 0.12, 0.09 and 0.06). When the lithium ions are extracted to the deeply lithium extraction region for NCM-811, H3 phase is mainly observed in addition to small amount of H2 phase. For x = 0.12, the mole fraction of H3 phase did not change significantly during relaxation time. On the other hand, excess amount of H3 phase is created at the charging for highly lithium extraction up to x = 0.09 or 0.06, and it turns into H2 phase with relaxation. For all the samples of NCM-811, Ni interlayer distance of H3 phase decrease with relaxation time, which is presumably due to the increase in valence of Ni for diminishment of lithium concentration in the remaining H3 phase. In comparison with $LiNiO_2$ and Co-3.1 NCA, less amount of transformation from H3 to H2 occurs during the relaxation for NCM-811. This suggests that the equilibrium structure is achieved more quickly in NCM-811 than in $LiNiO_2$ and Co-3.1 NCA.

In the chapter 5, I have carried out the relaxation analysis on $Li_xNi_{0.8}Co_{0.1}Mn_{0.1}O_2$ (NCM-811) and $Li_xNi_{0.35}Co_{0.35}Mn_{0.30}O_2$ (NCM-353530) after lithium extraction up to deeply lithium extraction region (x = 0.12, 0.09 and 0.06). In NCM-811 system, all the samples were observed at two-phase coexistence of H2 and H3 phases. 90% of the H3 phase was observed immediately after lithium extraction, and no significant change during the relaxation time. On the other hand, NCM-353530 was observed as only single H2 phase. It is thought that appearance of H3 phase is suppressed when the substitution amount of Co is increased in the NCM cathode materials, which is the same as the NCA cathode materials. Furthermore, to investigate the effect of current density, I compared

the results of NCM-811 with lithium extraction at 0.01 C and 0.1 C. Lithium extraction at 0.1 C showed a larger H3 phase and *c*-axis than that of the 0.1 C. And the change in the mole fraction and *c*-axis of H3 phase during the relaxation process was small for both 0.01 C and 0.1 C. I also compared the Li and Ni interlayer distances. The sample extraction with 0.01 C shows a larger Li interlayer distance and a smaller Ni interlayer distance during the relaxation. In the sample charged at 0.1 C, the H3 phase with low concentration is formed first because the lithium ion extracted from the part of the particle that is easy to be removed first. And the low Li concentration in the H3 phase results in a small Li interlayer distance and a large Ni interlayer distance because the Ni valence is small, and the average ionic radius is large. Comparing the relaxation time change, the Li concentration in the H3 phase of the sample charged at 0.1 C is low, but the lithium moved slowly from the H2 phase to the H3 phase toward the equilibrium state during the relaxation time. This behavior is more pronounced that at 0.01 C, suggesting that the Li interlayer distance increase and the Ni interlayer distance decrease rapidly.

$LiNiO_2$-based cathode materials are used in electric vehicles, while it is still difficult to use in the high potential region. It has been reported that not only large structural gaps in the H2 and H3 phase, but also surface deterioration and particle cracking during the cycling in the high potential region can degrade the cycle performance. Even though, after resolving these problems by surface modification or development of electrolytes, relatively higher potential region would be utilized to exploit energy density. I believe the present structural relaxation study on NCA and NCM cathode materials would provide valuable information for the use of higher potential region.

List of Publications

This dissertation entitled "Relaxation analysis of $LiNiO_2$-based cathode materials in the deeply lithium extracted region" is based on the following publications.

<Chapter 2>

Jian Kang, Shigeomi Takai, Takeshi Tabutsuka, and Takeshi Yao

"Structural Relaxation of $Li_x(Ni_{0.874}Co_{0.090}Al_{0.036})O_2$ after Lithium Extraction down to x = 0.12"

Materials, **11**, 1299 (2018)

Jian Kang, Shigeomi Takai, Takeshi Tabutsuka, and Takeshi Yao

"Structural Relaxation of $Li_x(Ni_{0.874}Co_{0.090}Al_{0.036})O_2$ after Lithium Extraction down to ($x \leq 0.12$)"

Journal of The Electrochemical Society, **166**, A5153 (2019)

<Chapter 3>

Jian Kang, Shigeomi Takai, Takeshi Tabutsuka, and Takeshi Yao

"Relaxation analysis of NCAs in high-voltage region and effect of cobalt content"

Journal of The Electroanalytical Chemistry, **878**, 114566 (2020)

<Chapter 4>

Jian Kang, Shigeomi Takai, Takeshi Tabutsuka, and Takeshi Yao

"Relaxation Analysis of $Li_xNi_{0.8}Co_{0.1}Mn_{0.1}O_2$ after Lithium Extraction to High-Voltage Region ($x \leq 0.12$)"

Journal of The Electrochemical Society, **168**, 010518 (2021)

<Chapter 5>

Jian Kang, Shigeomi Takai, Takeshi Tabutsuka, and Takeshi Yao

"Structural Relaxation of $Li_xNi_{0.8}Co_{0.1}Mn_{0.1}O_2$ and $Li_xNi_{0.35}Co_{0.35}Mn_{0.30}O_2$ after Lithium Extraction to high potential Region ($x \leq 0.12$) at 0.1 C"

(To be submitted)

Acknowledgement

I would like to my deepest gratitude to Associate Professor Shigeomi Takai for his valuable and constructive suggestion, and continuous encouragement throughout this study. He gave me an opportunity to take the master's and doctor's courses. His kind and stimulating guidance led me to how to solve problems as a scientist.

I would like to express thanks to Professor Rika Hagiwara and Professor Takashi Sagawa of Kyoto University for their helpful suggestions, discussions and comments for this study.

I gratefully acknowledge Assistant Professor Takeshi Yabutsuka for his help and adbice on this research.

I would like to express my deep appreciation to Ms. Yamamura, secretaries of Functional Solid State Chemistry Laboratory for a lot helps on studying in the master's and doctor's course.

I would like to express my sincere gratitude to Mr. Song Fangzhou, Mr. Chen Heng, Mr. Xiao Linxu and Mr. Wu Yuwei for their cooperation and discussion as members of the international students in our laboratory.

I would like to express my gratitude to the Iwatani Naoji Foundation for providing me with a scholarship to facilitate my life and research.

I would like to thank all the people who have helped me during my 11 years of study in Japan.

Finally, I would like to express my gratitude heartily to my parents and my sisters.